



UNIVERSITÀ
DEGLI STUDI
DI PADOVA

Administrative unit: **University of Padova**

Department: **Land, Environment, Agriculture and Forestry (TESAF)**

PhD Program: **Land, Environment, Resources and Health (LERH)**

Batch: XXXV

**LARGE INFREQUENT DISTURBANCES (LIDS) ON MOUNTAIN BASINS: PRIMARY AND
CASCADING MORPHOLOGICAL AND SEDIMENTOLOGICAL RESPONSES**

PhD Program Coordinator: Prof. Marco Borga

Supervisor: Prof. Lorenzo Picco

Co-supervisor: Prof. Luca Mao

PhD candidate: Giacomo Pellegrini



UNIVERSITÀ
DEGLI STUDI
DI PADOVA

Sede amministrativa: **Università degli Studi di Padova**

Dipartimento Territorio e Sistemi Agro-Forestali (TESAF)

Corso di Dottorato di Ricerca in: **Land, Environment, Resources and Health (LERH)**

Ciclo: XXXV

**EVENTI ESTREMI SUI BACINI MONTANI: RISPOSTE MORFOLOGICHE E
SEDIMENTOLOGICHE PRIMARIE ED A CASCATA**

Coordinatore: Prof. Marco Borga

Supervisore: Prof. Lorenzo Picco

Co-supervisore: Prof. Luca Mao

Dottorando: Giacomo Pellegrini

Table of contents

Summary.....	I
Riassunto.....	III
Introduction.....	1
Research objectives and thesis structure.....	7
Chapter 1 The morphological response of the Tegnias alpine catchment (Northeast Italy) to a Large Infrequent Disturbance.....	9
Chapter 2 Hydrological, geomorphic and sedimentological responses of an alpine basin to a severe weather event (Vaia storm).....	31
Chapter 3 The morphological evolution of a step-pool stream after an exceptional flood and subsequent ordinary flow conditions.....	63
Chapter 4 Surprising suspended sediment dynamics of an alpine basin affected by a large infrequent disturbance.....	83
Discussions and Conclusions.....	105
Future challenges and perspectives.....	107
Appendix.....	109
Acknowledgements.....	113
References.....	115

Summary

Large Infrequent Disturbances (LIDs) overturn the dynamic equilibrium of mountain basins by causing changes (i) to the entire morphological setting, (ii) to the stability of the affected areas and (iii) to the sensitivity to future disruptions. Therefore, the following PhD thesis focused on the mountain basins' primary and secondary impacts and processes caused by the LID "Vaia" (27th -30th October 2018).

The first two chapters have the aim of analysing the hydrological, geomorphic, and sedimentological responses of two mountain catchments characterized by different specific peculiarities: the Rio Cordon Basin and the Tegnás Torrent Basin. Both cases dealt with a catchment-scale holistic approach. In these analyses, particular attention was devoted to the morphological changes along the channel network and to the sediment sources (re)activated on the hillslopes. The two basins showed different predominant responses: mostly mixed (colluvial and alluvial) on the one hand and alluvial on the other. In the former, both the hillslope's sediment sources (landslides; debris flows) and the entire channel network (hyperconcentrated flows; debris flood) were registered as the main sediment suppliers while, in the latter, streambed remobilization, boulder mobility, incision and lateral erosion were identified as the main sediment-contributing processes.

The last two chapters focus attention at reach-scale and have the objectives of providing knowledge on the evolution of mountain streams' morphological units and on the changes in the sediment fluxes and yields of a mountain basin affected by a large infrequent disturbance (Rio Cordon basin). The availability of pre-event data (i.e. remote sensing and sedimentological-hydrological data) combined with the post-event data collected during the period of the project offered the unique opportunity to understand the post-extreme event hydrological and sedimentological responses of a mountain basin. Both the current morphological condition and sedimentological processes suggest that the Rio Cordon is now heading back to the original state but with a new dynamic *equilibrium* since (i) the morphology of the system changed during the Vaia event and (ii) the sediment fluxes and stability of the step-pool configuration resulted in line with the prior event condition.

As a whole, this thesis has the aim of providing deeper knowledge on the morphological impacts and ongoing recovering processes of mountain basins affected by LIDs in order to deliver possible management tips while considering the resilience state of mountain basins.

Sommaro

Gli eventi estremi sono in grado di stravolgere l'equilibrio dinamico dei bacini montani comportando variazioni (i) all'intero setting morfologico, (ii) alla stabilit  delle aree impattate ed (iii) alla vulnerabilit  a disturbi naturali futuri. Pertanto, la seguente tesi di dottorato si focalizza sugli impatti primari e sui processi secondari innescati dall'evento Vaia lungo i bacini montani.

I primi due capitoli hanno l'obiettivo di analizzare le risposte idrologiche, morfologiche e sedimentologiche di due particolari bacini idrografici dolomitici che si differenziano per caratteristiche specifiche: il bacino del Torrente Tegn  e il bacino del Rio Cordon. In entrambi i capitoli si applica un approccio olistico a scala di bacino. In particolare, le analisi si focalizzano sulle variazioni morfologiche lungo tutta la rete idrografica e sulle aree sorgenti (ri)attivate lungo i versanti. I due bacini presentano diverse risposte predominanti: perlopi  miste (alluviali e colluviali) da un lato e solamente alluviali dall'altro. Nel primo caso, sia le aree sorgenti dei versanti che l'intera rete di canali si registrano come principali zone di apporto di sedimento mentre, nel secondo caso, la mobilitazione del letto del fiume, la mobilit  dei grossi massi, l'incisione e l'erosione spondale sembrano essere i principali processi di contribuzione del sedimento.

I successivi due capitoli (Capitolo 3 e 4), invece, focalizzano l'attenzione a scala di tratto e hanno gli obiettivi di fornire conoscenza sia sull'evoluzione delle unit  morfologiche che sui flussi di sedimento in sospensione di un torrente montano (Rio Cordon) impattato da un particolare evento estremo. La disponibilit  di dati pre-evento (i.e. sia dati da remoto che idrologici e di trasporto solido in sospensione) combinati a quelli post evento raccolti durante il periodo di questo progetto di dottorato offre un'opportunit  pi  unica che rara per provare a capire le risposte idrologiche e sedimentologiche del Rio Cordon post evento estremo. Sia la condizione morfologica attuale che i processi sedimentologici suggeriscono che il Rio Cordon stia tornando allo stato originale ma con un nuovo equilibrio dinamico (i) poich  la morfologia dell'intero sistema fluviale   cambiata durante l'evento Vaia e (ii) poich  i flussi di trasporto solido in sospensione e le unit  morfologiche sono in linea con quanto registrato prima dell'evento estremo.

Nel complesso, il seguente progetto di Dottorato ha l'obiettivo di offrire una conoscenza molto approfondita degli impatti morfologici primari e dei successivi processi di ripristino dei bacini montani impattati da eventi estremi alluvionali. Tali risultati suggeriscono di tenere conto dello stato di resilienza dei bacini montani prima di intervenire con eventuali opere di sistemazione idraulico-forestali.

Introduction

The different interactions between physical processes and landforms define the landscape. In turn, landscape's composition, structure, and behaviour determine the river systems (Fryirs and Brierley, 2013). In this thesis, particular attention is devoted to mountainous river systems whose evolution, forms and processes are highly dynamic, especially after disturbances when the geomorphic systems constantly reshape and self-regulate (Knighton, 1998).

Mountain Rivers feature a wide variety of stream morphologies that are driven by the long-term interaction of geological, climatic, hydrological and hydraulic factors (Lenzi, 2001; Rainato, 2017). Mountain rivers share a series of common characteristics that Wohl (2010) summarized as (i) high channel gradient, (ii) high channel-boundary resistance with high boundary roughness, (iii) potentially highly turbulent flows with strong differences during seasonal discharge, (v) high spatial variability in channel morphology, (vi) low temporal variability because only infrequent disturbances are able to exceed channel-boundary resistance and (vii) potential for exceptional sediment yields over a period of few years following basin-scale disturbances (Wohl, 2010; Benito, 2013). At all events, today's literature defines mountain morphologies according to the five-type classification developed by Montgomery and Buffington (1997). Mountain streams are classified according to qualitative and quantitative specific features such as bed material, dominant roughness elements, sediment sources, sediment storage elements, bedform patterns, slope and confinement (Fig. 1). The five-type classes are: cascade, step-pool, plane bed, pool riffle and dune ripple. The cascade configuration features the presence of disorganized cobbles and large boulders that provide high stability to the reaches. Changes in the morphology are only possible when experiencing flood events exceeding 50-100 years of recurrence interval (Buffington, 2012). In those cases, the increase of sediment transport is given by the entrainment of fine material located underneath or around the large boulders. The step-pool morphology, instead, is characterized by a well-organized fluvial structure, which features the alternation of pools, and boulders positioned crosswise the main channel (step). Step-pool sequences represent a highly stable configuration up to floods with less than 40 years recurrence interval. Although this information is highly demonstrated (Montgomery and Buffington, 1997; Lenzi, 2001; Beylich and Sandberg, 2005), literature still lacks in accurate information as far as concerned the timing and hydraulic forcings needed to back-stabilize the channel bed configuration. The plane-bed configuration includes heterogeneous bed-material that ranges from sand to cobbles, pebbles and fine gravels. Plane-bed configuration features armoured layers that only bankfull or over-than bankfull events are able to entrain. Riffle-pool and Dune-ripple are, instead, the last two classes that highly differentiate from the others due to low channel gradients. On the one

hand the riffle-pool configuration promotes the formation of lateral bars while, on the other hand, the dune-ripple morphologies are characterized by sands and by a live bed that favours the sediment transport also during low discharges.

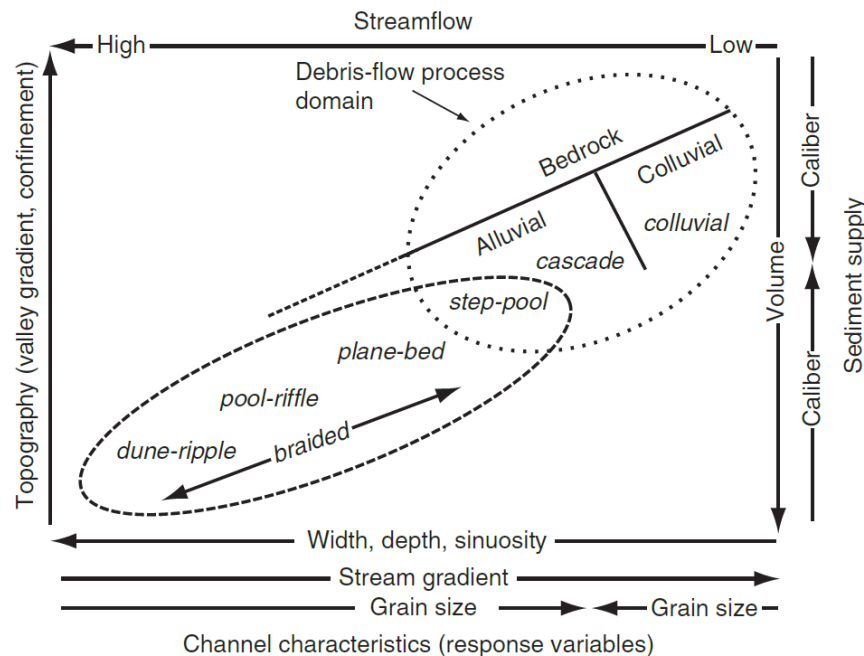


Figure 1. Montgomery and Buffington (1997) channel types and associated channel characteristics (width, depth, sinuosity, stream gradient, grain size) as a function of mountain basins' topography, streamflow, and sediment supply. The dotted circles indicate the process domains. Modified from Buffington and Montgomery, 2013.

Mountain stream morphologies, together with (i) the presence of sediment sources and their connection to the channel network (Cavalli et al., 2013), (ii) the sediment activity and supply type (Lenzi, 2004; Recking, 2012), (iii) the channel bed and composition (Mao et al., 2008; Picco et al., 2016b) and (iv) the hydraulic forcings (Rainato et al., 2021) control the sediment transport processes. According to the abovementioned conditions, sediment transport can occur either via alluvial or colluvial processes. The formers are in the form of suspended and bedload transport (Einstein et al., 1940) (Fig. 2) while the latters are identified as mass movements (Martinsen, 1994). Suspended sediment processes provide most of the total transport fraction (70-90%) (Lane and Borland, 1951; Walling and Webb, 1987) as regards large rivers while a larger range for what concerns mountain streams (10-100%) (Lenzi et al., 2003). Although the sizes of the suspended material change according to different hydraulic regimes, the diameters dimensions go from colloids with diameters smaller than 1μ to gravels up to 64 mm. The suspended sediment transport occurs for either long distances or long-time intervals without particles deposition, it affects the entire water depth, and it generally originates from the erosion of the hillslopes and during rainfall events (Lenzi et al., 2003). However, as intense rainfall events are supposedly becoming more frequent, there is still a worldwide

gap to understand what are the suspended sediment fluxes and dynamics during and after extraordinary events.

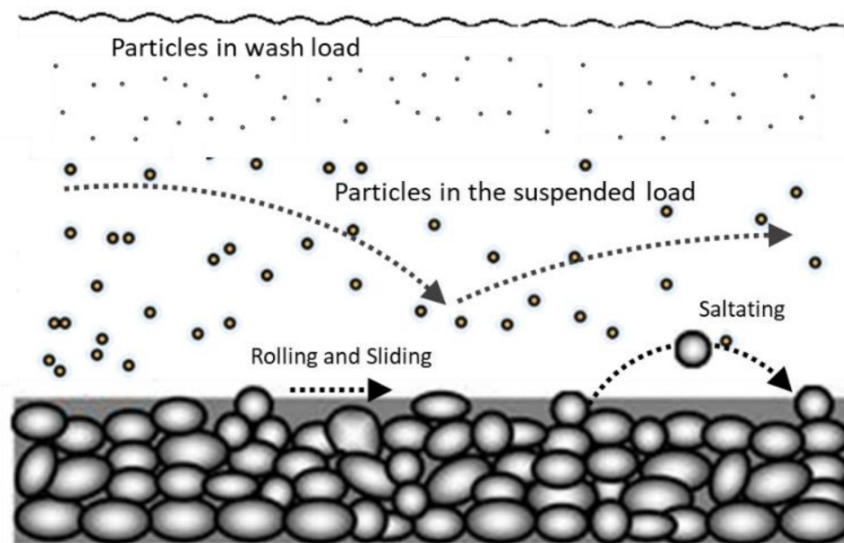


Figure 2. Fluvial sediment transport: suspended load and bedload (saltating, rolling or sliding processes)

Bedload processes, instead, move the sediments by saltating, rolling or sliding (Mazzuoli et al., 2022). The sediment can be moved either as single elements or as a set of granules of different sizes. Bedload is characterized by space-time discontinuity (Liébault et al., 2022) and constitutes the most important component of total transport as regards the steep waterways (Mao et al., 2020). The size of the bedload material is larger than the suspended one and it moves on the bed for short distances both by dragging and rolling or it can be continued by short and successive jumps. Since bedload affects the riverbed, both the riverbanks' and channel beds' erosions feed this process. As far as the colluvial transport is concerned, worth mentioning are the mass movement processes that can be major agents of sediment budgeting along small mountain basins of different morpho-climatic environments. By mass movements are intended those phenomena (i.e., debris flood, debris flows or mudflows) that produce gravitational mass transport that differ from each other due to grain sizes and rheological features (Martinsen, 1994).

When a mountain stream reaches a dynamic *equilibrium* that enhances a transport capacity consistent with the upstream sediment yields is defined as “graded” (Mackin, 1948). To become a graded stream, mountain streams modify their morphological, planimetric and roughness characteristics. If no external causes break this dynamic *equilibrium*, the stream maintains its own morphological characteristics (Fig. 3A) by moderating the catchment-related impacts that destabilized the morphology. The advent of natural (deposits of sediment from the slopes, mass movements, exceptional flood events, etc.) and anthropic disturbances (extraction of sediment from

the riverbed, channelling, water diversions, etc.), induce the unbalancing of mountain streams' dynamic *equilibrium* by either increasing or decreasing the sediment supply and the transport capacity (Rainato et al., 2020). However, predicting the changes in the sediment dynamics after disturbances is still an open question due to the complexity of understanding the fluvial systems. The interplay of geological, climatic and hydrological factors, in fact, leads to different perturbations' responses that can often be unpredictable and hard to understand. Low- and high-magnitude events, in fact, can produce either substantial or minor morphological changes to the systems, unbalancing to a greater or lesser extent the dynamic *equilibrium* (Fig. 3). Therefore, besides the magnitude of the events, it is extremely important to understand the degree of sensitivity and resilience state (Phillips, 2009) to which a hydro-system is subjected in order to predict the future processes needed to reach a stable dynamic *equilibrium* between water, sediment and energy.

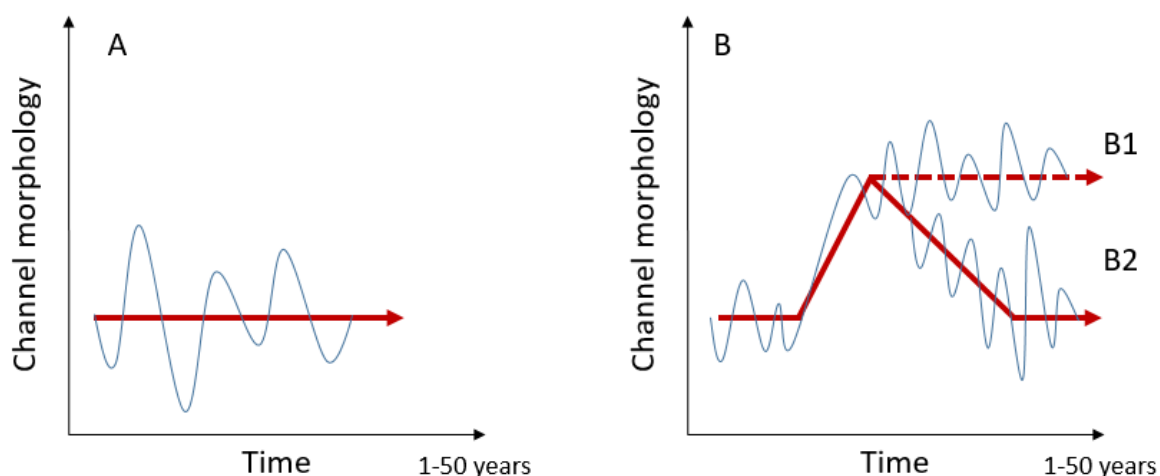


Figure 3. Dynamic equilibrium and instability (modified from Sear et al., 2010 and Rinaldi, 2015). (A) Dynamic equilibrium: channel in equilibrium with water and sediment load but minor morphological changes. (B) Instability; (B1) return to original state but morphology changed to new equilibrium; (B2) adjustment to previous equilibrium state.

If this concept of *equilibrium* is coupled to the context of climate change, things get even more complicated and unpredictable. At present, in fact, the general expectation driven by many studies on climate change impacts on the Alpine areas (e.g., mass movements) is that disturbances will increase in frequencies and magnitudes (IPCC, 2012). Several authors (Harris et al., 2009; Fischer et al., 2013; Ban et al., 2015, 2018; Giorgi et al., 2016; Turkington et al., 2016; Coe et al., 2018;) pinpointed that both the warming of permafrost and the retreat of glaciers will increase the availability of sediment sources areas that are likely to be moved by future intense rainfalls and, thus, to increase the exposure of downstream villages and human communities (Gariano and Guzzetti, 2016). However, the impacts of climate change on sediment production and transfer processes remains still a difficult task (Hirschberg et al., 2020).

Thus, assuming that the frequency of those that once were defined as Large Infrequent Disturbances (hereinafter LIDs) is likely to increase, the LIDs will lead to new and unfamiliar geomorphic processes that will establish new states of dynamic *equilibrium*.

LIDs are documented to be major landscape modification agents (Turner and Dale, 1998) (Fig. 4) and are normally classified as hurricanes, tornados and windthrows (Rich et al., 2007), wildfires (Schulte and Mladenoff, 2005), floods, glacial lake outburst floods (GLOFs), volcanic eruptions, and earthquakes (Stueve et al., 2011). However, due to their infrequency and wide spatial scale of impact as well as the lack of long-term data, very few LIDs-related studies are present in literature. This brought to light the importance of (i) comprehend the primary impacts and triggering mechanisms, (ii) the recovery time and (iii) the cascading sedimentological and morphological trajectories/processes. About this latter aspect, only Mazzorana et al. (2019) took stock of the current situation as far as concerned Chilean disturbances and cascading processes. The authors found intensification of landslides activity and changes in the structural and functional sediment connectivity after earthquakes, excess of sediment and large wood availability over the transport capacity and channel aggradation and subsequent widening in river systems affected by volcanic eruptions and mass movements, respectively.

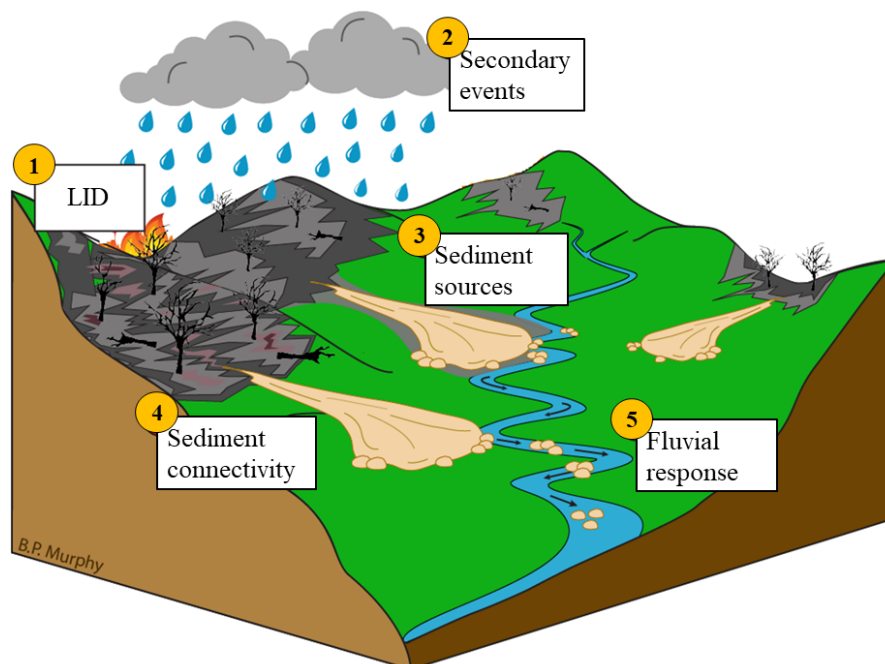


Figure 4. Conceptual cartoon showing the mountain basin's sediment cascade possibly occurring after a Large Infrequent Disturbance (1) and during secondary events (2): (re)activation of connected (4) sediment sources that could imply changes to the fluvial processes and morphologies. Modified from Murphy, 2019.

What emerges most from this first analysis on secondary processes is the need of large-scale analysis to better comprehend the impacts of LIDs in order to forecast and manage the expected

cascading processes. Therefore, in a climate change context, the need of increasing the knowledge and the monitoring worldwide is highly required. The need of increasing the knowledge is particularly required to understand the changes of risks during and after disturbances and to mitigate the risk itself by protecting humans' safety, villages, infrastructures, and economic activities placed neighbouring the hazardous areas (Keiler et al., 2010).

Considering all these aspects, studying and analysing the recent Vaia storm that recently affected the Northeast Alpine area of Italy has been a more unique than rare opportunity. The Vaia storm was an intense cyclone occurred between the 27th and 30th October 2018, which caused extraordinary severe weather all over the Italian Peninsula (Davolio et al., 2020). Exceptional rainfalls intensities and strong wind gusts were registered particularly in the Eastern Alps. Over this area, the Scirocco wind and the rainfall of deep-convection origin caused the strongest event ever recorded over the last 150 years (Davolio et al., 2020). Nonetheless, the exceptionality of the Vaia storm implied extensive impacts on mountain basins producing the loss of forested surfaces (Motta et al., 2018), the (re)activation of sediment sources and the triggering of outstanding colluvial (Macchi et al., 2022) and alluvial processes (Brenna et al., 2020; Rainato et al., 2021). Thus, Vaia broke the dynamic *equilibrium* of mountain basins and laid the foundations for secondary processes. Secondary processes that may entail simultaneous or separate variations on hillslope and channel dynamics affecting directly the morphology, stability and the safety (Montgomery and Buffington, 1997) of mountain basins. If on the one hand recent literature focused satisfactorily on how LIDs cause changes in the structural (dis)connectivity (i.e. the capability of a catchment to promote or impede the sediment cascade) (Lizaga et al., 2017; Ortíz-Rodríguez et al., 2017; Fernández et al., 2020; López-Vicente et al., 2020; Martini et al., 2020; Jautzy et al., 2021;), on the other hand, it showed few studies on the long-term effects of LIDS on sediment dynamics of mountain basins (Rainato et al., 2017; Uchida et al., 2018; Rickenmann, 2020) and barely no-one as far as concerned the timing and triggering forces and factors of such processes.

Therefore, although knowledge on mountain fluvial systems has reached top-level in the last decades, further progresses on river sciences to adapt these notions to the changing times are needed. The existing means, in fact, might be useful to fulfil the gaps of knowledge as far as concerned mountain basins' responses to climate change. Responses to large and ordinary events that could provide important insights on the understanding of the state of dynamic *equilibrium* to which a hydro-mountainous system tend which would be essential to predict the behaviour of fluvial systems and their sensitivity and/or resilience to future extra- and ordinary disturbances (Phillips, 2009; Fryirs, 2017; Piégay et al., 2020).

Research objectives and thesis structure

The main objective of the present thesis is to investigate the primary impacts and the ongoing cascading morphological and sedimentological processes of mountain basins following a specific large infrequent disturbance: the Vaia storm event. To achieve this objective, with regard to mountain basins' sensitivity and resilience state, the following PhD thesis focuses on the understanding of the state of dynamic *equilibrium* to which the mountain-system used to tend, and to which is currently tending.

Primary impacts of LID

Chapter 1:

The morphological response of the Tegnas alpine catchment (Northeast Italy) to a Large Infrequent Disturbance

Chapter 2:

Hydrological, geomorphic and sedimentological responses of an alpine basin to a severe weather event (Vaia storm)



Secondary processes

Chapter 3:

The morphological evolution of a step-pool stream after an exceptional flood and subsequent ordinary flow conditions

Chapter 4:

Surprising suspended sediment dynamics of an alpine basin affected by a large infrequent disturbance

Figure 2. Thesis structure: the first two chapters focus on the primary impacts at basin scale while the latter two investigate the secondary morphological and sedimentological processes at reach scale.

Specific objectives were built to pursue the general objective by using different approaches and temporal- spatial scales. Thus, each chapter addresses a specific objective.

The **first chapter** applies a catchment-scale integrated approach to analyse the impacts of a large disturbance on both the hillslopes and channel network of a managed mountain basin validating the overall structural approach of sediment connectivity.

The **second chapter** defines the responses of an alpine basin to the Vaia storm by focusing on: (i) the determination of rainfall and hydraulic forcing conditions, (ii) the analysis of the geomorphic and sedimentological responses showed by the hillslopes and main channels and (iii) the comparison of these responses with those exhibited by the alpine basin over the last three decades.

The **third chapter** provides an accurate study about the morphological response of an alpine step–pool stream to a large and infrequent flood, and subsequent ordinary flow conditions.

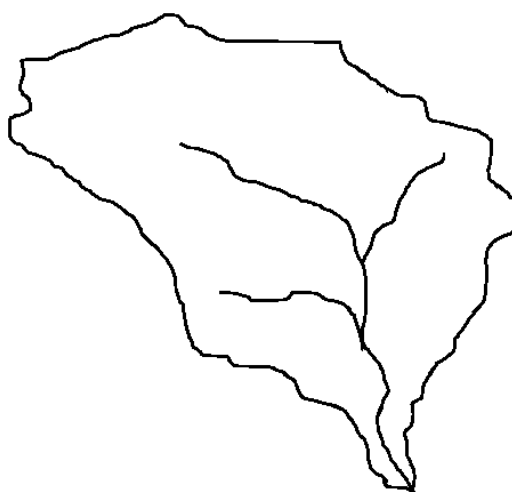
The **fourth chapter** aims at understanding the sediment fluxes after extreme events by (i) identifying the contribution of suspended sediment load from a windthrow-managed-affected area caused by the Vaia event in an alpine basin, (ii) quantifying the annual, seasonal and monthly variation of suspended sediment load, and (iii) analysing the changes in suspended sediment fluxes and dynamics both in the 2nd and 3rd year after Vaia and in comparison to those detected after a similar high magnitude event occurred in 1994.

Chapter 1.

The morphological response of the Tegnas alpine catchment (Northeast Italy) to a Large Infrequent Disturbance

Giacomo Pellegrini, Lorenzo Martini, Marco Cavalli, Riccardo Rainato,
Antonio Cazorzi, Lorenzo Picco

This chapter was published as Pellegrini, G., Martini L., Cavalli M., Rainato, R., Cazorzi, A., & Picco, L. (2021). The morphological response of the Tegnas alpine catchment (Northeast Italy) to a Large Infrequent Disturbance. *Science of the Total Environment*, 770. doi: 10.1016/j.scitotenv.2021.145209.



ABSTRACT

A recent storm (27th-30th October 2018), named Vaia, hit most part of the Northeast of Italy affecting the geomorphic aspect of almost all mountain catchments of the area. The event triggered new instabilities such as windthrows, landslides and debris flows. At present, few studies dealt with the analysis of the impact of a Large Infrequent Disturbance at large catchment scale. This work provides a focus on the Tegas Torrent Basin (Belluno Province) and aims at detecting how, where, and how much this storm affected the basin. Moreover, it integrates two different approaches considering both the dynamic and static aspects of the sediment, via DEM of Difference (DoD) and Index of Connectivity (IC), respectively. The Tegas sub-basins responded contrastingly: the Bordina (volcanic origin and covered by pastures and spruce forests) was mainly affected by windthrows (7% of the sub-basin area) and landslides (0.5%), while the Angheraz (outcropping dolomite rocks) was stricken only by debris flows (1.0%). Morphological changes were clear along the entire channel network, with predominant erosion in the steepest upstream parts (over 2 m of the channel elevation), and deposition in the lower main valley floor (over 3 m of the channel elevation). The IC analysis along the instabilities highlighted that the windthrows occurred mainly in areas of high connectivity, which may be important for future management strategies. Moreover, the proposed integrated approach, based on the combination IC-DoD, permitted a detailed identification of sediment routing and a contemporary estimation of erosion and deposition volumes generated by a high magnitude low-frequency event. Based on these results, cascading processes are expected and further analysis are required to fully consider the impact of a Large Infrequent Disturbance.

Keywords: Alpine catchment; Large Infrequent Disturbance (LID); Vaia storm; Geomorphic changes; Index of Connectivity (IC); Tegas Torrent

INTRODUCTION

Large Infrequent Disturbances (LIDs) drastically influence the riverine ecosystems, from the landscape to their functioning (Foster et al., 1998): the nutrient cycle and the rate and pattern of the energy flow change (Keiser et al., 2016), the entire morphological setting becomes different (Mazzorana et al., 2019), the stability of the affected areas decreases (Eaton and Giles, 2009) and the sensitivity to future disruptions increases (Turner and Dale, 1998). The LIDs are hurricanes, tornados and windthrows (Rich et al., 2007), wildfires (Schulte and Mladenoff, 2005), floods, glacial lake outburst floods, volcanic eruptions, and earthquakes (Stueve et al., 2011). In this work, a specific focus will be on the windstorms. The overall degree of impact of such disturbance depends upon the interaction between wind, forest composition and soil characteristics (Foster et al., 1998; Turner nd

Dale, 1998). Among others, the loss of forest cover reduces the overall evapotranspiration and rain interception increasing the total runoff, surface runoff, interflow and base flow (Langhammer et al., 2015). These changes promote an acceleration of the hydrological cycle, thus leading to a rapid flow response to rainfall event (Hlásny et al., 2015). Moreover, cascading processes such as channel instability, alteration of sediment yield and fluxes and increase in mass movements are highly expected (Mazzorana et al., 2019).

In a mountain environment, where the hillslopes are closely coupled to the active channel, the response to a large flood disturbance varies greatly between the upstream and downstream areas, especially under the combined effect of wind and precipitation (Orlandini and Lamberti, 2000). Therefore, when an extreme rainfall event occurs, the geomorphological aspect of the fluvial systems can be strongly affected (Hooke, 2016, Dong et al., 2016, Picco et al., 2016). The capacity of this specific flood to erode and deposit sediment all along the channel network entails morphological changes in the entire riverine environment (Yousefi et al., 2017). On the one hand, the upstream part of the mountain streams are frequently subject to erosion processes (DiBiase et al., 2012; Hurst et al., 2012; Clubb et al., 2016), favouring channel incision and slope instabilities (i.e., landslides and debris flows). In turn, slope instabilities are strongly related to the site specific morphological characteristics of the area and soil, as permeability, lithological properties and land use (McColl, 2015; Ivy-Ochs et al., 2017). On the other, in the downstream part, well-known geomorphic changes such as meander migration, channel widening (Krapesch et al., 2011), overbank sediment deposition (Knox, 2006), bar building and avulsions can occur (Beechie et al., 2006; Dean and Schmidt, 2013). In order to better comprehend these dynamics, two major concepts deserve to be taken into account: sediment-continuity (Joyce et al., 2018) and -connectivity (Cavalli et al., 2013). The continuity notion quantifies the storage and dynamics of the sediment (Joyce et al., 2018), while the connectivity represents the degree to which a fluvial system facilitates the transfer of water and sediment through itself (Heckmann et al., 2018; Cavalli et al., 2019). The grasping of such concepts simplifies the overall understanding (catchment related) of the sediment transport and the potential downstream geomorphic changes that a LID may induce in a short time due to the creation of new sediment stores and sources (Davies and Korup, 2010; Fryirs, 2013).

To study the LID effect on sediment delivery, the integration of sediment-continuity, intended as the dynamic or functional component, and -connectivity, as structural or static, is something still poorly used. Recent studies were mainly focused on small scale areas (Cucchiaro et al., 2019; Koci et al., 2020) while at larger scale the attention was paid to only one of those concepts (Cavalli et al., 2017; López-Vicente and Ben-Salem, 2019; Martini et al., 2020). The aspect of the sediment dynamics triggered by a LID is widely analysed through DoD (DEM Of Difference) approach. The

aspect of the sediment connectivity, instead, is commonly carried out through the geomorphometric Index of Connectivity (IC) (Cavalli et al., 2013). Thus, the integration of both techniques permits to better investigate the LID effect on large catchments in a more comprehensive way. To this end two main tools were used: Geomorphic Change Detection (Wheaton et al., 2010) and SedInConnect (Crema and Cavalli, 2018). Recent studies demonstrated the possibility of using them for analysing different disturbances such as debris flows (Tiranti et al., 2018), wildfires (Martini et al., 2020) and flood events (Croke et al., 2013; Cavalli et al., 2017). Therefore, the strong point of this methodology consists in considering all the areas of the catchment under assessment, even those that are difficult to consider with field surveys.

Thus, the general aim of this work is to apply a catchment scale integrated approach to analyse the impacts of a LID on both the hillslopes and channel network of a managed mountain basin validating the overall structural approach of sediment connectivity. The triggering factor is the unique windstorm Vaia that hit most parts of the Northeast Alpine area of Italy between the 27th and 30th October 2018. Given the magnitude of the event and the high natural and aesthetic recognition of the study area under assessment, the following work wants to propose a new integrated approach to characterize the impact of a large disturbance at catchment scale. Precisely, it focuses on how, where and how much this infrequent event affected a large mountain basin. Besides, it integrates the dynamic and functional aspect of sediment delivery through the DoD technique with the static and structural one of the IC. Furthermore, it discusses the latter aim using the IC through an alternative perspective in order to derive possible evolutionary trends at the basin scale.

STUDY AREA

Physio-geographical context

The Tegnass Torrent Basin (hereinafter Tegnass) belongs to the San Lucano Valley, located in the Northeast of the Italian Alps. The whole area is a famous touristic zone and, being highly recognized for its high natural and aesthetic value, it is part of the UNESCO World Natural Heritage (Gianolla, 2008). The study basin is characterized by a drainage area of around 52 km², which is delimited by the Pale di San Lucano Mountains to the North, by the Agnèr Mountain to the South and by the Pale di San Martino to the West (Bonat et al., 2019). The basin reaches elevations of over 2800 m a.s.l. and has its outlet at 620 m a.s.l. in the locality of Taibon Agordino (Belluno Province), where the torrent flows into the Cordevole Torrent. From the hydrographic point of view, the Tegnass can be divided into three parts (Fig. 1.1). These are the Bordina Torrent Basin (NW direction, hereinafter Bordina) limited to the north by Cima Pape and crossed by the Bordina Torrent, the Angheraz Torrent Basin (SW direction, hereinafter Angheraz), a glacial cirque surrounded by vertical and sub-vertical

slopes and debris flows and the San Lucano Valley (E direction, Lower-Tegnas) which sets itself apart for the peculiar U-shape and the crossing of the Tegnas Torrent (Testa et al., 2013). The basin is formed by 1000 m of thick Middle Triassic sequence of carbonate platforms (more information in Bonat et al., 2019), except for the Bordina, where middle Triassic volcanic rocks are predominant. Nowadays, especially along the valley bottom, the deposit of the Upper Permian Werfen Formation is covered by over 200 m of unconsolidated and semi-consolidated alluvial quaternary sediment (Testa et al., 2013). Additionally, worth highlighting is the presence of a buried moraine halfway down the valley floor of the Tegnas which stands out to form a stable morphological knickpoint of the Torrent (Castiglioni, 1939; Giordano, 2011).

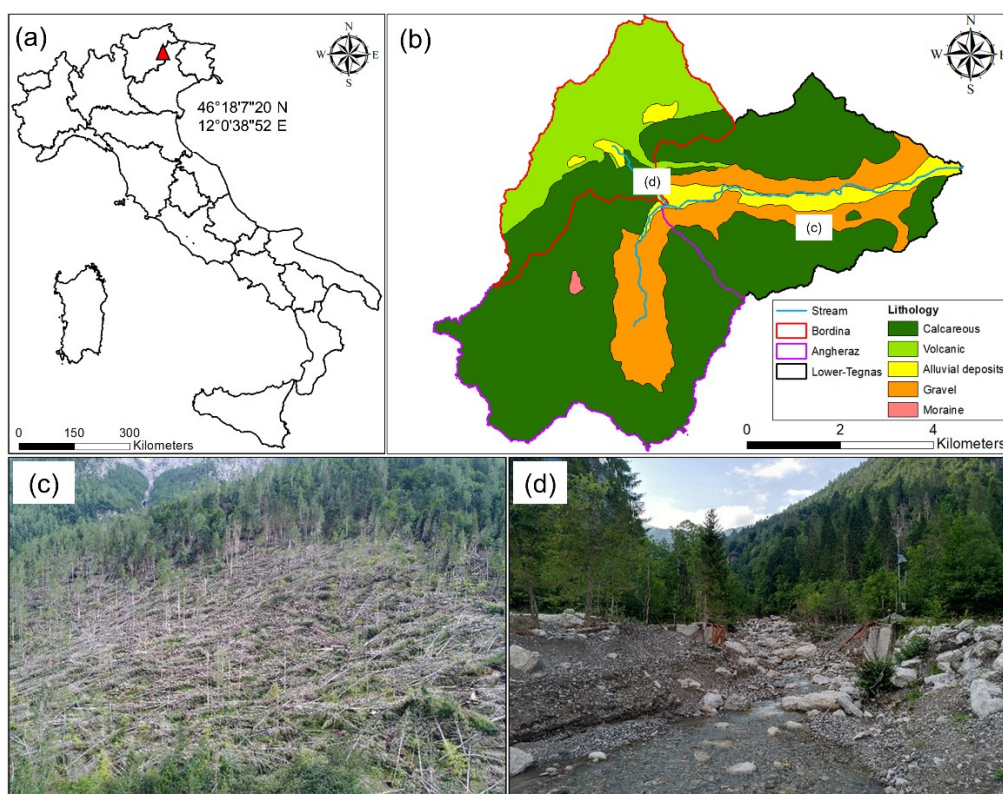


Figure 1.1 (a) Localization of Tegnas Torrent Basin in Italy and its (b) lithology (flow direction from left to right). Windthrows (c) and movement mass processes (d) with damages to infrastructures due to the Vaia event.

Concerning the Lower-Tegnas active channel, the torrent is characterized by a mean slope of 3%, a width ranging from 10 to 35 meters, a D_{50} of 34 mm and both wandering and braided river configurations. The Tegnas valley shows the presence of anthropic infrastructures; the overall basin is dominated by several ballasts, two hydropower stations, a municipal road all along the left side of the main valley bottom and a filtering check-dam around 200 meters upstream the Angheraz outlet. The vegetation is characterized by typical Alpine forest formations such as alder and willow (*Alnus incana* L., *Salix eleagnos* and *S. daphnoides*) along the riparian and peri-fluvial areas, maple and ash formations (*Acer pseudoplatanus* and *Fraxinus excelsior*) where the soil is more developed and rich

in terms of nutritional substances and Norway spruce (*Picea abies*), Larch (*Larix decidua*) and mountain pine (*Pinus mugo*) formations at higher elevations.

Vaia storm event

Between October 27th and 30th 2018, a low pressure system (named Vaia) hit all Northeast Italy, causing high Scirocco wind gusts, storm surges and intense precipitation all along the eastern Alps (Chirici et al., 2019). The highest peak of 72 hours cumulative precipitation was detected by the Veneto Regional Agency for the Environmental Prevention and Protection (hereinafter ARPAV) in Soffranco (Longarone, Belluno Province) and registered a value of 715 mm. Along with the precipitation, wind gusts up to 200 km h⁻¹ (Lucianetti et al., 2019) affected severely the mountain areas, causing extensive windthrows. From a first estimation, over 42,500 ha of forests (8.5 million cubic meters of wood) were affected (Chirici et al., 2019). Among the impacted areas, the San Lucano Valley was highly damaged. Specifically, the rain gauge station located in Col di Prà at the confluence between the Bordina and the Angheraz, managed by ARPA Veneto, registered rainfall until 12:00 a.m. of October 29th, when the instrument was damaged by the flood event. Up to that time, the cumulative precipitation recorded 376 mm. To better characterize the full event, the rainfall data collected in a neighbouring valley (4 km North, Biois of Cencenighe, ARPAV) were used. Here, the cumulative precipitation (72h) was 548 mm. In this sense, the precipitation intensity (mm 72h⁻¹) of the Vaia storm was compared to the larger events of same duration recorded during the period 1984-2017 (Fig. 1.2). This analysis suggested that the Vaia event was characterized by a recurrence interval (RI) of over 100 years which makes it the highest of the whole period by far (Fig. 1.2). Excluding the 2018 event, the highest intensity barely exceeded 10 years of RI in a period longer than 30 years.

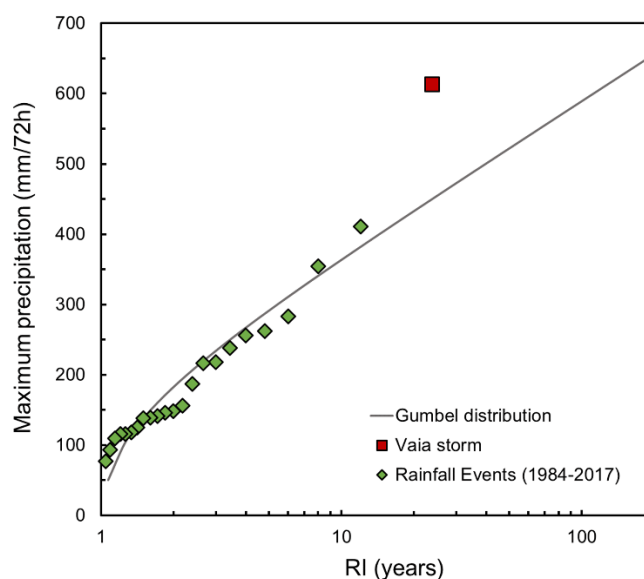


Figure 1.2 Graph representing the Gumbel distribution and the Recurrence Interval (RI) of the 72h events of the Tegnás basin since 1984. The red square represents the Vaia rainfall event. The precipitation between 29th-30th October 2018 were estimated by the Veneto Regional Agency for the Environmental Prevention and Protection.

Furthermore, early multi-model convection-resolving simulation of the Tegnás Torrent (more info in Regione del Veneto, 2020) defined a water peak discharge of $173.47 \text{ m}^3 \text{ s}^{-1}$ (Supplementary Fig. A S1). Hence, also according to the flow discharge, a $\text{RI} > 100$ years characterized the event.

MATERIAL AND METHODS

To understand the impact of the Vaia storm on the Tegnás, first slope instabilities were mapped to provide an overview of the primary effects; second geomorphic changes were quantified along the channel network and hillslopes to understand the sediment dynamics; lastly, the sediment connectivity analysis was carried out and the results were presented and discussed in reference to the outcomes of the previous analysis. The analyses were carried out taking advantage of two subsequent aerial photographs (2015 and 2019) and two LiDAR databases (2010 and 2019). Moreover, for the specific analysis of the Lower-Tegnás active channel changes, an additional ortophotos, dating 2018, was used. The ortophotos (0.2 x 0.2 m resolution) and LiDAR data were acquired during the period between June and October. The oldest LiDAR dataset was acquired by the Italian Ministry of the Environment, Land and Sea (MATTM), while the more recent one was provided by the Veneto Agency for the Payments in Agriculture (AVEPA). Firstly, the two point clouds were co-registered by applying the point-based method (Cheng et al., 2018) in the Cloud Compare software (version 2.7 - <https://www.danielgm.net/cc/>) and then used to produce 1 m Digital Terrain Models (DTMs).

Slope instability mapping

Through the use of the Esri ArcMap 10.5 software, the orthophotos were thereafter analyzed and compared. First, an inventory of the instabilities and active channels was accomplished using a geomorphological approach based on the orthophoto interpretations (Guzzetti et al., 2009; Rainato et al., 2018). Accordingly, these were classified into:

- i) Active channels: the geomorphic feature of the torrent which is defined by a break in bank slope and, typically, by the edge of the floodplain vegetation (Lawlor, 2004). In this case, it was considered from the confluence of Angheraz and Bordina to the outlet of the basin; The width was measured plotting transversal cross-section every ten meters for each orthophoto;
- ii) Windthrows affected areas: the forested areas affected by uprooting or overthrowing;
- iii) Debris flow channels: hillslope channels affected by debris flows that were identifiable through their light colour and their upstream Dolomite sources;
- iv) Landslides: mass wasted under the influence of gravity detectable because of both their brown colours and their locations in pastures and grasslands.

The investigation considered the percentages at basin scale of the areas affected by instability and the percentage variations between 2015-2019. The active channel, instead, was analyzed also in the 2018 orthophotos. Other type of instabilities (e.g., rills, gullies etc.) were not considered due to resolution constraints and the presence of dense forest cover.

To better comprehend the areas affected by instabilities (i.e., landslides and debris flows), three parameters were considered: slope, land use and permeability. The land use was considered according to the Veneto Region classification (<https://idt2.regione.veneto.it>), and regarded pastures, shrublands, screes, outcropping rocks and forest cover. For what concerns the permeability classes, still following the Regional data, it took into consideration two main classes: low permeability ($K=10^{-4}-10^{-6} \text{ cm s}^{-1}$) and the high permeability ($K>1 \text{ cm s}^{-1}$). Moreover, a distinction among the newly created instabilities and the reactivated one was applied, where the latter were defined as the already existing area that were modified during the Vaia storm. To pursue these aspects, the data were retrieved by the ARPAV regional maps and the LiDAR data previously mentioned.

Morphological evolution of the main channel network

The Geomorphic Change Detection (GCD) tool (Wheaton et al., 2010; Wheaton et al., 2013) was used for the volumetric changes estimation by computing the DoDs between pre and post Digital Elevation Models. This tool provides a suitable way to identify the changes occurred between the two surveys. In this way, it helps in distinguish the real changes from the noise by considering uncertainty in the individual DEMs and error propagation into the final DoD. Although the long timespan of 9

years between the two datasets, this analysis was possible since no remarkable events were detected during that period (view section 2.2). Moreover, since the main interest of this analysis was the characterization of the morphological changes occurred within the active channel, the DoD was computed focusing on the main channel network of Tegnás. The HYDROLOGY module in Esri ArcMap 10.5 software was used (Lin et al., 2006) in order to derive the channel network which was then buffered and manually adjusted according to the 2019 post event ortophotos.

In order to generate an uncertainty map to be considered in the DoD analysis to derive reliable morphological change, the DTMs were used as input into a Fuzzy Inference System (FIS) (Oss Cazzador et al., 2020), which took into account the slope and the point density (Wheaton et al., 2010; Neverman et al., 2016; Cavalli et al., 2017). Two separate sets of FIS rules were applied to better capture the potential source of elevation uncertainty mostly driven by the two highly different point densities (Bangen et al., 2016). Finally, once the rules and the inputs were defined, a probabilistic threshold with 90% confidence interval was applied to discretize the real elevation changes from the noise (Wheaton et al., 2013). In this way, the GCD output quantifies the volumes of sediment displaced during the flood, highlighting the main areas of deposition and erosion. To better comprehend the changes that occurred during the Vaia storm, those analyses were developed considering separately the three sub-basins (Fig. 1.1) and by giving particular attention to the percent imbalance of both the volume (hereinafter VPI) and area (hereinafter API) of each sub-basin. The VPI and API were computed as the volumetric and areal percentage of the bigger of erosion and deposition terms, minus the percentage (Wheaton et al., 2013).

Connectivity Index at basin the catchment scale

The analysis of sediment connectivity at the catchment scale was carried out by applying the topography-based Index of Connectivity (Cavalli et al., 2013), first conceptualized by Borselli et al. (2008). The Index of Connectivity (hereinafter IC) was computed using the stand-alone tool SedInConnect 2.3 (Crema and Cavalli, 2018), which needs a high-resolution DTM to derive an index of the potential linkages between upstream and downstream areas of the catchment. The 2010 DTM was used as the topographic base for the IC analysis. Moreover, the tool exploits the DTM also for the computation of the topographic roughness, which is used, following the approach by Cavalli et al. (2013), as weighting factor (W) to represent the impedance to sediment fluxes within the potential sediment linkages/pathways. Over other types of W factor, the topographic roughness was used for the following reasons: more objectivity and lack of land use heterogeneity. In the following analyses, the reference sink used for the analysis is the outlet of the Tegnás basin.

The IC equation (Eq. 1.1) is expressed as follow:

$$IC = \log_{10} \left(\frac{D_{up}}{D_{dn}} \right) \quad (1.1)$$

where D_{up} = upslope component which means the potential downward routing of sediment capability produced upslope; D_{dn} =the potential flow path length that sediment has to travel to reach the nearest target or sink.

Precisely, these two components are computed through the following equations (1.2 and 1.3):

$$D_{up} = \bar{W} \bar{S} \sqrt{A} \quad (1.2)$$

where \bar{W} = average weighting factor of the upslope contributing area; \bar{S} = average slope gradient of the upslope contributing area (m/m); A =upslope contributing area (m²).

$$D_{dn} = \sum_i \frac{d_i}{w_i s_i} \quad (1.3)$$

where d_i = length of the flow path along the i^{th} cell according to the steepest downslope direction (m); w_i =weighting factor for the i^{th} cell; s_i = slope gradient of the i^{th} cell (m/m).

A further analysis concerning the IC distribution for each type of instability areas was performed at catchment and sub-catchment scale. Additionally, the IC values regarding the instabilities of the entire Tegnás and the sub-basins were classified into four upscaling classes based on the natural breaks algorithm (Parida et al., 2019; Martini et al., 2020) applied on the entire Tegnás. The classes were: low connectivity, low intermediate connectivity, high intermediate connectivity and high connectivity. Hence, the potential variation (2015-2019) of each instability was considered according to the four classes of IC.

RESULTS

Areal changes at basin scale

In 2015 the Tegnás showed few active instability areas (i.e., landslides, debris flow channels and windthrows affected areas) of small extent and mainly located in the upstream sub-basins Bordina and Angheraz (Table 1.1). Windthrows and landslides represented most of Bordina's instabilities. Concerning the Angheraz, very few landslides were detected compared to the windthrows and active debris flows channels. Because of the Vaia storm, the two distinct sub-basins (Bordina and Angheraz), increased their instability areas (Fig. 1.3) except for the windthrows of the Angheraz, which halved. In 2019 the Bordina was highly affected by windthrows and partially by landslides, causing a 2015-2019 variation of nearly 900% and 19%, respectively (Table 1.1). Debris flows and landslides mostly impacted the Angheraz, causing a 2015-2019 variation of about 114% and 88%,

respectively. As regards the Tegnás, the overall area affected by windthrows rose dramatically by about 1588%, while the debris flow channels increased by 215% (Table 1.1). However, few new landslides were detected in the basin. Windthrows were mainly situated in areas along the valley floor and in a larger patch located in the NE part of the Bordina with respective surfaces of 1.28 km² and 0.80 km². The Lower-Tegnás was also affected by the re-activation of 8 debris flows channels on both the left and right side of the valley, besides triggering those already present on the sides of the Angheraz.

Table 1.1 Instability areas recognized in the Tegnás, Bordina and Angheraz sub-basins in 2015 and 2019.

Tegnás (52 km ²)	Area (%) 2015	Area (%) 2019	Variations 2015-2019 (%)
Debris flow channels	0.21	0.70	215.00
Landslides	0.12	0.13	13.00
Windthrows	0.24	4.00	1588.00
Bordina (12 km²)			
Landslides	0.38	0.46	19.00
Windthrows	0.67	6.66	897.00
Angheraz (22 km²)			
Debris flow channels	0.46	1.00	114.00
Landslides	0.02	0.03	88.00
Windthrows	0.22	0.12	-47.00

Most of the newly created debris flows were found in high permeability soils covered by screes and shrublands for the 76% and 24%, respectively (Table 1.2). Concerning the landslides, almost the totality of the new areas were registered under low permeability soils identified as pastures (73%) and shrublands (26%), respectively (Table 1.2). Compared to the reactivated instabilities, the location of the landslides moved towards the shrublands. As regards to the debris channels, instead, it moved to the screes rather than to the outcropping rocks as occurred prior Vaia. In both instabilities, a similar gradient of slope was registered (~ 40°).

Table 1.2 Data regarding the permeability and land use classes of 2019 debris flows channels and landslides. The low permeability is characterized by a $K=10^{-4}-10^{-6}$ cm s⁻¹ while, the high permeability to $K>1$ cm s⁻¹.

	Land use	Reactivated Area (m ²)	Newly created Area (m ²)	Permeability class
Debris flow channels	Shrublands	57818	48702	High
	Outcropping rocks	13343	/	High
	Screes	77091	146107	High
Landslides	Shrublands	3499	10505	Low
	Pastures	18368	28403	Low
	Screes	/	389	High

As regards the changes occurred along the active channel, the results revealed a reduction of the area of 0.23 km² between 2015 and 2018. Additionally, the average width detected in 2015 was greater than the one of 2018. In both cases the minimum width was found 2 km downstream the confluence of the Bordina. The maximum width, instead, was found approximately halfway to the active channel (Fig. A S2). Considering the period 2018-2019, opposite dynamics were detected. In fact, the active channel area increased over 100%. In 2019, the average width of the channel greatly increased, resulting two fold larger than in 2018. Both the minimum and maximum values increased (Table 1.3).

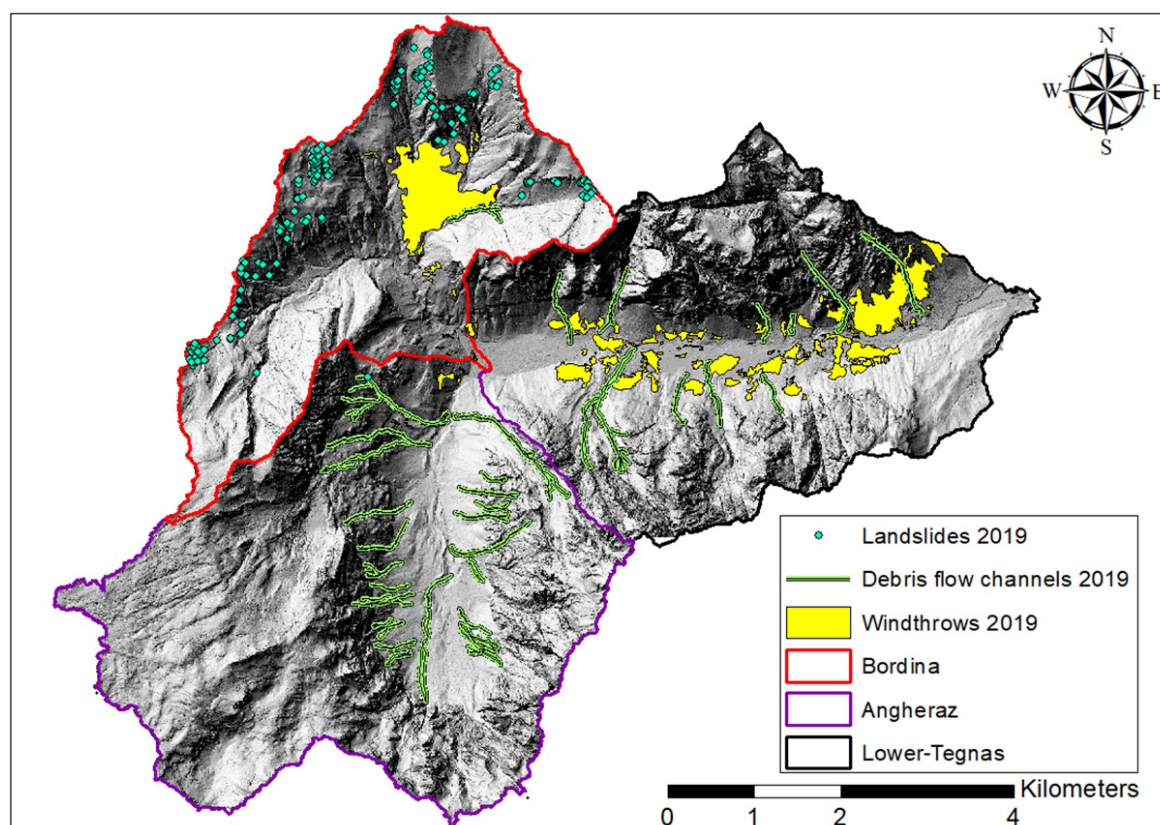


Figure 1.3 Distribution of the instability areas after the Vaia storm event.

Table 1.3 Data regarding the evolution of the active channel.

Active channel	2015	2018	2019	Variations 2018-2019 (%)
Maximum width (m)	77	64	115	49 %
Minimum width (m)	3	3	6	100 %
Average width (m)	19	16	41	156 %
Total area (km ²)	1.38	1.15	2.88	109 %

Morphological evolution along the main channel network

The 2010-2019 changes in the sediment storage ($\Sigma V_{\text{Erosion}}$ and $\Sigma V_{\text{Deposition}}$), together with the specific thresholded values of erosion, deposition and net change, are expressed in Table 1.4.

Table 1.4 DoDs results divided for the channel network of the Bordina, Angheraz and the Tegnás (Valley floor).

	Erosion			Deposition			Net Change			Total Change
	Σ Volume (m ³)	Error (%)	Area (m ²)	Σ Volume (m ³)	Error (%)	Area (m ²)	Δ Volume (m ³)	VPI (%)	API (%)	Σ Vol (m ³)
Bordina	125,970 ± 27,929	22	95,021	115,834 ± 20,196	17	65,506	-10,140 ± 34,466	-2	-9	241,808
Angheraz	167,182 ± 34,205	20	165,75	129,817 ± 21,599	17	109,639	-37,365 ± 40,453	-6	-10	296,999
Lower-Tegnás	66,964 ± 8,200	12	67,728	152,502 ± 14,987	10	138,246	85,538 ± 17,084	19	17	219,466

The Volume and Areal Percentage Imbalance (VPI and API) of the Bordina were in both cases calculated as erosional, respectively as -2% and -9%. As Fig. 1.4 shows, most of the secondary channels located along the upstream hillslopes were greatly eroded causing high values of deposition (over + 4 meters) in correspondence to the Bordina alluvial fan, the main area of deposition. Focusing on the West part, this spot featured evidence of over 3 m of erosion in the left side secondary channels and contributing to deposition of over 1 m (Fig. 1.4a). Moving East, in the channel neighboring the windthrows (Fig. 1.4b), a huge erosion of over 4500 m³ was found, implying a deposition of around 1200 m³ downstream. Similarly occurred at the outlet, where the flood after eroding over 5 m of the left bank (Fig. 1.4c) deposited the material in the alluvial fan.

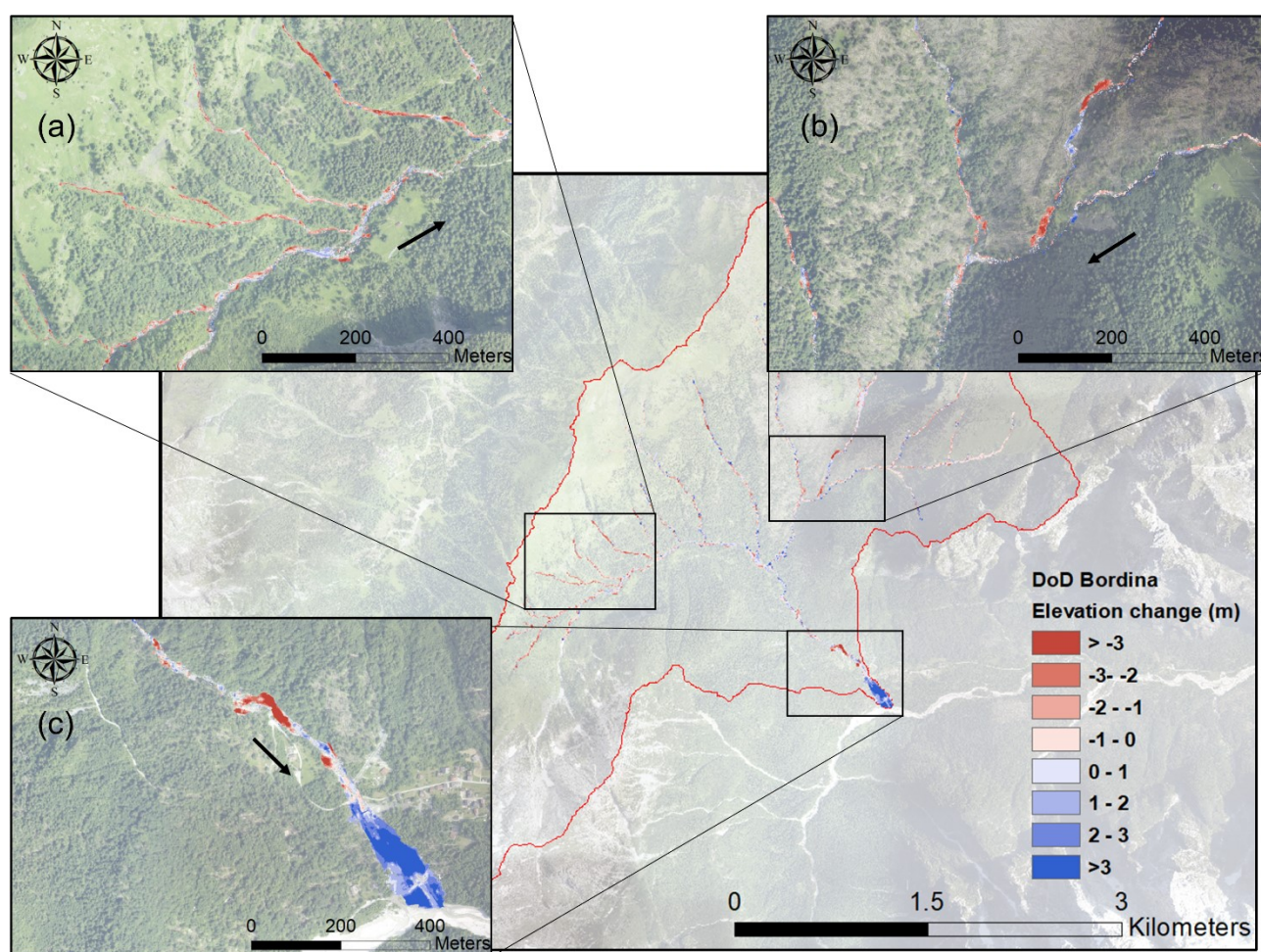


Figure 1.4 Representation of the thresholded DoD regarding the Bordina sub-basin. (a) (b) Evidence of erosion in the upstream part of the Bordina was registered, while (c) deposition by the confluence of the Bordina torrent with the Tegnaz was detected. The black arrow indicates the flow direction.

The VPI and the API regarding the Angheraz were registered equal to -6% and -10%, respectively. In this case, evidence of erosion was detected along the debris flow channels located on the sides of the Angheraz (Fig. 1.5a), as well as very high values of over 3 m of deposition upstream the filtering check-dam. Moreover, 2.5 m of sediment deposition was detected in correspondence of the vegetated alluvial fan located downstream the confluence of the last debris flow channel (Fig. 1.5b). Here the deposited volume was assessed around 20,000 m³. Regarding the upstream part (Fig. 1.5c), an alternation of both areas of deposition and erosion.

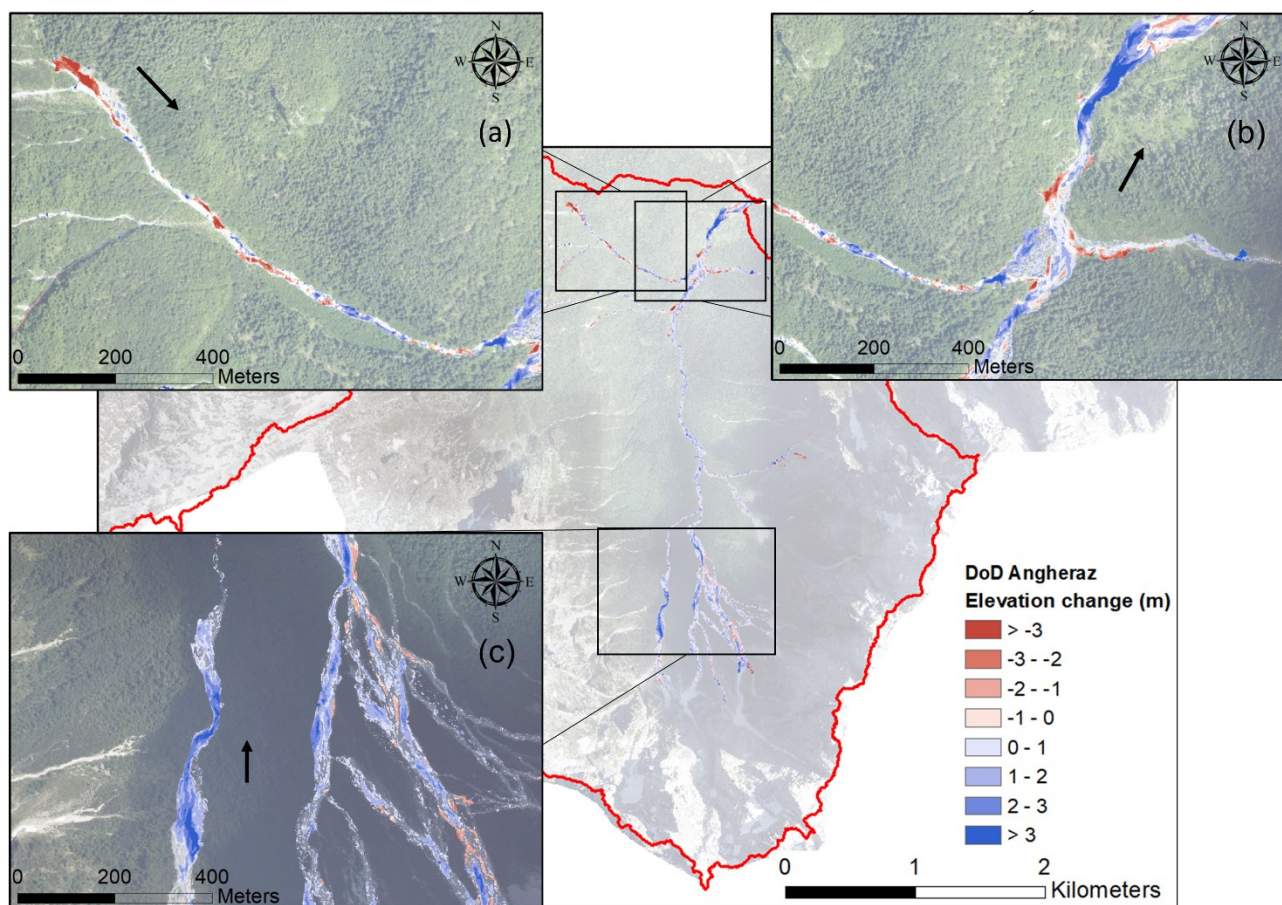


Figure 1.5. Representation of the thresholded DoD of the Angheraz. (a) Evidence of erosion by the lateral debris channels, (c) evidence of deposition at the check-dam and (b) both erosion and deposition in the upstream part of the Angheraz. The black arrow indicates the flow direction.

As regards the VPI and API of the Lower-Tegnas valley floor, these were computed as depositional reaching values of about 19% and 17%, respectively. The Lower-Tegnas valley floor, however, showed different responses to the Vaia event, highlighting deposition all along the upper 4 km of the channel, and of erosion starting from the immediate proximity of the moraine (Fig. 1.6). In this sense, the analysis registered over 100,000 m³ of net volume in the former part while, just below -40,000 m³ in the latter. In this respect, the torrent eroded most of the riverbanks and the fluvial bars.

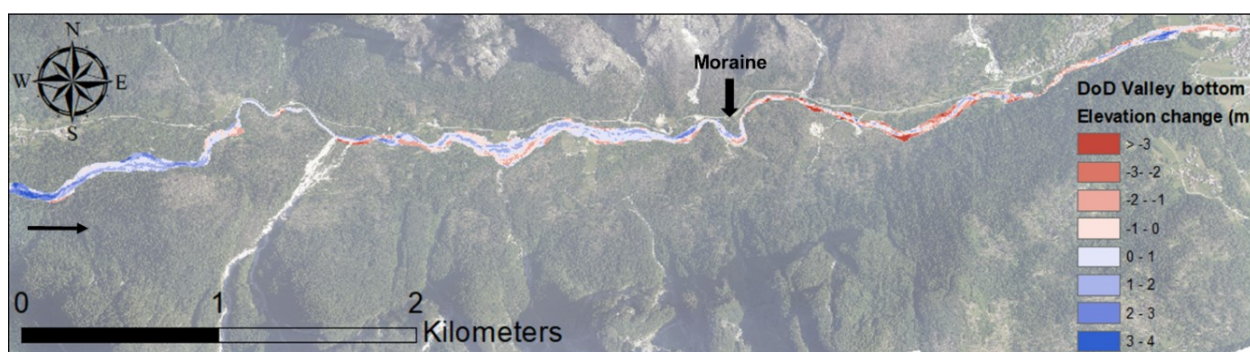


Figure 1.6. Representation of the Thresholded DoDs of the Tegnás valley floor. The black arrow indicates the flow direction.

Index of connectivity analysis

Focusing on the Bordina, high connectivity patterns all along the hillslopes of the basin were identified (IC index between -4 and -3). Nevertheless, also in this case evidence of low connectivity was found throughout the entire minor valley bottom, especially where the torrent flows South-West (Fig. A S3) and by the confluence between the Bordina Torrent and the Tegnás Torrent. In this specific case, the IC reached values between -8 and -7. Concerning the Angheraz, it is worth highlighting the presence of high connectivity areas both on the left and right side of the main valley. Precisely, the IC is characterized by values ranging between -3 and -2. Low IC values can be observed along the Angheraz valley and, particularly, in the South-West part of the catchment, where the low connectivity values are due to the presence of the Pale di San Martino plateau, as well as by the filter check-dam. Taking into consideration the Lower-Tegnás basin, the analysis pointed out high values of IC nearby the outlet of the basin, where the floodplain drastically reduces and the gradient of the hillslopes increases. Obviously the high values in the proximity of the outlet are also due to the choice of the outlet as the target of the analysis. Therefore, the areas close to the outlet have reduced flow path lengths and consequently high IC values. Low connectivity values of IC, ranging between -8 and -7, were registered along the large floodplain of the Tegnás, which has the role of decoupling the active channel from the surrounding slopes (Fig. A S3).

Moreover, the spatial variation of the IC in the Bordina, revealed a substantial increase in both percentage of the high connectivity class (Fig. 1.7), especially regarding the landslides (+ 20%). Focusing on the Angheraz (Fig. 1.7a), it is worth noticing the increase of the area of landslides under the high connectivity class. Additionally, even though characterized by a small amount of affected area, the windthrows increased their percentage of both high connectivity and low connectivity from 1% to 7%. With respect to the windthrows of the Lower-Tegnás, it is important to underline the increase of the high connectivity class.

Concerning the entire Tegnás basin (Fig. 1.7b), the major change was observed for the high connectivity class of the landslides, where the area decreased from over 20% to less than 6%. The four classes of the debris flows remained stable. It is worth highlighting the class of high connectivity related to the windthrows affected areas. Such information reveals that most of those instabilities occurred in high connectivity areas, demonstrating an increase of nearly 30%. Consequently, the low intermediate and high intermediate classes reduced from over 60% to less than 20% in the former, and from 30% to less than 20% in the latter.

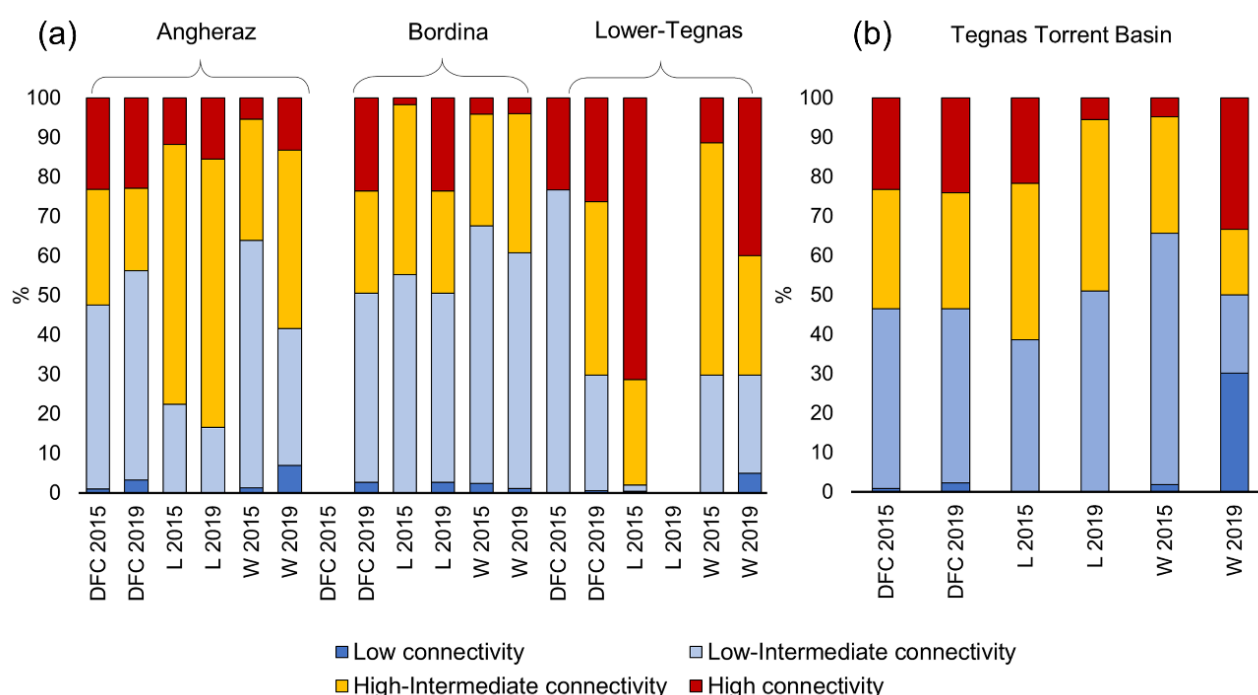


Figure 1.7 Area (%) of the Landslides (L), Debris flows Channels (DFC) and Windthrows (W) under the four classes computed with respect to the entire Tegnás and the sub-catchments according to their spatial variation 2015-2019.

DISCUSSION

The 2015 sediment sources and instabilities of the Tegnás were found to be few and with limited areas able to directly supply sediment to the channel network. Therefore, before the Vaia event, the Tegnás was considered stable as most of the well managed forested basins (Megahan and King, 2004). According to the precipitation data (section 2.3) and the active channel analysis (3.1) no major events occurred during the period 2015-2018. This consideration is supported also by the increasing extent of the riparian vegetation along almost entirely the river corridor (Perucca et al., 2007). With the occurrence of the Vaia storm, the morphological and topographical aspect of the entire alpine catchment changed. Worth considering is the response of the three main areas of the Tegnás: the

Bordina, the Angheraz and the Lower-Tegnas. Specifically, the various lithology of the two sub-catchments revealed different disturbance affected areas.

Concerning the Bordina, windthrows and landslides were the wider instabilities. On the one hand, the presence of spruce (*Picea abies*) forests, characterized by shallow roots (Lange et al., 1981), was more prone to be affected by windthrows (Tsvetanov et al., 2018). On the other, the extensive pastures and shrublands surrounding the basin favoured the triggering and widening of both new and already existing landslides (Tasser et al., 2003). Additionally, the lithological volcanic origin of the Bordina led to the erosion of several ephemeral channels located on the upper sides of the sub-basin (Pellegrini et al., 2020) promoting high sediment yields and erosion rates (Eiriksdottir et al., 2008; Thouret et al., 2014; Chalov et al., 2017). On this, the recent work of Brenna et al. (2020) identified the flow type from the evidence of the post-event deposits (crudely stratified, poorly selected, and from clast-supported to partially openwork deposits) and classified it as a debris flood. As result, the eroded material was deposited, almost entirely, at the alluvial fan located at the confluence between the Bordina and the Angheraz.

As regards the Angheraz, the typical calcareous and Dolomitic lithology as well as the high gradient slopes and availability of sediment (Testa et al., 2013) favoured the triggering of both new and old debris flows (Tiranti and Deangeli, 2015; Pastorello et al., 2020). Such results are also confirmed by the analysis of Brenna et al. (2020) who identified, in most of the Angheraz reaches, the presence of debris flows deposits (massive, extremely poor selected, and matrix-rich deposits). From those processes, the sediment moved to the channel network and was mostly stopped by the check-dam.-Worth adding, is the analysis applied on the substrate and land use of the landslides and debris flows affecting the Tegnas. Having verified similar gradients of slope for both instabilities, significant differences were found considering the permeability of the soils: high and low permeability for the debris channels and landslides (Muddle et al., 2015), respectively. Such results were strictly dependent on the lithological origin of the areas which correspond, almost entirely, to the two sub-basins (Eiriksdottir et al., 2008; Thouret et al., 2014). The only exception regarded one debris flow registered in the Bordina that turned out to be located in the only carbonatic and high permeable spot of the basin. Moreover, also the characterization of the land use of both instabilities suggested two different responses, shrublands and pastures favoured landslides while screes triggered debris flows (Chalov et al., 2017).

Concerning morphological changes, a different response between the upstream and downstream part of the Lower-Tegnas was detected. As well explained by Testa et al. (2013) the presence of the knick point (view section 2) promotes a sudden variation of the hydraulic regime of the Tegnas Torrent leading to different morphodynamics. In the upstream part, the DoD showed

evidence of sediment deposition, while within the downstream reach erosion was predominant. Thus, the upper part of the Tegnias seemed to have responded as a typical piedmont river, widening and depositing sediment all along the reach (Yousefi et al., 2017). On the contrary, the steeper downstream part was mostly eroded (DiBiase et al., 2012; Hurst et al., 2012; Clubb et al., 2016), in both the river bed and the banks, behaving like a mountain stream seeking the dynamic equilibrium (Cyr and Granger, 2008). As a whole, the entire channel network was affected by considerable variations in terms of landforms (i.e., erosion of floodplains, creation of wide bars or avulsions), topography (wider section) and sediment dynamic (Knox, 2006; Beechie et al., 2006; Dean and Schmidt, 2013).

However, despite the high resolution of both the aerial imagery and the LiDAR data, several limitations need to be highlighted. Firstly, the extension of the smaller areas of instability located under canopy cover (Section 3.1), implies an intrinsic error due to the operator interpretation and digitalization. Secondly, as expressed in Cavalli et al. (2017), the outcomes of a DoD LiDAR-based estimation on sediment erosion and deposition in a wide time window do not include minor impacting events (e.g. snowmelt or spring events) that may have occurred during the time between the old dataset and the one made after a major event. The time window considered was 9 years which implies an acceptable quantification of the sediment displaced at large scale (i.e. the entire channel network), but requires further analyses at smaller scale to exactly quantify the volume of sediment displaced by the Vaia event.

The application of the IC in this work resulted extremely useful to identify the transfer paths of the sediment to better understand the sediment dynamics related to a large disturbance, as the Vaia storm. As also found in other studies (Cavalli et al., 2013; Heckmann et al., 2018), lower connectivity values were found all along the main and minor valley floors, by the filter check-dam, by the Bordina alluvial fan and in the glacial cirque surrounding the Angheraz. Higher values of IC, instead, were mostly present all along the sub-basin hillslopes, highlighting old and new ephemeral channels, debris flow channels as well as gullies as possible sediment sources, sinks, and pathways. Moreover, the analysis on the IC spatial variation of the instabilities pinpointed an increase in the high connectivity class concerning the windthrows of the entire Tegnias and the landslides of the Bordina, highlighting the fact that the remaining instabilities either occur in disconnected areas or in the same as prior Vaia. The application of IC using the topographic roughness as W factor promotes the reproducibility of the analysis in similar mountain areas. Land managers can easily assess potential routes of sediment transfer, even if in a preliminary way, having only the DTM. However, other important features can be included for a deeper, but less reproducible, sediment connectivity analysis: soil properties, hydraulic characteristics and rainfall data could be taken into consideration for future research.

In accordance to the DoD analysis, although granted, most of the low connected areas were found to be preferential spots of sediment deposition (i.e., check-dam, alluvial fan, valley floor), as well as the high connected zones were characterized by preferential erosion (i.e. hillslope ephemeral channels) (Cavalli et al., 2013; Calle et al., 2020). Therefore, as recently highlighted by Najafi et al. (2021), the morphological approach (Eltner et al., 2018) seems to be a helpful tool to fill the gap between structural and functional aspects of connectivity (Cucchiaro et al., 2019). Following their idea (Najafi et al., 2021), the proposed integrated approach of using DoD within the connectivity context at catchment scale, permits a detailed identification of sediment routing and a contemporary estimation of erosion and deposition volumes generated by a high magnitude low frequency event (Bracken et al., 2015). In this context, it was possible to identify hot spots areas (i.e., alluvial fan, check-dam, hillslope ephemeral channels).

To better stress out the correspondence between the connectivity and the DoD, an additional analysis, based on a different perspective of the IC maps, was carried out. The aim of this alternative perspective does not concentrate on the instabilities (i.e., landslides, debris flows or windthrows), but rather on the potential sediment paths identified through the IC and, later, validated by the DoD results. Being the high IC path a direct result of high flow accumulation and low surface roughness (Koci et al., 2020), it can be expected having erosional processes going on along this area. The preliminary evidence on the IC-DoD correspondence, makes the analysis reasonable and promising. Such preliminary evidence was obtained in two specific areas, i.e., a newly created 105 m long gully (Fig. 1.8) and a 660 m long ephemeral channel (Fig. A S4). In both cases, the high IC paths matched well the DoD and the field evidence.

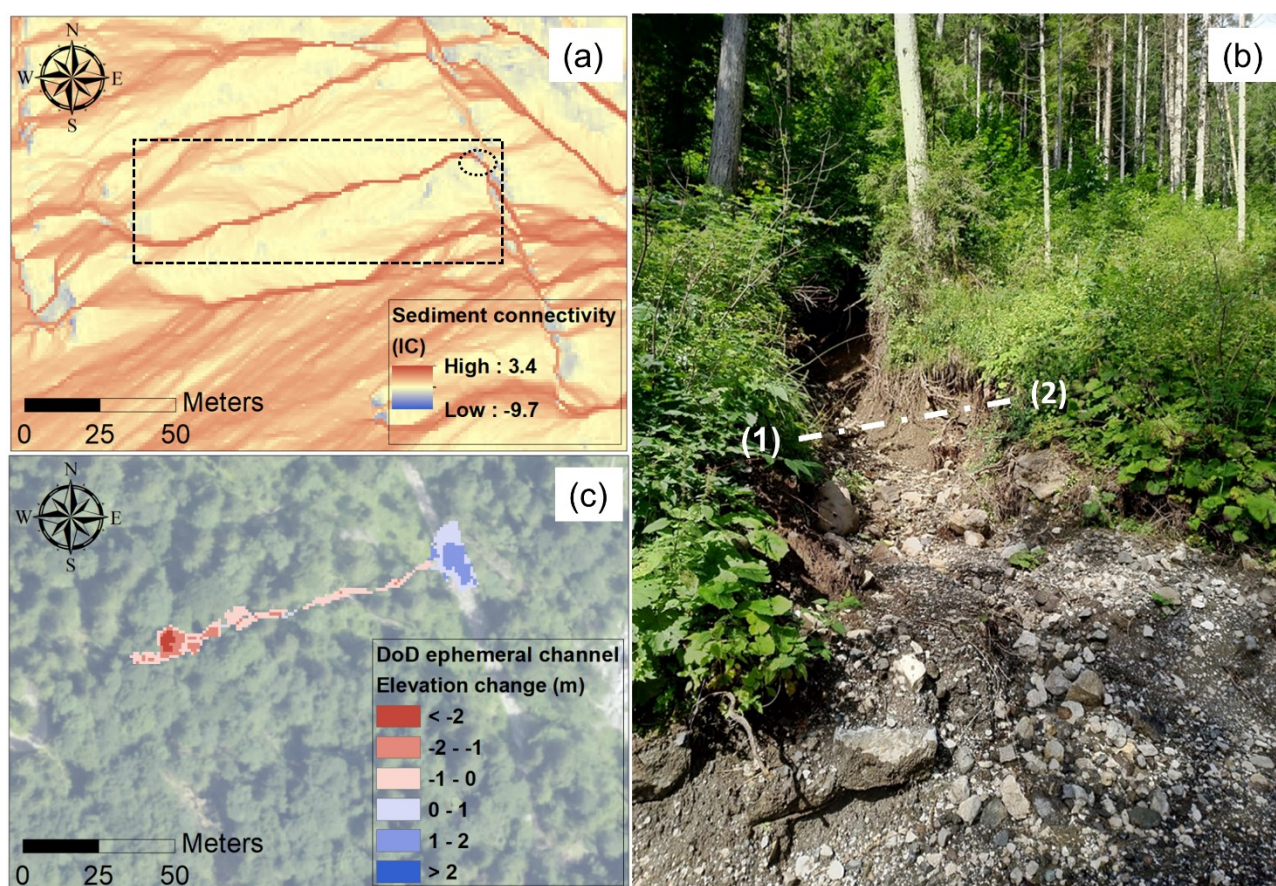


Figure 1.8 (a) IC map, (b) field evidence and (c) DoD regarding one of the ephemeral channels detected on the sides of the Bordina; (a) the dotted ellipse indicates the position from where the picture was taken. (b) the distance between (1) and (2) is approximately equal to 2.7 m.

Thus, although this approach was applied in a merely qualitative way, we can hypothesize, as stated by Koci et al. (2020), that hillslopes with higher connectivity are generally more susceptible to erosion and therefore, to geomorphic changes and sediment delivery to the downstream part. However, although the interpretation applied in this work considers a limited number of areas, there are some good foundations to start and discuss further assessments and improvements on this new IC perspective. Undoubtedly, a broad analysis considering a more conspicuous number of paths should be required and needed. Thus, considering a LID, it would be extremely important to know a priori which flow pathways can be triggered according to their level of connectivity. Therefore, the pre-event IC maps could represent a tool to predict the location of those sediment pathways otherwise not easily detectable from the pre-event orthophoto interpretation.

Therefore, the findings of this work suggest future research perspectives and possible management guidelines. And specifically recommends:

- Further improvements with respect to the alternative perspective of the IC analysis;

-
- Continuous monitoring of the new instability areas where cascading processes, such as changes in sediment fluxes and dynamics, can be triggered;
 - The application of this methodology to analyse the impacts on the morphodynamics of a large size mountain basin and to identify the areas where *ad hoc* mitigation measures and interventions should be applied.

CONCLUSIONS

The availability of high-resolution remote sensing data, such as aerial images and LiDAR, has been revealed a helpful tool to generally identify and characterize the impact of a large disturbance on a large mountain basin. Additionally, the application and integration of such data on different software permitted an integrated vision of the sediment dynamics. On the one hand, the static and structural function of the sediment was described by the IC while, on the other hand, the factual dynamics were outlined by the DoD analysis. Worth noting is how the former, applied on the prior Vaia dataset, validated the latter. In this sense, also as suggested from the qualitative analysis, the simple and objective IC application may predict what a LID may trigger.

As far as the results on the spatial variation of IC are concerned, particular attention has to be devoted to the windthrows of the overall basin as well as to the debris flows channels detected along the Lower-Tegnas. The increase in the high-connectivity class suggests a hot spot for future cascading processes due to the increase of sediment availability.

Chapter 2.

Hydrological, geomorphic and sedimentological responses of an alpine basin to a severe weather event (Vaia storm)

Riccardo Rainato, Lorenzo Martini, Giacomo Pellegrini, Lorenzo Picco

This chapter was published as Rainato, R., Martini L., Pellegrini, G., & Picco, L. (2021). Hydrological, geomorphic and sedimentological responses of an alpine basin to a severe weather event (Vaia storm). *Catena*, 207, 105600.

doi:10.1016/j.catena.2021.105600.



ABSTRACT

To achieve a reliable analysis of the impacts induced in mountain basins by large and infrequent floods, all their main components, from the spatial-temporal distribution of meteorological agents to the hydrological, geomorphic and sedimentological response should be considered. Comprehensive study of the hydro-geomorphic responses is extremely valuable to increase the awareness of large floods, especially, in highly populated mountain areas. Such type of investigation requires a solid and wide dataset, which is why only few studies had the chance to describe the response in such a holistic way. This work comprehensively analyzed the high magnitude/low frequency Vaia event, a severe storm that affected northeastern Italy in October 2018 and thus the Rio Cordon study basin. The 80 h precipitation registered in the basin showed a total rainfall equal to 29.8% of the mean annual precipitation. The temporal distribution of rainfall presented two phases, i.e., a first characterized by moderate but persistent precipitation and a second more intense, exhibiting recurrence intervals over 50 years. A combination of indirect methods permitted the reconstruction of the hydraulic forcing acted in the Rio Cordon. Despite the implicit uncertainty, these methods clearly highlighted the high magnitude expressed by October 2018 flood, which generated a unit peak discharge equal to $3.3 \text{ m}^3 \text{ s}^{-1} \text{ km}^{-2}$ and a peak of unit stream power of 3865 W m^{-2} , i.e., the highest hydraulic forcing conditions ever observed in 34 years. In terms of geomorphic changes, the use of pre- and post-event LiDAR data stressed out a moderate response of the hillslopes, where the (re)activation of the sediment sources was limited. Only few of these acted as sediment supplier to the main channel. The channel network instead, exhibited an evident response, with the Rio Cordon severely altered by wide lateral widening, deep streambed incision and armouring removal. The hydraulic and geomorphic forcing generated by October 2018 flood caused extensive streambed remobilization and boulder mobility that, in turn, induced the transport of a massive sediment volume. In this sense, the match between bedload observed and bedload predicted suggested the outstanding hydraulic forcing occurred and the quasi-unlimited supply conditions acted during the flood. The long-lasting monitoring program maintained in the Rio Cordon basin provided the rare opportunity to compare two high magnitude/low frequency floods and their induced effects. The September 1994 and October 2018 events were caused by different rainfall conditions, which resulted in different hydrological- and, especially, geomorphic- and sedimentological-responses. Particularly, the October 2018 flood induced an unprecedented alteration on the fluvial system, the effects of which could persist over the long-term.

Keywords: Vaia storm; Mountain basin; Large flood; Geomorphic changes; Sediment transport; Boulder mobility

INTRODUCTION

Large and infrequent floods are hydrological events characterized by high magnitude and low frequency occurrence, which can impact mountain basins and their fluvial systems over large temporal and spatial scales. In alpine environments, these flood events can be induced by intense summer thunderstorms (Shakti et al., 2018), prolonged rainfalls (Brogan et al., 2019), rapid snowmelt (Friele et al., 2020), rain-on-snow event (Pomeroy et al., 2016) and sudden water release from glacier sources (Bohorquez and Darby, 2008). All these triggering factors converge in a main effect that is the generation of massive runoff characterized by high water discharges and stream power peaks. An extensive literature found these conditions associated to flash floods, i.e., rapid and severe floods (McEwen and Werrity, 1988; Batalla et al., 1999; Borga et al., 2014; Marchi et al., 2016; Lucía et al., 2018), whereas they were observed less frequently in large floods of long duration (Cassandro et al., 2002; Sholtes et al., 2018; Bucala-Hrabia et al., 2020). The characterization of the hydraulic forcing conditions expressed by high magnitude/low frequency events can be challenging, with the frequent need to rely on indirect methods as post-flood measurements, dendrogeomorphic analysis, paleoflood estimation and hydraulic modelling in order to reconstruct hydrographs and peak discharges (Rico et al., 2001; Stoffel and Bollschweiler, 2008; Victoriano et al., 2018; Wyzga et al., 2020). In this sense, a delineation of large and infrequent events based on peak of water discharge or unit peak discharge appears not fully defined, with values spanning over several orders of magnitude (Marchi et al., 2016; Amponsah et al., 2018), while a minimum threshold of 300 W m^{-2} was reported in terms of unit stream power (Miller, 1990; Magilligan, 1992). However, it is worth noting that this threshold was based on geomorphic effectiveness of floods and that mountain basins responses are highly variable. Indeed, the geomorphic response to a high magnitude/low frequency flood can include: (i) the formation of rockfalls (Heckmann and Schwanghart, 2013), debris flows (Pastorello et al., 2020) and landslides (Korup, 2005) along the hillslopes; (ii) bedforms alteration (Lenzi, 2001), channel narrowing (Liébault and Piégay, 2002), chute cutting and channel migration (Gorczyca et al., 2013), reach straightening (Bauch and Hickin, 2011), lateral widening with floodplain erosion (Wicherski et al., 2017) or increase in channel bars extent (Hajdukiewicz et al., 2016) along the fluvial system. The investigation of these geomorphic changes is traditionally accomplished by multi-temporal geomorphological mapping, using both field and remote sensing products, such Digital Elevation Models (DEMs) and aerial photos (Messenzehl et al., 2014; Carrivick et al., 2016; Vericat et al., 2017). Additionally, geomorphic variations in mountain streams are quantified using the widely known DEM of Difference (hereinafter DoD) technique, which can be also used to infer in-channel sediment transfer's efficiency (Lane et al., 2003; Vericat et al., 2014; Cucchiario et al., 2019; Calle et al., 2020). In mountain basins, the hydraulic forcing and geomorphic changes generated by high

magnitude/low frequency floods can intensify the ordinary sediment transfer processes, altering the sediment cascade from source areas to the fluvial system (Brierley et al., 2006; Burt and Allison, 2010; Fryirs, 2013). However, during and after a large infrequent event, the capability of a catchment to promote or impede the sediment cascade depends on the impact of such event on the degree of (dis)connectivity. Specifically, highly connected catchments react transmitting a sediment pulse throughout the system, whereas in disconnected catchments the pulse is stopped by landform impediments (Fryirs et al., 2007). Along the fluvial system, the sediment dynamics promoted by high magnitude/low frequency floods can stretch over various time scales. Typical effects induced at event scale are streambed remobilization (Piton and Recking, 2017), boulder mobility (Turowski et al., 2009; Gob et al., 2010), high transport rates (D'Agostino and Lenzi, 1999; Pagano et al., 2019) and massive transported volumes (Rickenmann, 1997; Baewert and Morche, 2014). Nonetheless, the induced effects can also act on longer time scales, augmenting the transport rate of subsequent floods and favoring a memory effect on the sediment dynamics (Rainato et al., 2017; Uchida et al., 2018; Rickenmann, 2020).

High magnitude/low frequency floods caused by severe weather events were poorly investigated and rarely analyzed from the rainfall-runoff conditions to geomorphic and sedimentological effects. A recent example of severe weather event was the Vaia storm, which affected the Northeast Italy on October 27-30, 2018. This storm generated extremely high wind gusts, storm surges and heavy precipitation that caused landslides, floods, interruption of electric supply, road traffic disruption and the worst forest loss ever documented in Italy, consisting of about 8.5 million m³ of growing stock felled over 41000 ha (Biolchi et al., 2019; Cavaleri et al., 2019). This work aims at defining the responses of an alpine basin to the Vaia storm, focusing on: (i) the determination of rainfall and hydraulic forcing conditions, (ii) the analysis of the geomorphic and sedimentological responses showed by hillslopes and main channel, (iii) the comparison of these responses with those exhibited by the alpine basin over the last three decades.

MATERIAL AND METHODS

Study area

The Rio Cordon basin (Fig. 2.1) is a mountain basin extending for 5 km² in the eastern Italian Alps (Dolomites). It is characterized by typical alpine climatic conditions with a mean annual precipitation of 1180 mm (1986-2018). The runoff regime can be defined as nivo-pluvial due to the predominance of snowfalls between November-April, while short rain showers and persistent precipitations prevail in summer and autumn, respectively. The basin is part of the Southern Limestone Alps with the geological substrate mainly composed by dolomites, limestones, volcanic conglomerates (Wengen

group) and calcareous-marly rocks (Buchenstein group). A rugged topography can be appreciated throughout the basin, which exhibits an average slope of 27° . Due to the basin elevation between 1763-2763 m a.s.l., spruce and larch forest covers merely 7% of catchment area, while bare rock (14%), shrubs (18%) and grassland (61%) are more widespread. In the basin, the third-order Rio Cordon stream flows on a rough channel bed, featuring boulder-cascade and step-pool morphologies (sensu Montgomery and Buffington, 1997). In 2014, the surface streambed material resulted poorly sorted with $D_{16}/D_{50}/D_{84}/D_{90}$ of grain size distribution (GSD) equal to 29/114/358/455 mm, respectively, and a well-developed armour layer (Rainato et al., 2018a). The main channel (hereinafter Rio Cordon) had an average slope of 17% with a mean bankfull width equal to 5.3 m and a bankfull discharge (Q_{Bf}) = $2.30 \text{ m}^3 \text{ s}^{-1}$ (Lenzi et al., 2006a; Mao and Lenzi, 2007). Along the basin, the Rio Cordon is interrupted by a waterfall, which represents a topographic knickpoint that conventionally divides the whole basin into the upper part (upper plateau) and lower part (Rainato et al., 2018b). In 2016, 420 sediment source areas were detected throughout the basin, classified in debris flow channel/deposit, erosional area, stream bank erosion, landslide, rockfall deposit and active talus (Ferrato et al., 2017). From the sources, the sediment can be transported downstream and eventually deposited at the outlet (1763 m a.s.l.), where a permanent monitoring station is built.

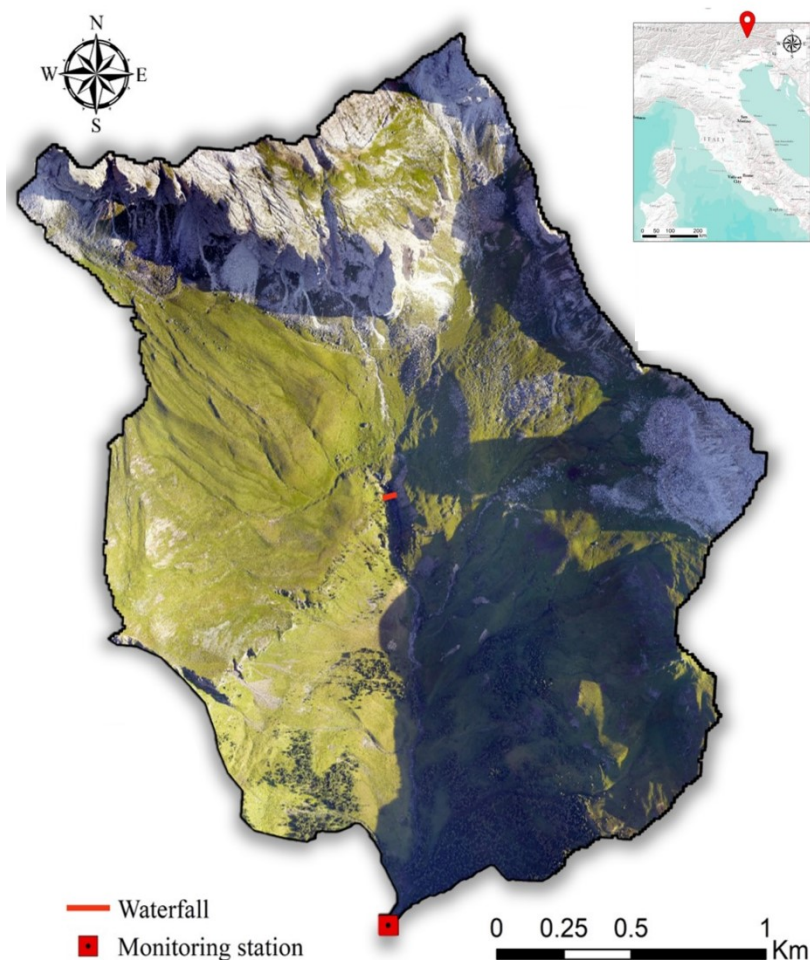


Figure 2.1. The Rio Cordon basin, located in the eastern Italian Alps. The waterfall represents the topographic knickpoint that divides the upper part (upper plateau) and lower part of the basin.

In 1985, the Rio Cordon basin was instrumented thanks to a collaboration between University of Padova and Veneto Region, and operating since 1986 under the ARPA Veneto management (Regional Department for Land Safety). Specifically, a permanent monitoring station was set up at the basin outlet with the aim of continuously monitor water discharge (Q), suspended sediment load (SSL) and bedload (BL). In 1994, the monitoring station was provided with a meteorological station, which measure continuously air temperature, wind speed and precipitations through a heated rain gauge. Between September 1986 and September 2018, the monitoring station recorded 33 flood events (Supplementary Table B S1). Overall, these events mobilized 1850 m^3 of coarse material, corresponding to a bedload yield of 3154 t. Considering instead the total sediment yield (BL+SSL), the Rio Cordon basin delivered $\sim 15125 \text{ t}$. Among the 33 events recorded, the highest magnitude was expressed by the September 1994 flood, when an intense summer shower triggered a flash flood with a peak of water discharge (Q_P) equal to $10.40 \text{ m}^3 \text{ s}^{-1}$ (Rainato et al., 2017). This event altered the basin by modifying the streambed configuration, creating new sediment sources throughout the catchment

and causing the transport of about 900 m³ of coarse material, which corresponds to ~ 50% of the total bedload volume observed between September 1986 and September 2018.

Rainfalls

Consistently to the previous flood event investigations realized in the Rio Cordon basin (Lenzi and Marchi, 2000; Rainato et al., 2018a; Oss Cazzador et al., 2020), to describe the rainfalls induced by the Vaia storm the data from the heated rain gauge were used. This sensor measures every 5 min with an accuracy of 0.2 mm, permitting to determine the total precipitation and the rainfall intensities exhibited by the storm event. Specifically, the maximum rainfall intensities in 5, 15, 30 min and 1, 3, 6, 12, 24, 48, 72 h were determined and named, $I_{5\text{min}}$, $I_{15\text{min}}$, $I_{30\text{min}}$ and $I_{1\text{h}}$, $I_{3\text{h}}$, $I_{6\text{h}}$, $I_{12\text{h}}$, $I_{24\text{h}}$, $I_{48\text{h}}$, $I_{72\text{h}}$, respectively. To better comprehend the magnitude expressed by Vaia storm in the Rio Cordon basin, the measured rainfall intensities were compared to the rainfall depth-duration-frequency (DDF) curves compiled by ARPA Veneto for the “Passo Falzarego” meteorological station. This was chosen as the nearest rain gauge with a long-lasting monitoring. In fact, it is located 9.4 km north-west of the Rio Cordon basin, at 2040 m a.s.l., and operates since 1985.

Hydrological conditions

The wind and rainfall generated by the Vaia storm caused the arrest of the water level gauges installed in the Rio Cordon monitoring station. Therefore, no discharge measurement was realized during the Vaia induced flood event (hereinafter October 2018 event). In light of this, to describe the hydraulic forcing conditions that acted in the Rio Cordon, indirect methods were used. To reconstruct the hydrograph, the nearest gauging station operating during the Vaia storm was tested. This was the “Sottorovei” Arpa Veneto gauging station (5.2 km south-west of the Rio Cordon basin), which recorded the discharge of the Fiorentina Stream (Q_{Fi}). Worth noting is that the Rio Cordon is a sub-basin of the Fiorentina basin (58 km²). To test the capacity of Fiorentina discharge (Q_{Fi}) to describe the Rio Cordon discharge (Q_{Rc}), two recent floods (November 2012 and November 2014) recorded in the sub-basin were isolated and the measured Q_{Rc} were compared to the Q_{Fi} simultaneously recorded. Using linear regression and comparing 1762 discharge measurements, it was possible to observe that Q_{Fi} and Q_{Rc} were statistically correlated ($R^2 = 0.897$, p-value < 0.01). Therefore, the Q_{Fi} measured during the Vaia storm were scaled according to the linear equation obtained, permitting to reconstruct the hydrograph of the October 2018 flood in the Rio Cordon. However, it should be stressed that this reconstruction was affected by a certain degree of uncertainty as based on the analysis of near-bankfull events. In fact, in terms of Q_{P} , the November 2012 and November 2014 floods ranged between 2.06 and 2.10 m³ s⁻¹ in the Rio Cordon, while in the Fiorentina Stream spanned

between 23.60 and 32.00 m³ s⁻¹. Therefore, given the high magnitude expressed by October 2018 flood, a specific investigation about Q_P was made in order to integrate the hydrograph reconstructed with a portion devoted to describing the peaking part. The latter was intended as the hydrograph part simulated between the maximum discharges estimated by hydrograph reconstruction (Q_{Fi} - Q_{Rc} relationship) and the Q_P estimated. A simple triangular shape was used to describe this peaking part, according to the hydrograph shapes generated in mountain basins by high magnitude/low frequency floods (Lenzi et al., 1999; Turowski et al., 2009).

The value of Q_P was calculated through two different approaches. Firstly, post-event surveys permitted to clearly identify high-water marks along a cross section located in a final downstream reach, straight and embanked on the right side. Therefore, this cross section provided the best conditions for Q_P definition by the slope conveyance method (Gaume and Borga, 2008; Marchi et al., 2016). A differential Global Position System (dGPS) device, featuring an average vertical and horizontal accuracy < 0.05 m, was used to survey this cross section, which was used to compute Q_P through the Manning-Strickler equation (Eq. 2.1):

$$Q = \frac{A R^{\frac{2}{3}} S^{\frac{1}{2}}}{n} \quad (2.1)$$

in which Q is the water discharge (m³ s⁻¹), A the flow area (m²), R the hydraulic radius (m), S the stream slope (m m⁻¹) and n the Manning roughness coefficient. Based on field observation of the boundary roughness conditions and on the n observed in mountain streams (Reid and Hickin, 2008; Zink and Jennings, 2014, Oss Cazzador et al., 2021) a Manning roughness coefficient = 0.125 s⁻¹ m^{-1/3} was applied. Secondly, the equation (Eq. 2.2) proposed by Bravard and Petit (1997) to determine Q_P through a basin area scaling ratio was used:

$$q = Q(a/A)^c \quad (2.2)$$

in which q is the water discharge occurred in a sub-basin (in m³ s⁻¹), Q the water discharge measured at the basin outlet (in m³ s⁻¹), a is the sub-basin area (in km²), A the basin area (in km²), while c is a site specific coefficient that in literature varies between 0.4 and 1.0 (Gob et al., 2010). The maximum Q_{Fi} recorded during the Vaia storm were used as Q, while c equal to 0.8 was applied according to Liébault et al. (2012) and Oss Cazzador et al. (2021). Once determined the hydrograph and its peaks, the bedload duration (T_{Bl}) and the effective runoff (ER) were estimated. These describe the hydrograph-duration and -volume exceeding the threshold for bedload motion. To this end, the critical

discharge (Q_C) for motion of coarse streambed material observed in the Rio Cordon during the period 2012-2018 was used, which corresponds to $Q_C = 2.06 \text{ m}^3 \text{ s}^{-1}$ (Rainato et al., 2020). This is consistent with the observations made in the Rio Cordon by Lenzi et al. (1999), who documented Q_C constantly around $Q = 2.00 \text{ m}^3 \text{ s}^{-1}$ in the flood events of 1987-1994.

The hydraulic forcing conditions were expressed even in terms of unit stream power (ω), through Eq. 2.3:

$$\omega = \frac{\rho g Q S}{w} \quad (2.3)$$

where ρ is the fluid density (kg m^{-3}), g the acceleration due to gravity (m s^{-2}), Q the water discharge ($\text{m}^3 \text{ s}^{-1}$), S the stream slope (m m^{-1}) and w is the flow width (m). Specifically, to calculate the peak of unit stream power (ω_P) acted during the October 2018 flood, the flow width was determined by analyzing the Digital Terrain Model (DTM) of the Rio Cordon dated 2006, which suggested a $w = 6.30 \text{ m}$.

Geomorphic setting

To investigate the geomorphic response induced in the Rio Cordon basin by the Vaia storm, two LiDAR surveys dated, respectively, 2006 and 2019 were exploited. Both surveys produced classified point clouds and orthophotos. The latter with resolution of 0.5 m and 0.2 m, for 2006 and 2019, respectively. From the point clouds, only the ground points were used to derive the DTMs for the following analyses. The post-processing was carried out using CloudCompare software (www.danielgm.net/cc; version 2.10.2 Zephyrus), with the primary aim of co-registering the point clouds. The co-registration was performed using a combination of automatic Iterative Closest Point (ICP) algorithm and manual definition of point correspondences. The compound use of these methods wants to provide a suitable solution to reduce unrealistic differences between the point clouds that often exist in rugged environments (Cucchiari et al., 2020). The orthophotos were exploited for different purposes: from the qualitative assessment of the changes throughout the basin to the analysis of the variations along active channel and sediment source areas. However, due to the time interval between the two LiDAR surveys, other events might have contributed to alter the geomorphic setting of the catchment. To distinguish the alterations induced by these events from the October 2018 effects, an additional pre-event orthophoto and previous studies were used. Specifically, the 2015 orthophoto (Web Map Service service for AGEA, 0.20 m resolution) and the geomorphic effects documented in Rainato et al. (2017), Rainato et al. (2018a) and Oss Cazzador et al. (2020) were taken

advantage of. Instead, the two DTMs permitted to determine the topographic differences and, then, any significant geomorphic change related to the Vaia storm.

The topographic differences were determined by comparative analysis between the 2006 and 2019 DTMs, using the DEM of Difference, hereinafter DoD, technique. The old-2006 DTM was subtracted to the new-2019 DTM using the Geomorphic Change Detection 7.4.4, AddIn for ArcGIS (Wheaton et al., 2010). To overcome the mere representation of all the changes, hence to distinguish those changes produced by noise from the real ones, a widely used approach accounting for spatially distributed elevation uncertainty was adopted. Also, this approach overcomes spatially uniform methods, i.e. minimum level of detection (minLOD), in which real geomorphic changes risk to be removed. The methodology proposed by Wheaton et al. (2010) mainly regards three steps to generate a robust DoD output: (i) computation of cell-by-cell DEM uncertainty (spatial distribution of elevation uncertainty) using the Fuzzy Inference System (FIS); (ii) propagation of the uncertainty into the DoD; (iii) statistical significance of the propagated uncertainty based on probabilistic thresholding. The first step was accomplished using a three inputs-FIS, i.e., point density, slope and roughness. Particularly, the roughness information was derived using the Roughness Index, proposed by Cavalli and Marchi (2008), and already applied in other geomorphological studies as part of the three inputs-FIS (Oss Cazzador et al., 2021). The second step regards the propagation of the uncertainty from the individual DEM into the DoD, still on cell by cell basis. This step was accomplished by applying the well-known combined error formula proposed by Brasington et al. (2000). The third step assessed the statistical significance of the DoD output using a 95% probabilistic thresholding, which means that all the elevation changes that do not fit within a confidence interval of 95% were discarded. The application of such probabilistic thresholding relies upon the choice of the corresponding t-value, as proposed by Taylor (1997) and then by Brasington et al. (2003) and Lane et al. (2003). In this work, a conservative 95% confidence interval (t-value = 1.96) was assigned because of the high values of elevation uncertainty and the willingness to quantify the minimum compatible volume of sediment mobilized in the Rio Cordon basin. The DoD was performed to investigate sediment displacement occurred along the hillslope, within the lower Rio Cordon and at the bedload storage area of the monitoring station. Specifically, for the hillslopes, the aim was to outline potential new sediment sources that may or not have contributed to supply sediment in the channel network. At the bedload storage area, the DoD was performed over a polygon of 4200 m², which includes also the lateral and downstream zones buried by sediment. However, an area of ~ 500 m² was affected by the presence of a bridge that passes over the deposit. Here, no suitable LiDAR data were found so that the 2006 and 2019 DTMs have been roughly interpolated causing an estimated source of error of about 11%.

The detection of the new sediment sources was accomplished through orthophotos and DoD interpretation with a focus to the lower part of the basin. In addition, a previous sediment source inventory (Ferrato et al., 2017), was used to help the detection of those areas (re)activated only during the Vaia storm. The sediment sources were then grouped according to the classification already proposed for the Rio Cordon basin in: landslide, debris flow channel/deposit, surficial erosion, stream bank erosion, rockfall and active talus. Knowing the coupling state of the sediment sources, it is possible to have an idea of the volume of sediment supplied to the channel network and eventually to the outlet. To assess the coupling state and the potential supply from sources to active channel, an approach based on the Index of Connectivity (IC) (Cavalli et al., 2013) and the DoD was proposed. First, using the 2019 orthophoto, the sources that did not reach the active channel and, therefore, visibly decoupled were excluded. Then, the IC map was computed with SedInConnect 2.3 (Crema and Cavalli, 2018), using the pre-event (2006) DTM, selecting the active channel as target. The mean IC value for each sediment source was extracted and only those having a value higher than a threshold were considered. The threshold was set as the median (50th percentile) of all the mean IC values of each area. In other terms, a boundary based on the central value was set, to distinguish areas of high- and low-IC. Finally, the sediment sources showing predominant erosion (negative net volume difference) were selected. In this way, we assumed that only the sediment sources highly coupled with the active channel supplied a significant volume of sediment. Conversely, the decoupled or balanced (erosion and deposition balanced) sediment sources were not considered suppliers. In particular cases, e.g. landslides recharging debris flow channels/deposits, the balance was obtained as the overall DoD result of the single areas composing the same potential supplier.

The active channel variations were first investigated through qualitative analysis of orthophotos. To further investigate the geomorphic changes as well as its causes and effects along the Rio Cordon, the active channel was segmented into sub-reaches. The segmentation, which draws part of the criteria from Rinaldi et al. (2013), considered homogeneous sub-reaches based on stream slope, channel width and confluences with tributaries. Stream slope was derived from the 2006 DTM, while channel width and confluences from the orthophotos. Hence, six sub-reaches (1-6) ranging from 154 m to 623 m in length were identified in the lower basin, resulting in 2023 m totally investigated along the active channel. Upper Rio Cordon was excluded from this analysis due to its semi-colluvial nature and sediment disconnectivity documented during Vaia storm (Oss Cazzador et al., 2021). The width ratio (W_r), the peak of unit stream power (ω_{Pi}) acted during the October 2018 event and the DoD segregation (Wheaton et al., 2013) were calculated for each sub-reach. W_r is intended as the ratio between the post- and pre-flood average channel width (Scorpio et al., 2018), which were assessed on the 2019 and 2006 orthophotos, respectively. The peak of unit stream power occurred in the sub-

reaches ($\omega_{P1} - \omega_{P6}$) was determined according to Eq.3. To this end, each S and w were calculated analyzing the 2006 DTM and considering the stream slope and the channel width averaged on the upstream channel portion. Instead, the maximum water discharge flowed in each sub-reach (i.e. Q in Eq.3) was determined using the Eq.2, with Q equal to the Q_P calculated for the Rio Cordon outlet (see previous section), while a and A were the basin area subtended by the sub-reach and the whole basin, respectively. Finally, the potential correlations between W_r , ω_{P1} and DoD were investigated through linear regression.

Sedimentological setting

The sedimentological response of the study basin to the Vaia storm was explored by investigating the variation in the grain size distribution of the main channel and by characterizing and quantifying the coarse material transported. To determine the post-flood GSD of the Rio Cordon, 202 particles were collected and measured along the main channel using the grid by number method. The same method was used to describe the GSD of bedload transported to the monitoring station, which was estimated by sampling 224 particles. Also, the ten largest boulders deposited at the bedload storage area were characterized in terms of a-, b- and c-axis in order to describe the boulder mobility triggered by the October 2018 flood. To determine the volume of coarse material mobilized by the event (BL_{Obs}), the bedload storage area of the monitoring station was surveyed. Therefore, using the DoD technique it was possible to quantify a reliable volume resulting from the elevation difference between the post-event storage unit (2019 DTM) and the pre-event one (2006 DTM). The reconstruction of hydraulic forcing conditions occurred during the October 2018 event enabled the volume of coarse material transported to be predicted (BL_{Pred}) as well. To this end, consistently with previous Rio Cordon flood investigations (D'Agostino and Lenzi, 1999; Lenzi et al., 1999; Lenzi et al., 2006b; Rainato et al., 2017), the bedload equation (Eq. 2.4) proposed by Schoklitsch (1962) was used:

$$Q_s = \frac{2.5}{\rho_s/\rho} S^{\frac{3}{2}} (Q - Q_c) \quad (2.4)$$

where Q_s is the bedload rate ($m^3 s^{-1}$); and ρ_s is the sediment-density ($kg m^{-3}$), respectively. The use of Schoklitsch equation permitted to calculate BL_{Pred} but also to analyze its performance under the different hydrological conditions examined in the Rio Cordon over the last decades.

RESULTS

Rainfall characterization

In the Rio Cordon basin, the Vaia storm induced a rainfall event that lasted about 80 h, starting on October 27th at 06:55 (CET) and ending on October 30th at 14:45 (Table 2.1). During this time interval, a total precipitation of 352.0 mm was recorded, corresponding to the 29.8% of the mean annual precipitation. The rainfall event was not continuous but exhibited a hiatus of ~ 9 h (Fig. 2.2). Therefore, it is possible to identify a first and a second phase, hereinafter Phase 1 and Phase 2. The Phase 1 lasted 36.8 h with 199.8 mm, while 152.0 mm were recorded in the 34.2 h of Phase 2.

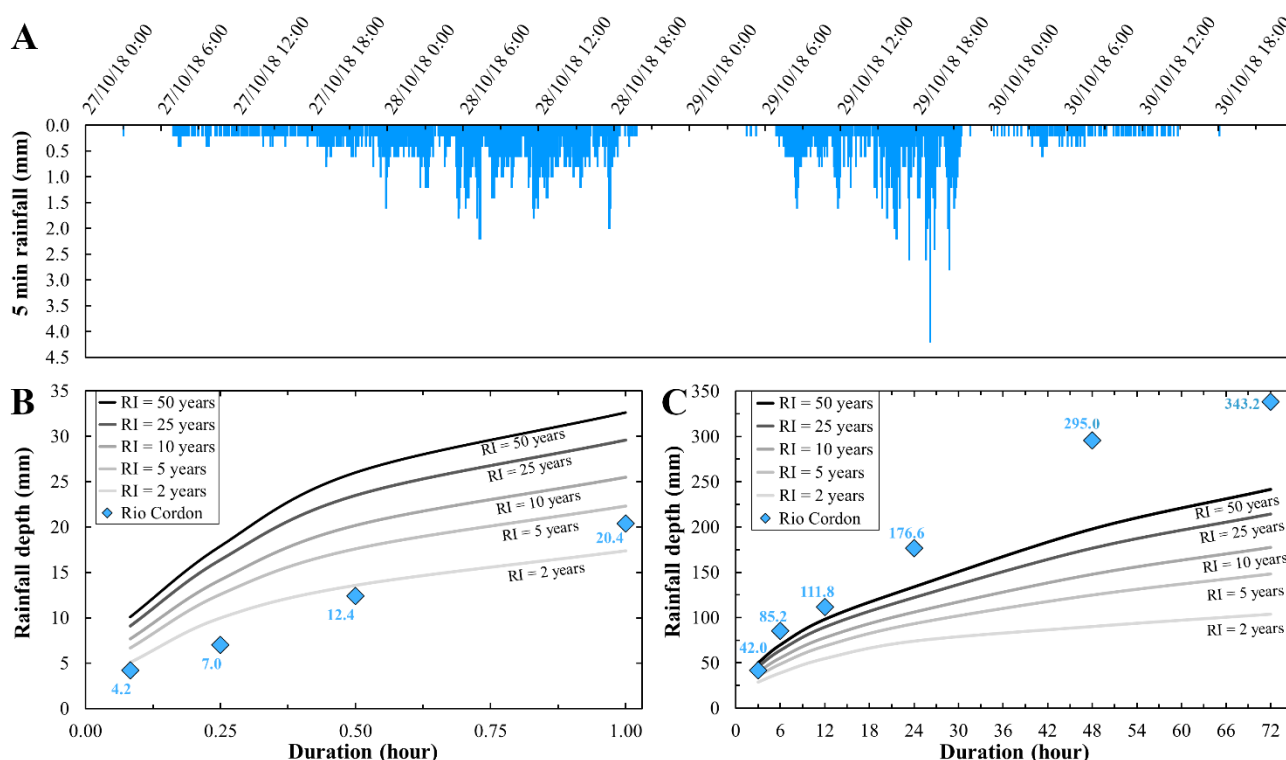


Figure 2.2 (A) Rainfall recorded by Rio Cordon meteorological station during Vaia storm; (B) Maximum rainfall intensities recorded in 5 (I_{5min}), 15 (I_{15min}), 30 (I_{30min}), 60 (I_{1h}) minutes and (C) in 3 (I_{3h}), 6 (I_{6h}), 12 (I_{12h}), 24 (I_{24h}), 48 (I_{48h}) and 72 (I_{72h}) hours compared to the rainfall depth-duration-frequency curves of Passo Falzarego rain gauge.

The event registered a mean rainfall intensity equal to 4.4 mm h^{-1} , while Phase 1 and Phase 2 expressed an average of 5.4 and 4.4 mm h^{-1} , respectively (Table 2.1). Phase 1 showed a higher mean intensity due to the more continuous precipitation over time compared to Phase 2 that exhibited an abrupt decrease after peaking (Fig. 2.2). However, the highest intensities between I_{5min} and I_{12h} were constantly observed during Phase 2, particularly, between 8:30 and 21:30 of October 29th. In this sense, the maximum rainfall intensities recorded (I_{5min} - I_{72h}) were compared to the DDF curves of the “Passo Falzarego” meteorological station. Figure 2.2b and Figure 2.2c show that I_{5min} , I_{15min} and I_{30min}

resulted lower than DDF curve estimated for recurrence interval (RI) of 2 years, while from I_{1h} progressively exceeded the DDF curves by culminating in I_{6h} - I_{72h} that showed RI clearly higher than 50 years.

Table 2.1 Main characteristics of the first and second phase of the rainfall event recorded by the Rio Cordon rain gauge during the Vaia storm, as well as of the entire rainfall event. I_{5min} , I_{15min} , I_{30min} describe the maximum rainfall intensities measured in 5, 15 and 30 minutes, respectively. I_{1h} , I_{3h} , I_{6h} , I_{12h} , I_{24h} , I_{48h} and I_{72h} are the maximum intensities recorded, respectively, in 1, 3, 6, 12, 24, 48 and 72 hours.

	Phase 1	Phase 2	Event
Time of rainfall initiation (CET)	27/10/2018 06:55	29/10/2018 04:30	27/10/2018 06:55
Time of rainfall end (CET)	28/10/2018 19:45	30/10/2018 14:45	30/10/2018 14:45
Total precipitation duration (h)	36.8	34.2	79.8
Total precipitation (mm)	199.8	152.0	352.0
Mean rainfall intensity (mm h^{-1})	5.4	4.4	4.4
Time of I_{5min} (CET)	28/10/2018 07:15	29/10/2018 19:05	29/10/2018 19:05
I_{5min} (mm/5 min)	2.2	4.2	4.2
I_{15min} (mm/15 min)	5.6	7.0	7.0
I_{30min} (mm/30 min)	9.2	12.4	12.4
I_{1h} (mm/1 h)	14.6	20.4	20.4
I_{3h} (mm/3 h)	34.8	42.0	42.0
I_{6h} (mm/6 h)	74.4	85.2	85.2
I_{12h} (mm/12 h)	111.2	111.8	111.8
I_{24h} (mm/24 h)	176.6	142.8	176.6
I_{48h} (mm/48 h)	-	-	295.0
I_{72h} (mm/72 h)	-	-	343.2

Hydraulic forcing conditions

The reconstructed hydrograph estimated Q persistently $> 1.10 \text{ m}^3 \text{ s}^{-1}$ (i.e. $> 0.5 Q_{BF}$) from October 28th at 7:00 through October 31st at 9:30. Two consecutive peaks were determined, respectively, on October 28th at 18:45 and on October 29th at 20:00, interspersed by ~ 21 h of under-bankfull conditions (Fig. 2.3). Therefore, similarly to what observed in the rainfall analysis, also in the flood event caused in the Rio Cordon by the Vaia storm two phases can be observed (Fig. 2.3).

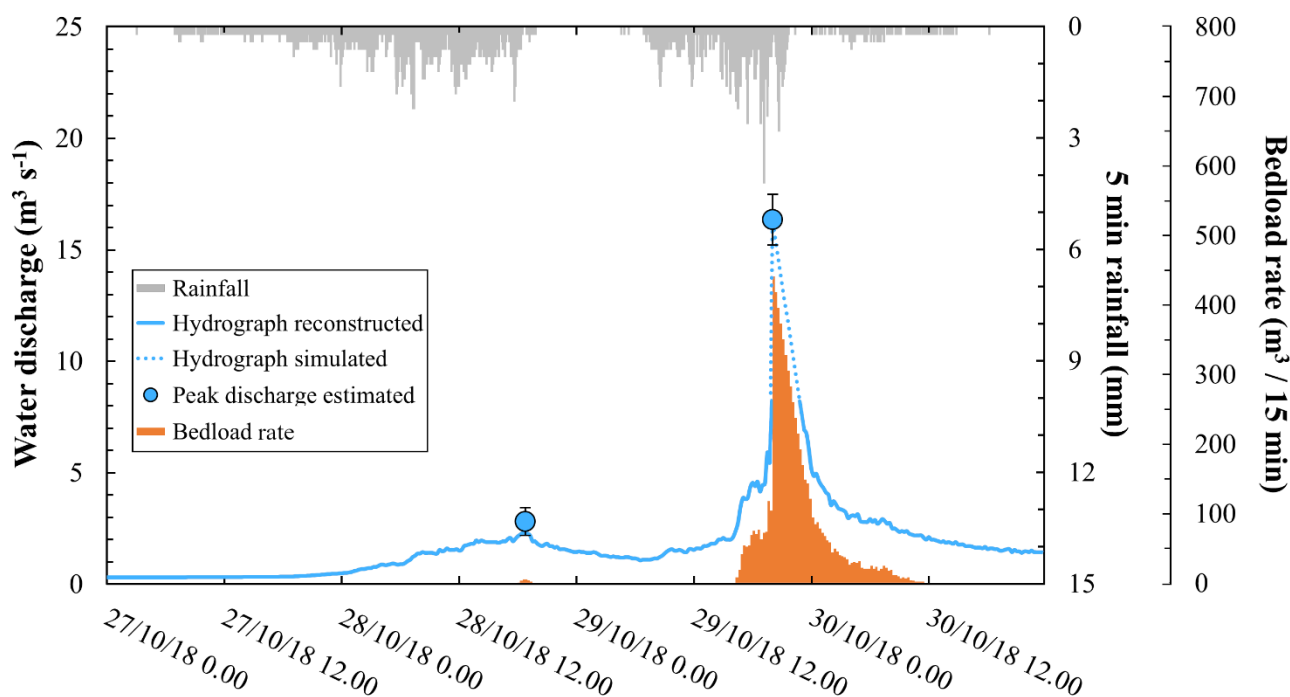


Figure 2.3. Rainfall, water and bedload discharges estimated for the October 2018 event. The blue line represents the hydrograph reconstructed starting from the Fiorentina discharge measurements; the blue dotted line are the parts of hydrograph simulated between the maximum values estimated by discharge reconstruction (Q_{Fi} - Q_{Re} relationship) and the peaks discharge estimated for the first and second phase of flood event. The peaks discharge are represented by the blue circles, the error bars are the lower and upper bounds of the Q_P considered. The orange lines express the bedload rate calculated by the Schoklitsch (1962) equation.

The reconstructed hydrograph suggested Q_P for the Phase 1 and Phase 2 equal to $2.31 \text{ m}^3 \text{ s}^{-1}$ and $8.24 \text{ m}^3 \text{ s}^{-1}$, respectively. Interestingly, the maximum discharge exhibited a delay respect to the maximum I_{5min} of 55 min (Table 2.2). The high-water marks detected in the post-flood surveys enabled to calculate, via Eq. (1), a maximum peak flowed = $17.50 \text{ m}^3 \text{ s}^{-1}$. Such peak was related to the maximum discharge occurred, i.e., Q_P of Phase 2. No field evidences permitted to determine the Q_P of Phase 1. For both phases, the peak of water discharge was estimated through the basin area scaling ratio (Eq. 2) applied to the maximum Q recorded in the Fiorentina Stream. Thus, the Q_P estimated were $3.43 \text{ m}^3 \text{ s}^{-1}$ and $15.21 \text{ m}^3 \text{ s}^{-1}$ for Phase 1 and Phase 2, respectively (Table 2.2). These peaks resulted roughly consistent to those estimated for the Phase 1 by the hydrograph reconstruction (lower by a factor of 0.67) and for the Phase 2 by the post-flood surveys (higher by a factor of 1.15). Therefore, considering the uncertainty and limits associated to each method used, the average between Q_P estimated by hydrograph reconstruction ($2.31 \text{ m}^3 \text{ s}^{-1}$) and the one determined by basin area scaling ratio ($3.43 \text{ m}^3 \text{ s}^{-1}$) was considered representative in describing the water discharge peak of Phase 1. About Phase 2, the average between Q_P obtained by post-flood surveys ($17.50 \text{ m}^3 \text{ s}^{-1}$) and the one resulted by application of basin area scaling ratio ($15.21 \text{ m}^3 \text{ s}^{-1}$) was considered. Hence, Phase 1 and Phase 2

expressed $Q_P = 2.87 (\pm 0.56) \text{ m}^3 \text{ s}^{-1}$ and $Q_P = 16.36 (\pm 1.14) \text{ m}^3 \text{ s}^{-1}$, respectively (Fig. 2.3). In terms of unit stream power, these peaks corresponded to 678 W m^{-2} and 3865 W m^{-2} . The resulted hydrograph shows a Phase 1 characterized by a lower magnitude compared to Phase 2. In terms of flow duration, in Phase 1 about 0.50 h with $Q > Q_{Bf}$ and 1.75 h of bedload duration (T_{Bl}) were assessed. Such conditions led to an effective runoff (ER) equal to $1.0 \times 10^3 \text{ m}^3$ (Table 2.2). Phase 2 exhibited a clear higher magnitude: over-bankfull discharge for ~ 18 h was observed and Q two- and three-fold higher than Q_{Bf} were noted for 5.75 h and 3.50 h, respectively. In Phase 2, $ER = 200 \times 10^3 \text{ m}^3$ and T_{Bl} equal to 20.25 h were estimated, leading the total bedload duration for the October 2018 flood to 22 h (Table 2.2). Overall, the October 2018 flood expressed the largest Q_P ($16.36 \text{ m}^3 \text{ s}^{-1}$) and ER ($201 \times 10^3 \text{ m}^3$) ever documented in the Rio Cordon basin, with a unit peak discharge equal to $3.3 \text{ m}^3 \text{ s}^{-1} \text{ km}^{-2}$.

Table 2.2 Main characteristics of first and second phase of the flood event induced in the Rio Cordon by Vaia storm, and of the entire flood. Q_{Bf} indicates the Rio Cordon bankfull discharge (i.e., $2.30 \text{ m}^3 \text{ s}^{-1}$), while Q_{2Bf} and Q_{3Bf} represent discharges, respectively, two and three fold larger. T_{Bl} is the estimated bedload duration, while ER is effective runoff. BL_{Pred} and BL_{Obs} describe the bedload volume calculated by applying the Schoklitsch (1962) equation and by DoD analysis, respectively.

	Phase 1	Phase 2	Event
Duration of $Q > Q_{Bf}$ (h)	0.50	17.75	18.25
Duration of $Q > Q_{2Bf}$ (h)	-	5.75	5.75
Duration of $Q > Q_{3Bf}$ (h)	-	3.50	3.50
T_{Bl} (h)	1.75	20.25	22.00
ER (10^3 m^3)	1.0	200.0	201.0
Time of Q_P (CET)	28/10/2018 18:45	29/10/2018 20:00	29/10/2018 20:00
Q_P (hydrograph reconstructed ^a ; $\text{m}^3 \text{ s}^{-1}$)	2.31	8.24	8.24
Q_P (post-flood survey; $\text{m}^3 \text{ s}^{-1}$)	-	17.50	17.50
Q_P (basin area scaling ratio ^b ; $\text{m}^3 \text{ s}^{-1}$)	3.43	15.21	15.21
BL_{Pred} (m^3)	32	6858	6890
BL_{Obs} (m^3)	-	6656	6656

^a hydrograph reconstruction based on the Fiorentina discharge measurements

^b based on Bravard and Petit (1997) equation

Geomorphic effects

The detection of the sediment sources led to the mapping of 9 newly formed instabilities and 17 source areas reactivated or enlarged during the October 2018 flood (Fig. 2.4A). The new sediment sources were exclusively located in the lower part of the Rio Cordon basin, covering a total area of 31179 m², with a minimum extent of 49 m² and a maximum of 4927 m². According to the sediment sources' classification used in the Rio Cordon basin, 5 sources were classified as debris flow channels/deposits, 20 as landslides and 1 as stream bank erosion.

The sediment connectivity analysis pointed out the presence of 6 sources coupled to the channel network and potentially sediment suppliers (Fig. 2.4A). Conversely, 20 sources were classified as non-supplier, either because decoupled to the active channel or because they did not show net erosion. This result agrees with the historic knowledge of the basin and with post-event observations. The estimated volume of sediment eroded from the 6 coupled sources was 1219 m³, mostly conveyed by the landslides-debris flow system located close to the outlet (Fig. 2.4A). This volume was reduced, subtracting the bedload yields expressed by November 2012 and June 2014 events (Supplementary Table B S1) to avoid double counting, thus obtaining a potential volume supplied during the October 2018 flood of 1140 m³.

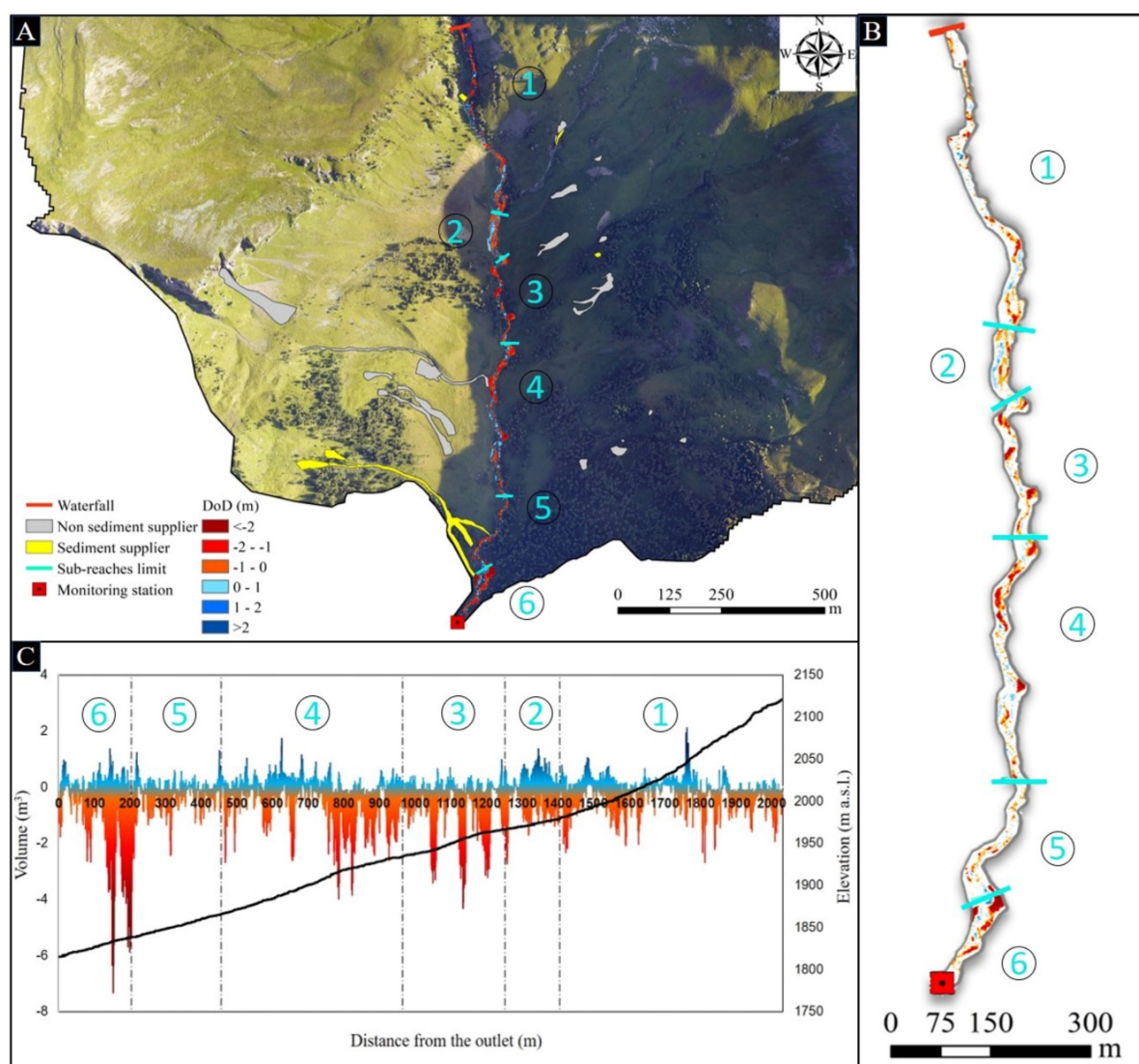


Figure 2.4 The geomorphic response of the lower Rio Cordon basin: A) location of the source areas and their potential role as sediment supplier to the active channel (sub-reaches 1-6); B) zoom of the spatial pattern of geomorphic changes along the Rio Cordon obtained from the DoD; C) DoD represented as the sum of eroded (red) and deposited (blue) volume along the longitudinal profile of the active channel.

Between pre- and post-event conditions, over the 2023 m analyzed, the active channel widened from an average width of 6.30 m to 10.60 m, expanding from 8607 m² to 38696 m². Considering the geomorphic change detection, the DoD analysis computed a total net erosion of 6979 m³ ± 2059 m³ unevenly distributed along the reach (Fig. 2.4A). The average depth of surface lowering (erosion) was 1.06 m, while the average depth of surface raising (deposition) was 0.63 m. Many of the deeper erosional areas were located along the banks (Fig. 2.4B). Notably, the deepest erosion of 4.70 m was located in the downstream part of the basin, along banks affected also by windthrows. Conversely, the depositional areas were predominantly located in the middle of the stream and the highest deposit was 3.10 m. The DoD segregation pointed out that all the sub-reaches were eroded and the downstream sub-reach has the highest average net thickness of difference with - 0.45 m (Table

2.3). Therefore, sub-reach 6 presented the highest averaged rate of erosion (averaged to the area of the sub-reach), followed by sub-reaches 3, 4 and 1 with remarkable erosion rates. Differently, sub-reaches 2 and 5 exhibited the lower average net thickness of difference with - 0.07 m and -0.08, respectively, stressing that they were closer to balancing the erosional and depositional volumes than other sub-reaches. These results were confirmed in the DoD profile (Fig. 2.4C), in which the DoD was presented as the sum of all the values hydrologically equidistant from the outlet. Sub-reach 6 exhibited predominant erosion values, whereas sub-reach 2 and 5 showed erosion values almost balanced with deposition ones. As proven by the elevation profile, sub-reach 2 corresponds to a flatter part of the Rio Cordon. The unit stream power acted in each sub-reach (ω_{Pi}) showed a progressive increase by moving from upstream to downstream, spanning from $\omega_{P1} = 2487 \text{ W m}^{-2}$ to ω_{P6} equal to 3865 W m^{-2} . Interestingly, sub-reach 1 expressed a width ratio (Wr) close to 1, while sub-reach 6 experienced major planimetric variations with a Wr equal to 3.76 (Table 2.3). In this sense, the width ratio scaled roughly linearly with the unit stream power ($R^2 = 0.749$, $p\text{-value} < 0.05$), while a weak relationship was observed between ω_{Pi} and DoD values ($R^2 = 0.293$, $p\text{-value} > 0.05$). Therefore, the results suggest that stream power variation led to a linear variation in the channel width but not in the streambed elevation.

Table 2.3 Summary of the results for each sub-reach concerning unit stream power (ω_{Pi}), width ratio (Wr) and average net thickness of difference (DoD).

Sub-reach	Contributing area (km^2)	Length (m)	ω_{Pi} (W m^{-2})	Wr	DoD (m)
1	2.30	623	2487	1.21	- 0.12
2	3.37	154	2971	1.79	- 0.07
3	3.50	288	2984	1.39	- 0.24
4	4.28	510	3534	2.44	- 0.19
5	4.47	251	3586	2.01	- 0.08
6	5.00	197	3865	3.76	- 0.45

Sedimentological effects

The post-flood GSD of Rio Cordon resulted slightly finer than pre-event, with $D_{16}/D_{50}/D_{84}/D_{90}$ that varied from 29/114/358/455 mm, respectively, to 26/78/302/423 mm (Fig. 2.5). Particularly, it should be stressed the reduction of about a third experienced by D_{50} . The coarse material transported to the monitoring station exhibited a GSD comparable to that expressed by the streambed material, with $D_{16} = 38 \text{ mm}$, $D_{50} = 90 \text{ mm}$, $D_{84} = 248 \text{ mm}$ and D_{90} equal to 381 mm (Fig. 2.5).

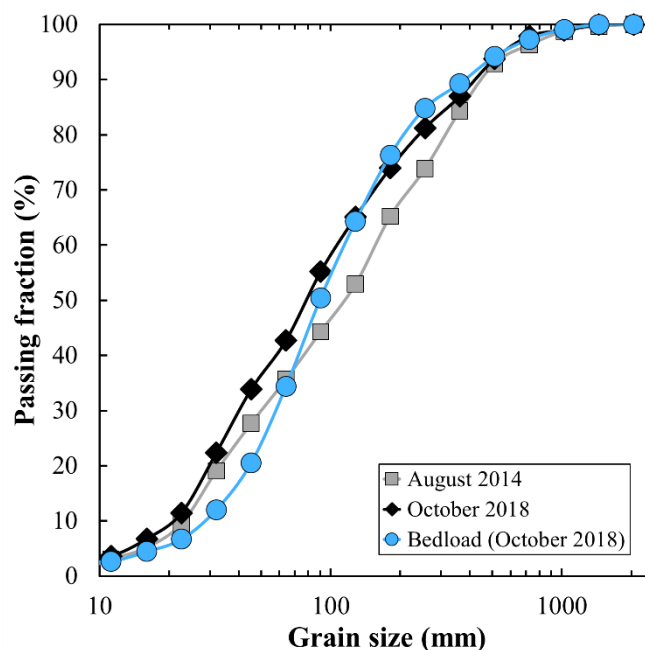


Figure 2.5 Comparison between grain size distributions of pre- (August 2014) and post-flood (October 2018) Rio Cordon streambed as well as of October 2018 bedload.

The ten largest elements were characterized measuring the axis and, thus, estimating the weight. These boulders had a b-axis between 400 and 1100 mm, corresponding to an estimated weight between 0.11 and 1.75 t. Field evidence suggested that these elements were recruited primarily from banks and cascade/step-pool sequences, being then transported for tens of meters. The relationship observed in the period 2012-2018 between critical unit water discharge (q_c) and particle size (Rainato et al., 2020) permitted to roughly determine the hydraulic forcing that caused the boulder entrainment. Considering the ten largest elements, the analysis suggested q_c between $0.68 \text{ m}^2 \text{ s}^{-1}$ and $1.51 \text{ m}^2 \text{ s}^{-1}$. The bedload storage area located at the measuring station was completely filled with coarse sediment (Fig. 2.6). In this area, the DoD analysis determined a bedload volume (BL_{Obs}) equal to $6656 \text{ m}^3 \pm 769 \text{ m}^3$, over an extent of about 4200 m^2 . Therefore, the average net thickness of difference was 1.58 m, with the maximum elevation change reaching 5.96 m of deposition. The reconstruction of the hydrograph also permitted to determine the bedload volume predicted (BL_{Pred}) by bedload equation. The application of the Schoklitsch (1962) equation suggested a bedload volume of 6890 m^3 , of which 32 m^3 were associated to Phase 1 and 6858 m^3 to Phase 2 (Fig. 2.3). Interestingly, the total 6890 m^3 resulted higher by a factor of 1.04 respect to the BL calculated by DoD analysis. Thus, the bedload volume expressed by the October 2018 flood was considered as the average between BL_{Obs} and BL_{Pred} , i.e., equal to about 6800 m^3 .



Figure 2.6 Bedload storage area (A) pre- and (B) post-October 2018 flood.

In terms of BL, the October 2018 flood appeared the largest event recorded in the last 34 years (1986 - 2018), resulting greater than the second flood by a factor of ~ 7.5 , i.e., the September 1994 event ($BL = 900 \text{ m}^3$), and by a factor of 3.68 than the cumulative bedload volume generated by the 33 previous events. Moreover, the bedload was transported over a T_{Bl} of 22 h, corresponding to a transport rate equal to $309 \text{ m}^3 \text{ h}^{-1}$. In terms of bedload yield, the October 2018 flood delivered 11713 t of coarse material, accounting for 99% of the annual bedload recorded in 2018 and 79% of total bedload observed in the period 1986-2018 (Fig. 2.7). Considering this period and accounting the October 2018 event, the Rio Cordon basin therefore exhibited a total sediment yield = 26840 t, which corresponds to a mean sediment yield of $162.6 \text{ t km}^{-2} \text{ y}^{-1}$. It is worth bearing in mind that this estimate does not account for the suspended sediment load generated by October 2018 event.

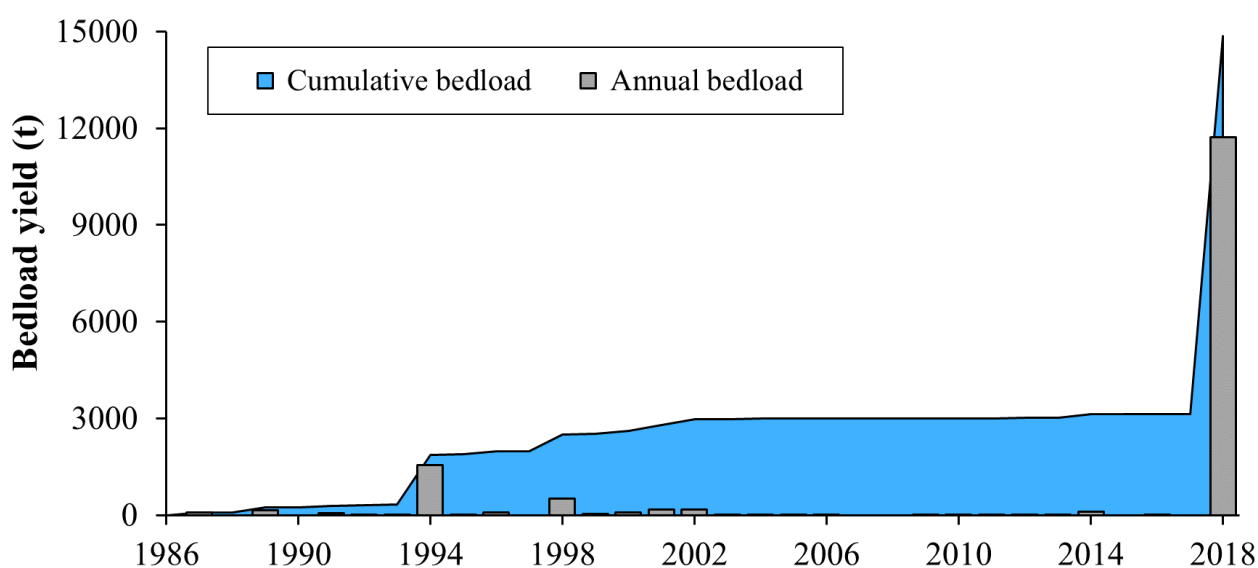


Figure 2.7 Annual and cumulative bedload yields in the Rio Cordon between 1986-2018

Considering the 34 floods recorded in the Rio Cordon basin in the period 1986-2018, it is possible to note a power law relationship between Q_P and BL ($R^2 = 0.719$, p-value < 0.01), in which the October 2018 flood represents the upper bound (Fig. 2.8a). In addition, the bedload GSD seems to be described by Q_P , with the transported $D_{16}/D_{50}/D_{84}/D_{90}$ well predicted by the peak of water discharge. Notably, the relationship performance increases with the coarsening of the percentiles (Fig. 2.8b). In fact, the relationships $Q_P - D_{90}$ and $Q_P - D_{84}$ showed $R^2 = 0.842$ (p-value < 0.01) and $R^2 = 0.813$ (p-value < 0.01), respectively, with the larger elements mobilized by October 2018 flood. Differently, $Q_P - D_{50}$ ($R^2 = 0.677$, p-value < 0.01) and $Q_P - D_{16}$ ($R^2 = 0.421$, p-value < 0.05) resulted more scattered, with October 2018 event that transported D_{50} and D_{16} similar to those entrained by lower magnitude floods. Overall, a progressive increase of both the factor a and exponent b can be noticed with the coarsening of the percentile considered (Fig. 2.8b).

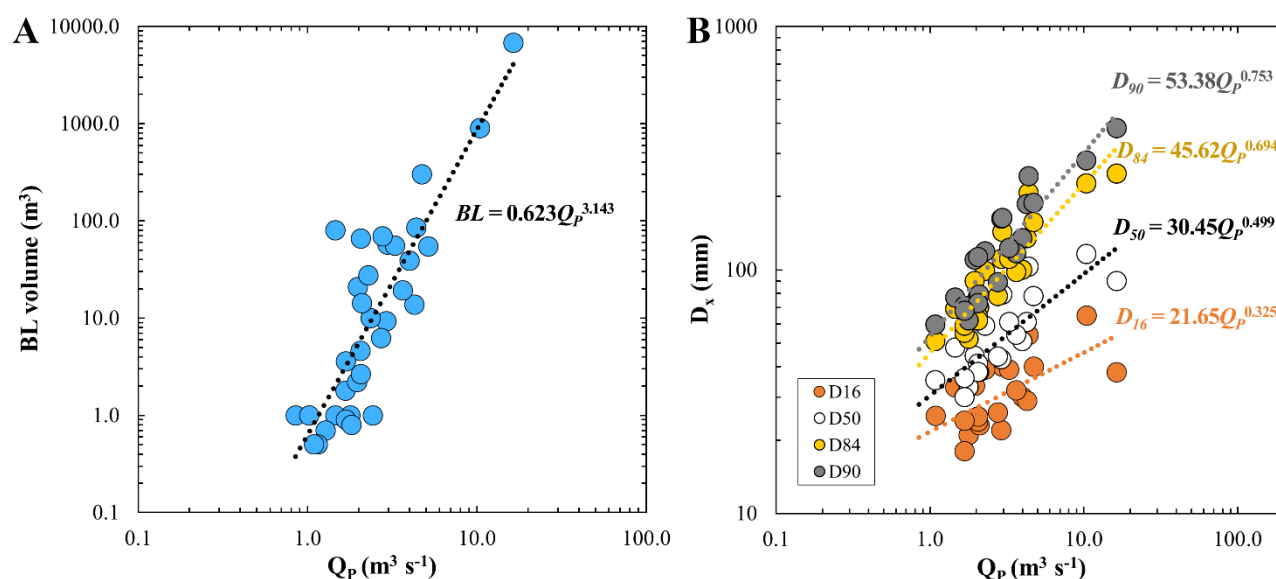


Figure 2.8 Relationship between Q_P and (A) BL volume, and (B) D_{16} , D_{50} , D_{84} , D_{90} , transported by the 34 flood events recorded in the Rio Cordon (1986-2018). The dotted lines are the best-fit lines for each relationship investigated.

The ratio between BL (in t) and ER expressed by each flood recorded (1986-2018) enabled to investigate the temporal trend of transport efficiency. Figure 2.9 shows a general decreasing trend over the long-term period, with most of the events characterized by a BL/ER ratio between 0.1 and 10.0. The only floods that clearly deviate from the general trend were the September 1994 (BL/ER = 58.0) and the October 2018 (BL/ER = 58.3).

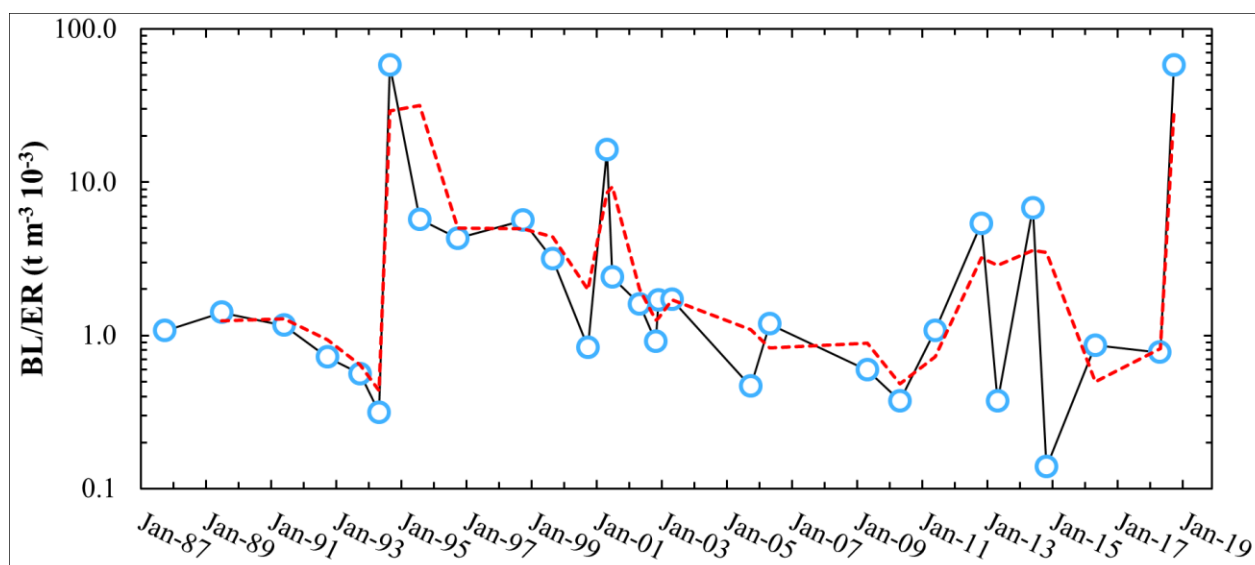


Figure 2.9 Temporal trend expressed by the BL/ER ratio over the 34 flood events recorded in the Rio Cordon (1986-2018). The red dotted line is the 2-event moving average.

DISCUSSIONS

Rainfall conditions

The heavy precipitation generated in the study basin by the Vaia storm was not continuous but exhibited a hiatus of about 9 h, permitting the identification of a Phase 1 and a Phase 2 in the rainfall event (Table 2.1). This temporal distribution is consistent to what was shown by Vaia storm over northeastern Italy (Davolio et al., 2020; Giovannini et al., 2021). The maximum rainfall intensities recorded in 5, 15, 30 min ($I_{5\text{min}}$, $I_{15\text{min}}$, $I_{30\text{min}}$) were characterized by RI < 2 years, while considering longer time intervals ($I_{6\text{h}}$ - $I_{72\text{h}}$) the RI resulted well over 50 years, emphasizing the persistence of rainfall occurred in the Rio Cordon basin. These results agree with Giovannini et al. (2021) who, investigating the main characteristics of the Vaia storm, reported 72 h accumulated precipitation with RI > 200 years in most of the eastern Italian Alps. The moderate but persistent pattern of rainfall was further stressed by the comparison of other high magnitude/low frequency events documented in mountain basins. Batalla et al. (1999) documented, in the Arás basin, a flash flood associated to boulder mobility and massive sediment transport and caused by a brief but intense summer thunderstorm that featured a mean rainfall intensity of 250 mm h^{-1} (Table 2.4). Similarly, Turowski et al. (2009) analyzed three high magnitude floods that affected the Erlenbach basin with large bedload and boulder mobility, identifying intense summer thunderstorms as triggering factor. These events were characterized by $I_{1\text{h}}$ ($40.4 - 61.3 \text{ mm}$) and mean rainfall intensity ($12.9 - 36.8 \text{ mm h}^{-1}$) clearly higher than those observed in the Rio Cordon basin during the Vaia storm, but associated to a total precipitation ($45.3 - 106.7 \text{ mm}$) and a total precipitation duration ($1.5 - 5.0 \text{ h}$) notably lower.

Few authors described high magnitude/low frequency events triggered by persistent precipitation. In the Fella River basin, Marchi et al. (2009a) analyzed a convective storm ($I_{12h} = 390$ mm) which caused a massive debris flow with a mobilized volume of ~ 78000 m³, while a 6 days rainfall event with a total precipitation of 501.0 mm and daily rainfall between 27.2 - 246.4 mm led to a flood with RI > 200 years in the Ligurian Alps (Nannoni et al., 2020).

Table 2.4: Main characteristics of the high magnitude/low frequency event analyzed in this work, compared with those observed in mountain basins by other authors. A is the basin area; S the mean channel slope; Rainfall description indicates the precipitation type triggering the flood event (PP = persistent precipitation, ST = summer thunderstorm); Basin responses describes the main effects induced by the high magnitude/low frequency event in each study basin (CC = channel changes, BM = boulder mobility, HF = Hyperconcentrated flow, DF = debris flows, LA = landslides).

Study basin	Event	A (km ²)	S (m m ⁻¹)	Rainfall description	Mean rainfall intensity (mm h ⁻¹)	Unit peak discharge (m ³ s ⁻¹ km ⁻²)	Unit stream power (W m ⁻²)	Basin responses	Reference
Rio Cordon	October 2018	5.0	0.17	PP	4.4	3.3	2487 – 3865	CC, BM	This work
Arás	August 1996	18.0	0.14	ST	250.0	20.0	–	CC, HF, BM	Batalla et al. (1999)
Emme	July 2014	94.0	0.02	ST	~ 87.0	2.7 – 4.7	–	CC, DF, LA	Ruiz-Villanueva et al. (2018)
Erlenbach	July 1984	0.7	0.18	ST	21.3	17.1	–	CC, BM	Turowski et al. (2009)
Erlenbach	July 1995	0.7	0.18	ST	12.9	14.0	–	CC, BM	Turowski et al. (2009)
Erlenbach	June 2007	0.7	0.18	ST	36.8	20.9	–	CC, BM	Turowski et al. (2009)
Fourmille	September 2013	65.0	0.03 ^a	PP	~ 2.6	–	2500	CC, BM, DF	Wicherski et al. (2017)
Grimmbach	May 2016	30.0	0.02	–	~ 6.4	22.6 – 25.1	–	CC, LA	Lucía et al. (2018)
Jamne	July 2018	8.9	–	ST	~ 2.0	4.6 – 4.8	770 – 2769	CC	Bucała-Hrabia et al. (2020)
Jaszcze	July 2018	11.4	–	ST	~ 2.0	4.1 – 4.5	767 – 2703	CC	Bucała-Hrabia et al. (2020)
Orlacher Bach	May 2016	6.0	0.06	–	~ 6.4	20.0	–	CC, LA	Lucía et al. (2018)
Rio Cordon	September 1994	5.0	0.17	ST	16.0	2.1	–	CC, BM, LA	Lenzi et al. (1999)
Selška Sora	September 2007	29.8	0.02	–	~ 20.0	4.4	–	CC, DF, LA	Marchi et al. (2009b)
Tegnas	October 2018	52.0	0.03	PP	5.7	3.3	–	CC, DF, LA	Pellegrini et al. (2021)

^a averaged value

Hydraulic forcing

The use of indirect methods to estimate the hydraulic forcing acted in the Rio Cordon led to an implicit uncertainty, which needs to be considered. In fact, the hydrograph reconstruction was based on the use of the discharge measured in the Fiorentina basin to describe what occurred in the Rio Cordon sub-basin. The $Q_{Fi} - Q_{Rc}$ relationship was statistically significant and based on 1762 discharge measurements recorded during floods triggered by persistent precipitation, i.e., same rainfall conditions that led to the October 2018 flood. However, it is worth noting that these floods were near-bankfull events and, therefore, the $Q_{Fi} - Q_{Rc}$ relationship may have allowed a better description of under- and near-bankfull discharge than over-bankfull conditions. Nevertheless, the reconstructed hydrograph seems reliable since it reflected the temporal distribution of rainfall registered. Thus, specific analyses were made to determine the corresponding Q_P using the slope conveyance method (Gaume and Borga, 2008) and the basin area scaling ratio proposed by Bravard and Petit (1997). This latter indirect method is characterized by an implicit source of uncertainty due to the basin to sub-basin discharge extrapolation. This uncertainty may have been somewhat reduced by means of the site specific coefficient c already used and tested in the Rio Cordon (Oss Cazzador et al., 2021). Thus, the Q_P inferred for Phase 1 ($2.87 \pm 0.56 \text{ m}^3 \text{ s}^{-1}$) and Phase 2 ($16.36 \pm 1.14 \text{ m}^3 \text{ s}^{-1}$) were associated to the hydrograph reconstructed and, in particular, in the Phase 2 the hydrograph was integrated by a part simulated to describe the peaking portion of flood. This simulated part involved 3 h of the 90 h investigated (October 27th – October 30th) and it was described as a triangular shape according to the hydrograph shape observed in mountain basins during high magnitude/low frequency floods (Lenzi et al., 1999; Marchi et al., 2009a; Turowski et al., 2009). Interestingly, this shape was consistent to the hydrograph generated by the Vaia storm in another basin of eastern Italian Alps, i.e., the Tegnasc catchment (Pellegrini et al., 2021). The hydraulic forcing conditions estimated clearly stressed the high magnitude expressed by the October 2018 flood event (Table 2.2). This high magnitude can be ascribed to the amount and intensity of rainfall but also to their temporal distribution and soil moisture. The soil conditions may have also influenced the perfluvial areas, where important windthrows were observed (Picco et al., 2020) likely to the high wind gusts of October 29th acting on a saturated and softened terrain.

In the Rio Cordon, the October 2018 flood resulted in a unit peak discharge of $3.3 \text{ m}^3 \text{ s}^{-1} \text{ km}^{-2}$. This value was lower than those described in the Erlenbach by Turowski et al. (2009), who observed a unit peak discharge between $14.0 - 20.9 \text{ m}^3 \text{ s}^{-1} \text{ km}^{-2}$ in large floods due to intense thunderstorms (Table 2.4). Higher unit peak discharges were documented even in the Fella River basin by Marchi et al. (2009a) and in Grimmbach and Orlacher Bach by Lucía et al. (2018), who reported $20.0 \text{ m}^3 \text{ s}^{-1} \text{ km}^{-2}$ and $20.0 - 25.1 \text{ m}^3 \text{ s}^{-1} \text{ km}^{-2}$, respectively. Hydraulic forcing comparable to that observed in the

Rio Cordon were detected by Marchi et al. (2009b) in the Selška Sora basin, where a flash flood expressed $4.4 \text{ m}^3 \text{ s}^{-1} \text{ km}^{-2}$, and by Ruiz-Villanueva et al. (2018) that reported a unit peak discharges between $2.7 - 4.7 \text{ m}^3 \text{ s}^{-1} \text{ km}^{-2}$ ascribed to heavy and extensive summer precipitation in the Emme River basin (Table 2.4). Particularly, the unit peak discharge calculated in the Rio Cordon resulted consistent to the $3.3 \text{ m}^3 \text{ s}^{-1} \text{ km}^{-2}$ experienced in the Tegnás catchment during the Vaia storm (Pellegrini et al., 2021). Also, the peaks of unit stream power inferred along the main channel ($\omega_{P1-6} = 2487\text{-}3865 \text{ W m}^{-2}$) appeared comparable, although at the upper limit, to those reported in literature. In fact, the small Jamne and Jaszczé basins, located in the Western Polish Carpathians, experienced ω between $767 - 2769 \text{ W m}^{-2}$ as a consequence of flood due to heavy summer precipitation (Bucala-Hrabia et al., 2020). In Fourmille Creek, Wicherski et al. (2017) documented a precipitation event of 350 mm in seven days, which generated over-bankfull discharge for 120 h and a maximum ω of about 2500 W m^{-2} (Table 2.4). Instead, the range of unit stream power determined in the Rio Cordon appeared in line to what observed by Yochum et al. (2017) in the Colorado Front Range as consequence of persistent heavy rainfall ($\sim 460 \text{ mm}$ in 10 days). These authors analyzed 531 stream reaches, estimating maximum ω between 30 and 7000 W m^{-2} .

Hillslopes and main channel responses

The limited response of hillslope and the only 26 sediment sources (re)activated could be attributed to the moderate rainfall intensity that, in combination with the hiatus in precipitation, may have precluded an extensive slope instability. Also, the lack of other high magnitude events in the period 1994-2018, might have reduced the erosional processes and favored a consequent stabilization trend along the hillslopes (Ferrato et al., 2017). Differently, in the Tegnás catchment characterized by a similar geological substrate, the Vaia storm caused a marked increase of sediment sources with the catchment area covered by instabilities, such as debris flows and landslides, augmented from 0.33% to 0.83% (Pellegrini et al., 2021), whereas in the Rio Cordon basin this extent increased only from 0.13% to 0.14%. The sediment sources were investigated as potential suppliers in the lower basin. According to Dalla Fontana and Marchi (1994), the lower Rio Cordon belt shows predominant erosion areas (e.g., landslides, debris flows, stream bank erosions), where the sources are potentially more capable of transferring sediment to the downstream outlet in respect to the upper basin (Cavalli et al., 2016). In this sense, recent analyses performed on the upper plateau by Oss Cazzador et al. (2021) demonstrated that, although the October 2018 flood caused the reconfiguration of the upper reach (estimated BL = $86.0 - 133.2 \text{ m}^3$), it did not effectively transferred sediment to the downstream part of the basin. According to the IC-DoD analysis, only few sources acted as sediment suppliers to the main active channel during the event. Although it proved to be sufficiently reliable, this approach

can be further improved. First, the DoD should consider more frequent surveys, second the IC analysis could involve a deeper and extensive field analysis to derive a more accurate threshold. However, the analyses stressed that the Rio Cordon basin showed evidence of limited lateral connectivity, since only few sediment sources supplied material to the channel network. On the contrary, it showed high longitudinal connectivity due to the evident linkage between active channel and outlet (Fryirs et al., 2007). The DoD analysis suggested that the moderate but persistent rainfall caused greater hydraulic forcing along the main channel than along the slopes, leading to a predominant alluvial response of the Rio Cordon basin. This hypothesis was supported by a volume eroded from Rio Cordon (6979 m^3) clearly larger than the potential volume supplied by sediment sources (1140 m^3). In fact, the DoD pointed out that along the active channel the October 2018 flood resulted in severe erosion processes, with large streambed incisions and banks scouring. Particularly, an evident widening was observed along the 2023 m analyzed, with the average channel width that varied from 6.30 m, pre-event, to 10.60 m post-event. In this sense, it is worth noting that the geomorphic changes measured can be affected by uncertainty due to: (i) the error range in the active channel DoD, corresponding to $\pm 2059 \text{ m}^3$ (29.5%); (ii) the inaccuracies related to the channel width measuring by means of orthophotos interpretation. Despite these sources of uncertainty, the results seem to suggest that the sediment transport benefited by quasi-unlimited sediment supply conditions mainly due to an extensive alteration of active channel, where the armoured layer was removed. From the DoD analysis a longitudinal pattern along the channel was hardly detectable as many avulsions caused the variation of the stream pathway and no clear erosional/depositional alternation can be used to infer in-channel sediment transfers (Calle et al., 2020). However, the subdivision in sub-reaches helped to reconstruct the linkage between the hydraulic forcing and the geomorphic response. As supported by Marchi et al. (2016), unit stream power was able to describe the major geomorphic changes at channel reach scale. In particular, consistency between ω_{Pi} and lateral geomorphic changes (W_r), rather than vertical (DoD), was found. This result appeared in line with Krapesch et al. (2011), who successfully predicted channel widening, caused by extreme floods in alpine gravel bed rivers, by using ω determined by means of the pre-event channel width. In the Rio Cordon basin, the definition of the hydraulic forcing conditions and the induced geomorphic changes supported also the hypothesis that the high magnitude/low frequency floods are the only events that can severely alter the rough boulder streams (Baker and Costa, 1987).

Sedimentological response

The hydraulic forcing and erosive processes triggered by October 2018 flood resulted in a massive sediment transport. The GSD investigation stressed that the entire streambed grain size, from fine

gravel to large boulders, was mobilized (Fig. 2.5). This finding supports the hypothesis that the Rio Cordon experienced structural bedload, condition under which a complete streambed remobilization occurred (Piton and Recking, 2017). Consistently, the mobility of large boulders was also observed, highlighting the outstanding hydraulic forcing expressed by October 2018 event. In this sense, it is interesting to note that, in literature, the transport of boulders was generally documented for higher unit peak discharges (Table 4). However, Wicherski et al. (2017) observed boulder mobility in the Fourmille Creek as a consequence of ω comparable to that exerted in the Rio Cordon by October 2018 flood. Therefore, these outcomes stressed out the need to better comprehend the boulder mobility, a condition that can strongly impact the mountain streams but that was only rarely investigated. The approaches used to determine the bedload volume, i.e., DoD analysis and bedload prediction, provided very similar volumes, with a BL_{Obs}/BL_{Pred} ratio equal to 0.97. In the Rio Cordon, this ratio was always lower due to the overestimation of BL_{Pred} by Schoklitsch (1962) equation and, in general, by bedload equations, with respect to BL_{Obs} (D'Agostino and Lenzi, 1999; Rainato et al., 2017). Therefore, the good match between BL_{Obs} and BL_{Pred} emphasized the high hydraulic forcing of October 2018 flood coupled with a high sediment supply, conditions under which the bedload equations can provide the highest predictive performance (D'Agostino and Lenzi, 1999; Recking, 2012; Rickenmann, 2020). However, it is worth noting that both BL_{Pred} and BL_{Obs} might be affected by a certain degree of uncertainty. On the one hand, BL_{Pred} was calculated by means of the Schoklitsch equation applied to the hydrograph reconstructed. Therefore, the intrinsic uncertainty affecting the discharges estimated may have propagated in the predicted bedload. On the other hand, the BL_{Obs} determined by DoD analysis presented an error range of $\pm 769 \text{ m}^3$, corresponding to about 11.5 % of the volume observed. Finally, BL_{Obs} might be affected by a partial underestimation as the October 2018 flood caused the complete filling of the bedload storage area, up to its maximum capacity (Fig. 2.6), and therefore a certain portion of bedload may have been transported further downstream.

Large and infrequent floods in Rio Cordon basin

The long-lasting monitoring program realized in the Rio Cordon basin provides the rare opportunity to compare two high magnitude/low frequency floods occurred in the catchment. These events were caused by markedly different rainfall conditions. In fact, the intense summer thunderstorm that triggered the September 1994 flash flood exhibited $I_{5min}/I_{15min}/I_{30min}$ about twice the Vaia storm's values but lasted 12 h, i.e., a total precipitation duration considerably shorter than the 79.8 h estimated in October 2018 (Table 2.1). The prolonged rainfalls of October 2018 produced the highest hydraulic forcing conditions among the 34 floods recorded in the Rio Cordon since 1986 (Supplementary Table B S1). Particularly, the estimated water discharge peak ($Q_P = 16.36 \pm 1.14 \text{ m}^3 \text{ s}^{-1}$) and effective runoff

($ER = 201.0 \times 10^3 \text{ m}^3$) were higher by a factor of 1.57 and 7.56, respectively, than those exhibited by September 1994 flood, which instead exhibited rainfall intensities ($I_{5\text{min}}/I_{15\text{min}}/I_{30\text{min}}$) about twice the Vaia storm but lasted 12 h. Despite this outstanding hydraulic forcing, the hillslope response to the October 2018 event was modest. In particular, the number of newly formed sediment source areas was relatively low compared to what produced by the September 1994 flood (Dalla Fontana and Marchi, 1994; Lenzi and Marchi, 2000). This diverse response appears to be due to the different rainfall intensity showed by the flood events (Table 2.4). However, in both high magnitude/low frequency floods, the main sediment source was identified in the active channel and, particularly, in the streambed that experienced armoured layer removal. In October 2018, the alteration faced by the main channel was clearly larger than in 1994, with unprecedented lateral widenings and avulsions. This finding confirmed that, with similar unit stream power and peak discharge, long-lasting floods can produce larger geomorphic changes than flash floods (Costa and O'Connor, 1995; Magilligan et al., 2015; Marchi et al., 2016). The hydraulic and geomorphic forcing exerted by October 2018 flood triggered boulder mobility in the Rio Cordon main channel, a condition that was previously observed only in the September 1994 event. In this sense, according to Rainato et al. (2020), the largest element (b-axis = 1100 mm) recovered in the bedload storage area after the October 2018 flood suggests a critical unit water discharge (q_c) of $1.51 \text{ m}^2 \text{ s}^{-1}$, thus, higher than $q_c = 1.25 \text{ m}^2 \text{ s}^{-1}$ observed in the September 1994 flood (Lenzi et al., 2006b). Also in terms of bedload volume, the October 2018 flood ($BL = 6800 \text{ m}^3$) was the largest event recorded in the Rio Cordon basin, and about one order of magnitude larger than the September 1994 event ($BL = 900 \text{ m}^3$). Interestingly, the two high magnitude/low frequency events showed comparable transport rate, i.e., $309 \text{ m}^3 \text{ h}^{-1}$ in October 2018 flood and $323 \text{ m}^3 \text{ h}^{-1}$ in September 1994 event but the latter lasted 3 h, while, during the former, bedload persisted 22 h. The BL magnitude expressed by October 2018 flood was also clearly noticeable in terms of sediment yield, accounting for 79% of the total bedload delivered during the period 1986-2018 and, then, leading to an abrupt increase over the annual trend (Fig. 2.7). In light of climate change, because of which a higher frequency of heavy rainfall event is expected (Fischer and Knutti, 2015; Peleg et al., 2020), the observed relationships Q_P -BL volume and Q_P -GSD transported seem to suggest that in the near future, in the Rio Cordon, other massive bedload transport accompanied by the mobilization of coarse grain size could be awaited. Additionally, the October 2018 flood induced a peak in the temporal trend of BL/ER ratio, similarly to what was caused by the September 1994 event, i.e., a condition that favoured about a decade of increased transport efficiency (Rainato et al., 2017).

CONCLUSIONS

In alpine basins, severe rainfall events and induced large floods can influence erosion processes, sediment dynamics and landscape evolution over large spatial and temporal scales. However, given the high magnitude/low frequency, these events and their effects are difficult to measure and, thus, to be documented. Additionally, even rarer are the studies proposing a comprehensive approach that encompasses all the main responses to the events. This work analyzed the hydrological, geomorphic and sedimentological responses of an alpine basin (Rio Cordon basin) to the Vaia storm, a severe weather event that affected northeastern Italy in October 2018. In the Rio Cordon basin, the Vaia storm resulted as a severe and persistent rainfall event, during which the rainfall intensities for sub-hourly intervals were ordinary, while for longer time intervals expressed $RI > 50$ years. The combination of different indirect methods helped the hydraulic forcing quantification. Despite the uncertainty associated to this approach, the analyses clearly stressed the outstanding hydraulic forcing occurred during the flood, pointing out the largest Q_P and ER ever recorded in 34 years. These conditions induced a moderate hillslope response, with only few new sediment sources capable of acting as sediment suppliers to the main channel. Instead, the precipitation favored a predominant alluvial response of the basin, with the Rio Cordon severely altered by lateral widening, deep streambed incision and armouring removal. In terms of sedimentological response, the hydraulic forcing and the erosive processes induced by the Vaia storm resulted in streambed remobilization, boulder mobility and in a bedload volume about four times the one produced cumulatively by the 33 previous events. Thanks to a monitoring program maintained over three decades, the Rio Cordon basin offered the uncommon chance to compare characteristics and effects of two high magnitude/low frequency floods. These two events exhibited different rainfall and hydraulic forcing conditions that favored in the September 1994 flash flood a hillslope response larger than in the October 2018 event, which instead altered the main channel more extensively. These conditions resulted in a different sedimentological response of the basin, clearly evident in terms of bedload volume, supporting the hypothesis that floods featuring high Q_P (or ω_P) combined with a long duration can severely influence the mountain fluvial systems. Therefore, bearing in mind the long-lasting effects induced by the previous large and infrequent event, what can be expected for the future? Has the October 2018 event represented the new ground zero for the Rio Cordon basin? To answer these questions, also in the framework of climate change, it will be fundamental to continue investigating over the long-term this and other alpine basins to understand how they will respond to forthcoming ordinary and high magnitude/low frequency events.

Chapter 3.

The morphological evolution of a step-pool stream after an exceptional flood and subsequent ordinary flow conditions

Giacomo Pellegrini, Riccardo Rainato, Lorenzo Martini, Lorenzo Picco

This chapter was published as Giacomo Pellegrini, Riccardo Rainato, Lorenzo Martini, Lorenzo Picco (2021). The morphological evolution of a step-pool stream after an exceptional flood and subsequent ordinary flow conditions. *Water*, 13, 3630.

doi: 10.3390/w13243630.



ABSTRACT

Mountain streams are frequently characterized by step–pool morphology that provides stability and energy dissipation to the channel network. Large flooding events can overturn the equilibrium of the step–pool condition by altering the entire configuration. This work focuses on the impact of the “Vaia” storm (27–30 October 2018) on a step–pool mountain stream (Rio Cordon, Northeast Italy) and on its evolution after two years of ordinary flow conditions. To achieve the aims, this work uses both remote sensing data (LiDAR and UAV) and direct field measurements (i.e., longitudinal profiles and grain sizes distributions) performed pre-event, post-event, and 2 years later (current conditions). The results show a significant widening (width +81%, area +68%) and the creation of a new avulsion after the storm and a substantial change between the number of units (51 in the pre-event, 22 post-event, and 51 in the current conditions) and characteristics of step–pool sequences between pre- and post-conditions. Furthermore, it proves the ongoing processes of morphological stabilization since the current step–pool sequences parameters are heading back to the pre-event values. Such results suggest clear susceptibility of step–pool to exceptional events and fast recovery of such setting during barely two years of ordinary flow conditions.

Keywords: Mountain Basin; Vaia storm; Exceptional flood event; UAV; LiDAR; Step-pool evolution; Ordinary flow conditions

INTRODUCTION

The morphological configuration of a fluvial system is the result of a complex interplay between different factors. In mountain environment, the latter are mainly constituted by climatic, geological, hydrological and sedimentological forcings, to which mountain streams have to adapt. To describe and better understand the mountain stream morphology, different classifications were proposed in literature. Up to now, the most used and shared is the classification proposed by Montgomery and Buffington (1997), which defines the streams according to the channel-reach morphologies. These are classified as follow: colluvial, bedrock, cascade, step-pool, plane bed, pool riffle and dune ripple. Worth adding is the typology “rapids” that was introduced firstly by Church and Zimmermann (2007) and then used by Gomi et al. (2003). In this work, particular attention is paid to the step-pool configuration that is one of the most common morphology in mountain streams (Lenzi, 2001). As the name suggests, the step-pool setting is characterized by the presence of an upstream step and a downstream pool. Higher water level upstream and a lower moving downstream characterize the pools. The steps are commonly composed of large boulders or wood logs that imbricate smaller boulders, cobbles or gravels, entailing stability and a heterogeneity in the streambed material.

Additionally to the steep slope ($> 5\%$), the step-pool setting develops mainly under the conditions of highly heterogeneous grain size, i.e., spanning from fine granules to large boulders (Lenzi, 2001; Turowski et al., 2009); near critical to supercritical flows (Comiti et al., 2009); persisting limited sediment supply conditions and limited transport rate (Turowski et al., 2009). This morphology is also known to be a configuration that effectively dissipates energy (Chin, 2003). Dissipation that is favored by both the grain- and form-roughness. The former is verified since the large elements provide resistance to the water flow, the latter, instead, occurs due to the presence of the vertical drop of the step that reduces the potential energy, which otherwise would be converted into a longitudinal component of the kinetic energy (Chin et al., 2019), influencing erosional and sediment transport processes (Marston, 1982). The mean flow velocity for a step-pool stream, in fact, is the minimum attainable for assigned values of slope, grain size distribution and roughness (Lenzi, 2001). The step-pool configuration can be described by a series of descriptive parameters, proposed by Whittaker and Jaeggi (1982) and Abrahams and Atkinson (1995), i.e. step width (W), step-step drop (Z), step-pool height (H), pool-pool spacing (L_p), step-step spacing (L_s) and mean slope (S). The mean H and mean L_s of a step-pool unit can be used to define the steepness factor (Abrahams et al., 1995; Davies and Sutherland, 1980; Whittaker and Jaeggi, 1982). Based on field and flume experiments, Abrahams and Atkinson (1995) suggested that the maximum resistance to the flow of a step-pool setting is satisfied when the steepness factor is equal to $1.5S$. Furthermore, field experiments by Lenzi (2001) demonstrated that such parameter equals $0.79S$ when the step-pool configuration faces unstable conditions. The addition of the S parameter to the steepness permits to compute the non-dimensional steepness (c) which gives further information on the slope of the pool bottom profile (Lenzi, 2001). Step-pool configuration plays an important role in controlling sediment transport processes and, in the mountain streams' sediment yield. This capacity to influence the sediment transport processes is also used for ecological and management issues. At present, in fact, step-pool settings are used to provide both watershed protection and restoration of mountain fluvial systems. The capacity of step-pool configuration to modulate the sediment fluxes was also proven by study cases that documented its removal. In fact, the suppression of step-pools led to an increase in sediment yields due to the reduction of grains inter-locking, and bedform roughness (Lenzi, 2001; Turowski et al., 2009). In addition, in highly confined valleys the step-pool configuration can act as a reinforcement of the banks and, therefore, its removal may promote hillslope instabilities and the increase of sediment supply (Schuerch et al., 2006; Turowski et al., 2009). As far as the alteration of step-pool is concerned, Crowe (Crowe and Wilcock, 2002) through flume experiments identified several processes such as: burial by sediments, collapse of key elements due to erosion of supporting fine particles, failure due to downstream plunge pool erosion and collapse due to collision by large particle as processes for

which a step can be removed. Nevertheless, the field analysis carried out in the Erlenbach by Turowski et al. (2009) identified an additional step removal process, consisting in the direct entrainment of key elements due to outstanding hydraulic forcing conditions. Large and infrequent floods are commonly the main causes of mountain streams' morphological alteration expressed as new avulsions (Valenza et al., 2020), channel widening (Pellegrini et al., 2021) and changes in the streambed configuration (Wyżga et al., 2021). Such morphological changes can be investigated by means of remote sensing approaches relying on LiDAR, UAV and aerial photos (Lucía et al., 2018; Picco et al., 2014; Tonon et al., 2018), which can be integrated by accurate field surveys in order to limit their uncertainty (Messenzehl et al., 2014; Misset et al., 2020).

Therefore, in light of the susceptibility of the mountain step-pool streams to a wide range of natural disturbances (Robson et al., 2013) and given the increase of intensity and frequency of such events, it is of crucial importance understanding their responses and evolutions after flood events of different magnitude. In this sense, the Northeast of Italy was recently affected by the “Vaia storm” (27-30th October 2018), a low-pressure system causing high Scirocco wind gusts ($> 200 \text{ km h}^{-1}$) and cumulative precipitation up to 715 mm (Lucianetti et al., 2019; Pellegrini et al., 2021). This work provides an accurate study about the morphological response of an alpine step-pool stream to a large and infrequent flood, and subsequent ordinary flow conditions. The unique opportunity of analyzing the Vaia storm provides new information concerning the step-pool morphological changes and new tips for future management guidelines in order to predict mountain streams evolution in a future scenario featuring climate change. Therefore, to analyze precisely the event, particular attention is given to: (i) the planimetric evolution, (ii) the alteration of step-pool configuration and (iii) the grain size variations.

MATERIAL AND METHODS

Study area

The Rio Cordon catchment is located in the eastern Alps of Italy, precisely in the Agordino valley (Belluno, Veneto Region) (Fig. 3.1). It has an extension of 5 km^2 and a typical alpine climate. The mean annual precipitation is stable (1986-2018) around 1180 mm (Rainato et al., 2021), while the mean annual temperature (T°) has distinctly increased over $1 \text{ }^\circ\text{C}$ during the last three decades (Rainato et al., 2018b). At present, the mean T° is around $7.5 \text{ }^\circ\text{C}$. The nivo-pluvial regime of the basin favors predominant snowfalls in the late fall, during the winter season and in the early spring. In the rest of the year, short and intense rainfalls feature the runoff regime.

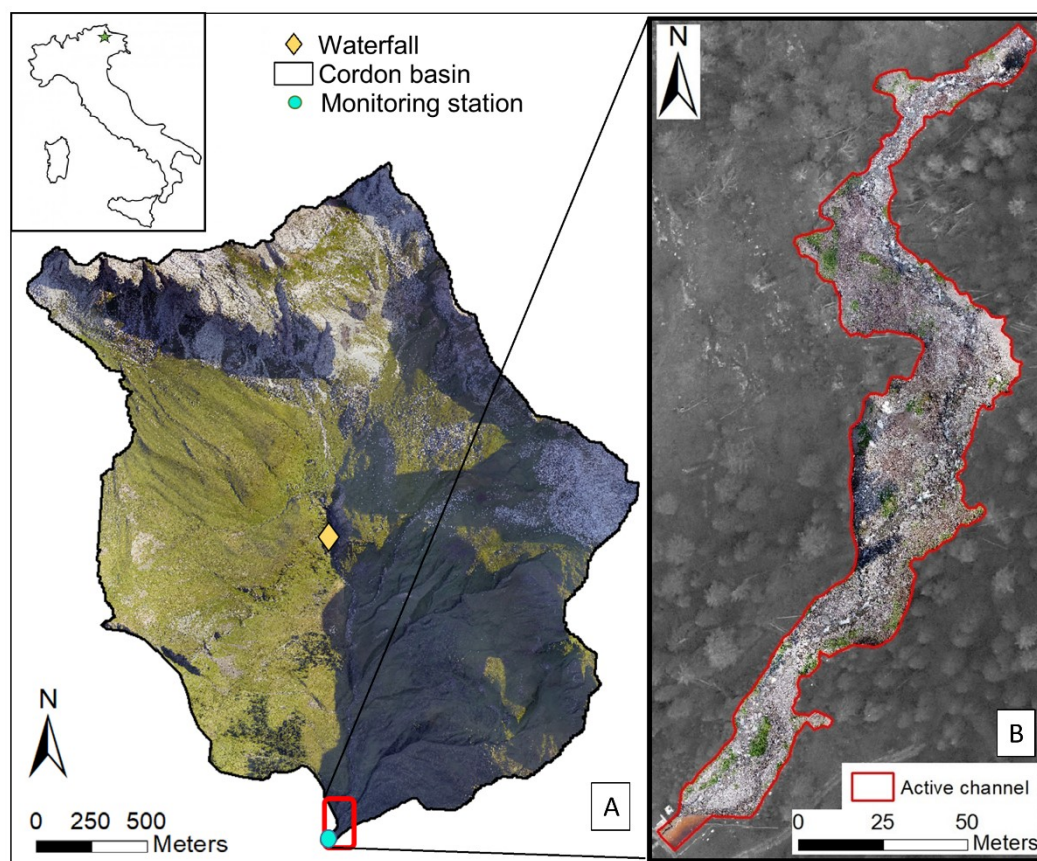


Figure 3.1. (A) Aerial picture of the Rio Cordon basin located in the northeast of Italy, the red square at the outlet of the basin represents the area where the UAV survey was made along the (B) study reach. In this part, the planimetric and step-pool analyses were made.

Being part of the Southern Limestone Alps, the substrate of the Rio cordon is characterized by dolomites, limestones, volcanic conglomerates and calcareous-marly rocks (Rainato et al., 2021). As the range of elevation goes from 1763 to 2763 m a.s.l., the vegetation cover is limited to 7% of the basin area. The vegetation is composed by spruce (*Picea abies*) and larch (*Larix decidua*). Bare rocks (14%), shrubs (18%) and grasslands (61%), instead, cover the rest of the area. The Rio Cordon main channel (hereinafter Rio Cordon) is characterized by cascade, step-pool and riffle-pool morphologies (Montgomery and Buffington, 1997). Worth mentioning is the presence of a waterfall just upstream the middle part of the channel. As known (Rainato et al., 2018b), such unit represents a knickpoint and a natural area of disconnection between the upstream and downstream part of the basin. As to the lower Rio Cordon, the mean average slope is around 17%. The bankfull discharge is around $2.3 \text{ m}^3 \text{ s}^{-1}$ (Fig. 3.2) which covers a mean channel width of around 5.3 m (Lenzi et al., 2006; Rainato et al., 2018b, 2018a). Thanks to a monitoring program activated since 1985 and based on a permanent measuring station, the Rio Cordon study site can be defined as a “field laboratory”. In fact, it was monitored for more than three decades, allowing to better understanding how climatic, hydrological, morphological and sedimentological dynamics can act in an alpine basin (Comiti et al., 2007;

D'Agostino and Lenzi, 1999; Oss Cazzador et al., 2021, 2020; Pagano et al., 2019; Rickenmann et al., 1998; Wilcox et al., 2011).

Flow conditions

To analyze the morphological evolution of the study reach channel of the Rio Cordon, three field campaigns were realized in 2015 (pre-event), 2018 (post-event) and 2020 (current conditions), respectively (Fig. 3.2, Table 3.1). In terms of hydraulic forcing, the period between pre-event and post-event surveys was characterized thanks to the water discharge (Q) recorded by the Rio Cordon monitoring station, which measured Q hourly (Pagano et al., 2019). In this study period, the Rio Cordon experienced Q mainly under- and near-bankfull flood (Fig. 3.2). However, in October 2018 a severe weather event (hereinafter Vaia storm) affected the study site (Picco et al., 2020). Particularly, the heavy rainfall occurred between 27th-30th October 2018 (352 mm in ~ 80 h) triggered a peak of water discharge (Q_P) equal to $16.4 \text{ m}^3 \text{ s}^{-1}$, i.e., the largest Q_P ever documented in the Rio Cordon (Rainato et al., 2021). This outstanding hydraulic forcing caused the transport of about 6800 m^3 of bedload to the monitoring station and the consequent interruption of all the operations, included the Q measurements. Therefore, from the Vaia storm, the hydraulic forcing conditions acting in the Rio Cordon had to be derived through indirect methods. To this end, the Q recorded by the nearest gauging station (“Sottorovei” Arpa Veneto station at Fiorentina Stream) was used, through a specific basin to-sub-basin discharge extrapolation (Rainato et al., 2021). The capacity of the Fiorentina Stream discharge to predict the Rio Cordon discharge was tested and validated by Rainato et al. (2021), permitting authors to characterize the Vaia storm flood. In light of this, the relationship between Fiorentina Stream discharge and Rio Cordon discharge was used to describe the hydraulic forcing condition occurred in the Rio Cordon from October 2018 onward. Fig. 3.2 shows that following the Vaia storm and, in particular, between the post-event field campaign and the survey of current conditions, the Rio Cordon experienced persistent ordinary flows. In this study, we defined as ordinary flow condition the discharge values lower than the bankfull value. Precisely, the peak of water discharge estimated between the pre-event and post-event surveys was equal to $16.4 \text{ m}^3 \text{ s}^{-1}$ (29th October 2018), while $Q_P = 1.7 \text{ m}^3 \text{ s}^{-1}$ (17th November 2019) was observed between the post-event field campaign and the survey of current conditions.

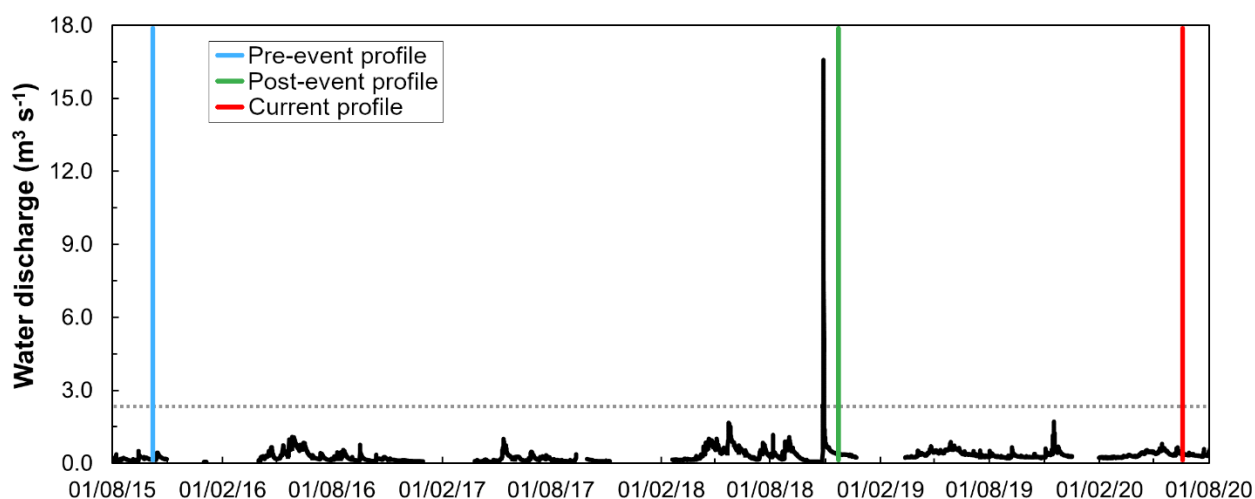


Figure 3.2. Water discharge experienced by the Rio Cordon during the study period. Until the Vaia storm, the water discharge was measured by the Rio Cordon monitoring station. From Vaia onward, due to the interruption in the monitoring station operations caused by the event, the water discharge acting in the Rio Cordon was determined starting from the Fiorentina Stream discharge and using a specific basin to sub-basin discharge extrapolation (see details in (Rainato et al., 2021)). The vertical blue, green and red lines identify the longitudinal profile surveys realized during the pre-event, post-event and the current conditions. The horizontal gray dashed line shows the bankfull discharge ($2.30 \text{ m}^3 \text{ s}^{-1}$).

Planimetric pattern

The planimetric analysis was carried out taking advantage of three subsequent aerial photos and Digital Elevation Models (hereinafter DEMs) with respect to the pre-event, post-event and current conditions (Table 3.1). For the first two years (pre-event and post-event) LiDAR surveys were exploited. The ortophotos were characterized by a resolution of 0.20 m while the DEMs of 0.50 m. Although the Vaia storm hit the basin in the late 2018, the remote sensing survey was taken the following winter in order to avoid snow covering along the basin area. The remote sensing data of the current conditions, instead, were obtained thanks to Structure From Motion workflow (SfM) (Iheaturu et al., 2020) using Unmanned Aircraft Vehicles (hereinafter UAVs). Particularly, the drone employed was a quadcopter DJI Phantom 4. The data processing was performed using the Agisoft Photoscan software (Rusnák et al., 2019) from which high-resolution aerial photos of 0.02 m and DEM of 0.10 m were produced.

Moving forward, through an aerial photos interpretation technique (Guzzetti et al., 2009; Rainato et al., 2018b), the active channels detected in the pre-event, in the post-event and in the current periods were measured and compared using the Esri ArcMap 10.5 software. Following Lawlor (Lawlor, 2004) definition, the active channel considered referred to the geomorphic feature of the torrent which is defined by a break in bank slope and, typically, by the edge of the exposed gravels. The talweg line position was detected via aerial photo interpretation. The combination of the active

channel polygon and the talweg position permitted to measure the mean width per each year plotting transversal cross-sections every 20 m.

Step-pool configuration

The analysis of the step-pool configuration was performed surveying the longitudinal profile of the Rio Cordon in the study reach 320 m-long. This segment partially matches with the 250 m investigated by Lenzi (2001), extending for over 70 m upstream. Specifically, the longitudinal profile was surveyed pre-event, post-event and in the current conditions (Fig. 3.2, Table 3.1). In these surveys, a uniform and consistent approach was used to measure the longitudinal profile. Particularly, a laser rangefinder (horizontal/vertical accuracy = 0.01 m) in conjunction with a target prism was used to measure the relative elevation and distance of each major breaks in the bed topography along the talweg of the Rio Cordon. Using such approach, 335, 149 and 220 points were measured pre-event, post-event and in the current periods, respectively. Therefore, the mean accuracy achieved was 1.05 points m^{-1} pre-event, 0.47 points m^{-1} post-event and 0.69 points m^{-1} in the current conditions.

Once obtained the longitudinal profiles, the analysis focused on the identification of step-pool units. A step-pool unit was defined as an accumulation of boulders or large cobbles separating an upstream backwater pool from a downstream plunge pool (Church and Zimmermann, 2007; Lenzi, 2001; Pampalone et al., 2021; Turowski et al., 2009). According to Lenzi (2001), only the step-pools that were part of a sequence of at least three consecutive units were considered. Hence, each step-pool unit was characterized in terms of step-pool height (H), step-step drop (Z), step-step spacing (L_s), pool-pool spacing (L_p) and mean slope (S) (Fig. 3.3). H and Z were measured considering the vertical distance while L_s and L_p were defined measuring the slope distance.

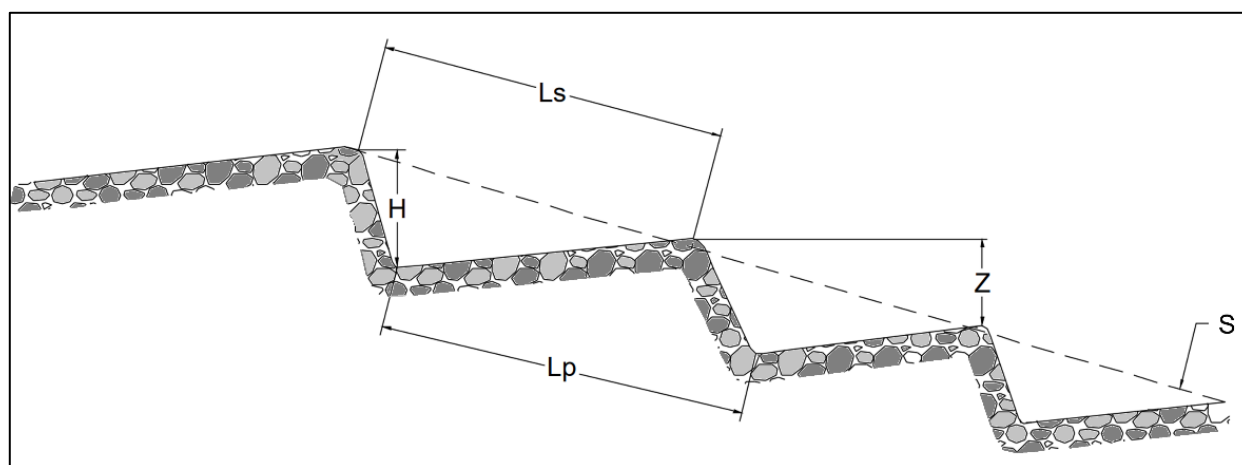


Figure 3.3. Graphical description of the variables analyzed in the step-pool sequence, i.e., the step-step drop (Z), step-pool height (H), pool-pool spacing (L_p), step-step spacing (L_s) and mean slope (S).

In this sense, only the step-pool units exhibiting $H > D_{84}$ of the pre-event grain size distribution were considered in the analysis. The use of D_{84} as minimum threshold is designed to operate an effective

identification of the step-pool configuration, relying on sedimentological feature of the study site. The step-pool sequences (SPS) were identified in clusters of three or more consecutive step-pool units, separated upstream and downstream by other channel forms for a distance of at least two times the mean bankfull width (10.6 m). Finally, to compute the steepness (Eq. 3.1) and non-dimensional steepness (Eq. 3.2) the following equations were used, according to Lenzi (2001) and Abrahams and Atkinson (1995):

$$\text{steepness} = \frac{H}{L_s} \quad (3.1)$$

$$c = \frac{\frac{H}{L_s}}{S} \quad (3.2)$$

Grain size distribution variation

To comprehensively understand the morphological evolution of the Rio Cordon over the study period, the surveys of planimetric variations and step-pool configurations were supported by the definition of the grain size distribution (GSD) of the Rio Cordon surficial material. The GSD analysis were made in the pre-event (Rainato et al., 2017), post-event and current conditions (Table 3.1). The three GSD analyses were conducted using the grid by number approach and sampling the surficial in-channel material along the most downstream part of study reach. Specifically, 326, 202 and 229 particles were collected and measured in the pre-event, post-event and current periods, respectively.

Table 3.1. Date and typologies of data used for the analysis.

Data	Pre-event	Post-event	Current conditions
Remote sensing device	LiDAR	LiDAR	UAV
Aerial photos	2015	2019	2020
Digital Elevation Model	2006	2019	2020
Grain Size Distribution	2014	2018	2020
Longitudinal profile	2015	2018	2020

RESULTS

Planimetric evolution

In the pre-event condition, the Rio Cordon active channel (Fig. 3.4A) covered an area of 3238.5 m² and was characterized by a mean channel width of around 10 m (Table 3.2). The talweg length was 350.8 m.

Table 3.2. Planimetric evolution of the study reach

	Talweg Length (m)	Mean channel width (m)	Active channel area (m ²)
Pre-event	350.8	10.3	3238.5
Post-event	352.5	18.6	5425.1
Current conditions	346.8	20.0	5993.8

After the Vaia storm event, the mean channel width and active channel area increased by 81% and 68%, respectively. Particularly, the former reached a value of 18.6 m while the latter registered around 5425.1 m². Furthermore, the talweg increased its length to 352.5 m (+ 0.48%). Compared to the post-event planimetric data, the current conditions exhibited further slight changes. The channel area increased by 10.5 %, covering an active area of 5993.8 m². Likewise, the width increased to 20.0 m (+7.5%). On the contrary, the talweg reduced its path by around 1.6%, registering a length equal to 346.8 m.

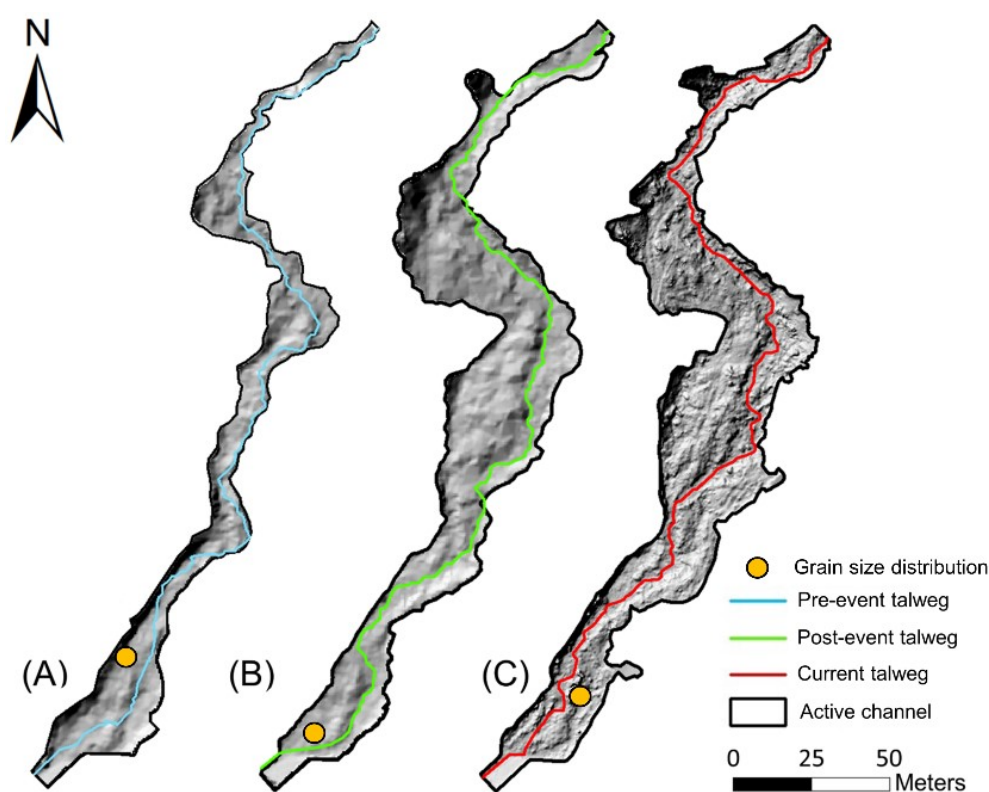


Figure 3.4. Visual planimetric changes of the active channel and talweg in the pre-event, post-event and current periods. The yellow dot identifies the area where the grain size analysis was realized.

Worth to mention, is the creation of an avulsion around 110 m upstream the outlet of the basin. Such area (Fig. 3.5) affected around 23.3 % of the post-event talweg length. Specifically, the avulsion measures 82.3 m and reduced the pre-event talweg length in that area by around 6 m (from 88.5 to 82.3 m).

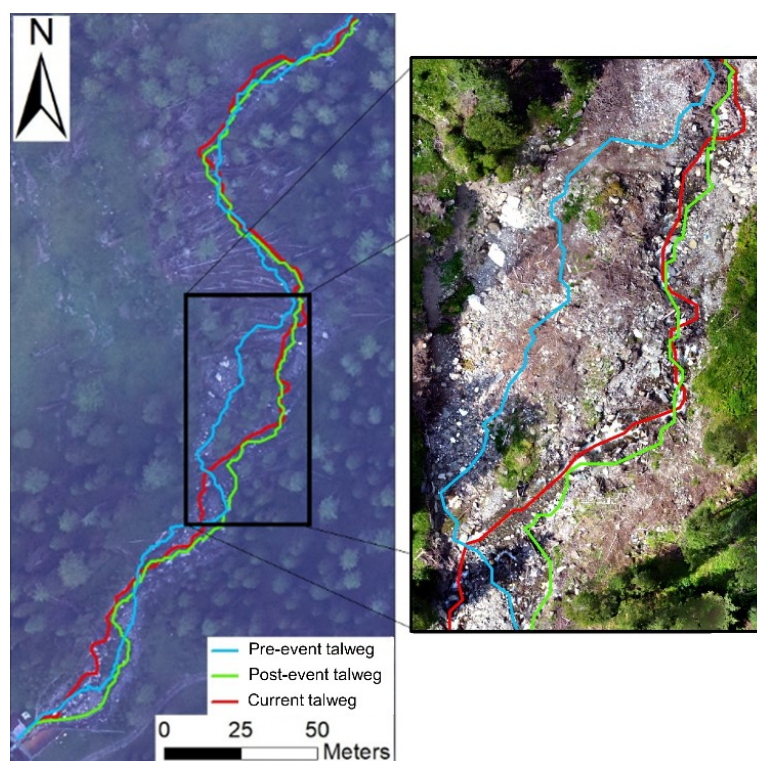


Figure 3.5. Visual planimetric changes of the talweg for the pre-event, post-event and current conditions. The aerial photo refers to the post-event condition. In the right part, a focus on the new avulsion created during the Vaia storm is shown.

Evolution of step-pool configuration

The number of step-pool units identified in the pre-event, post-event and current conditions was 51, 22 and 51, respectively. All investigated parameters exhibited a similar behavior over the study period, with larger L_s , L_p , H and Z in the post-event than in the pre-event situation. Hence, in the current conditions, these parameters showed a general decrease, returning to values very close to those observed in the pre-event (Fig. 3.6).

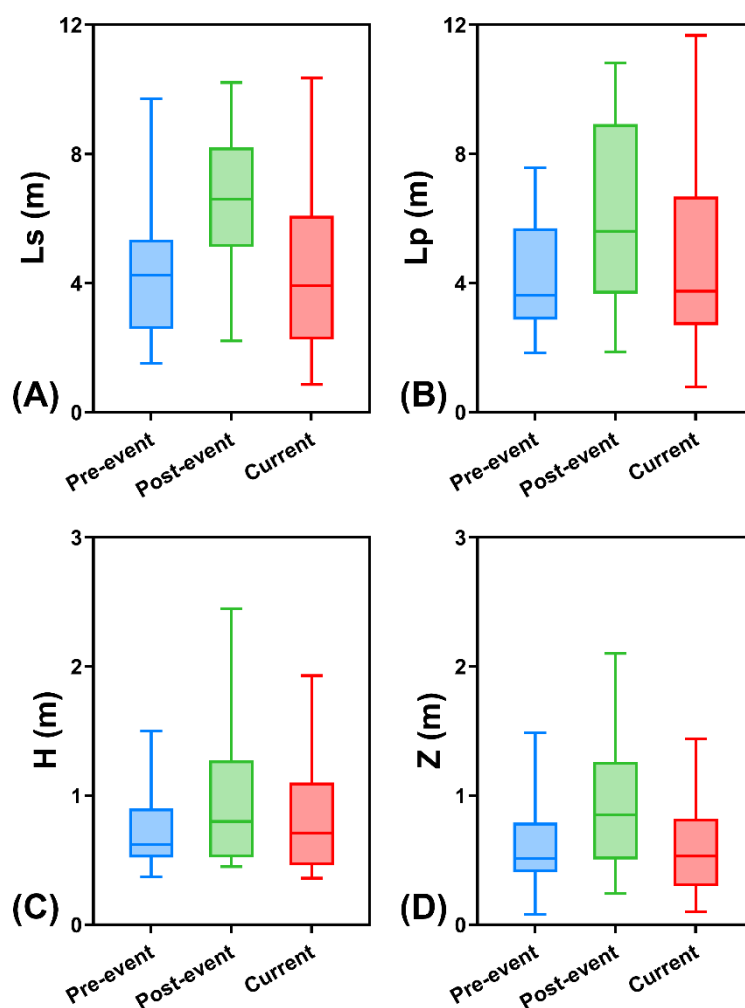


Figure 3.6. Distribution of (A) step-step spacing (Ls), (B) pool-pool spacing (Lp), (C) step-pool height (H) and (D) step-step drop (Z) values in the pre-event, post-event and current conditions.

A certain trend is observable also clustering the step-pool units in sequences (SPS). In the pre-event, in fact, 6 step-pool sequences were found, while post-event they decreased to 4. In the current conditions, instead, the sequences moved up to 8 (Table 3.3). Interestingly, the mean Ls, Lp, H and Z observed in the SPS showed, between the pre-event, post-event and the current conditions, a behavior similar to that identified in the units (Fig. 3.6). In fact, the average Ls observed in the step-pool sequences increased from 4.42 m in the pre-event to 6.80 m in the post-event (+ 53.9%) and, then, decreased to 4.07 m in the current conditions (- 40.2%). The mean Lp increased from 4.36 m to 6.68 m between the pre-event and post-event period (+ 53.3%), while in the current conditions was 4.23 m (- 36.7%). Similarly, H and Z showed higher mean values in the post-event than in the pre-event, increasing from 0.75 to 0.97 (+ 30.4%) and from 0.63 to 0.95 (+ 50.8%), respectively. Therefore, in the current conditions, both H and Z experienced a reduction in mean values, decreasing to 0.75 m (- 22.6%) and 0.54 m (- 42.8%), respectively (Table 3.3). Lastly, it is worth noticing that an opposite trend was appreciated in the mean slope of step-pool sequences, which exhibited S equal

to 0.14 m m^{-1} in the pre-event period, 0.13 m m^{-1} in the post-event (- 5.1%) and 0.15 m m^{-1} in the current conditions (+ 12.7%).

Table 3.3. Mean values of step-step spacing (Ls), pool-pool spacing (Lp), step-pool height (H), step-step drop (Z) and slope of each sequence (SPS) identified pre-event, post-event and in the current conditions.

		Mean Ls (m)	Mean Lp (m)	Mean H (m)	Mean Z (m)	S (m m^{-1})
Pre-event	SPS1	5.93	5.56	1.03	0.92	0.16
	SPS2	3.04	2.96	0.54	0.39	0.12
	SPS3	4.26	4.36	0.64	0.61	0.14
	SPS4	5.05	4.98	0.70	0.60	0.12
	SPS5	3.98	4.07	0.85	0.71	0.19
	SPS6	4.26	4.24	0.71	0.55	0.12
Post-event	SPS1	7.69	6.61	1.12	1.10	0.14
	SPS2	6.48	7.08	0.86	0.85	0.10
	SPS3	5.98	5.94	0.88	0.84	0.16
	SPS4	7.06	7.10	1.04	1.02	0.14
Current conditions	SPS1	4.06	3.36	0.86	0.64	0.17
	SPS2	5.67	5.63	0.80	0.64	0.12
	SPS3	5.72	6.57	1.04	0.66	0.12
	SPS4	1.52	1.59	0.57	0.37	0.24
	SPS5	2.51	2.23	0.75	0.46	0.19
	SPS6	5.75	6.40	1.12	0.82	0.16
	SPS7	4.04	4.83	0.41	0.29	0.07
	SPS8	3.28	3.23	0.49	0.49	0.14

The step-pool analysis also permitted to investigate the trend exhibited by the steepness over the study period. Specifically, the relationship between S and mean steepness (H/L_s) for each step-pool sequence observed pre-event, post-event and in the current conditions (Fig. 3.7) highlighted that the pre-event and, in particular, the current periods' sequences fit well the function $H/L_s = 1.5S$ (maximized flow resistance). Differently, the post-event sequences plot constantly lower. In this sense, the non-dimensional steepness (c) was 1.41 in the pre-event, 1.11 in the post-event and 1.44 in the current conditions.

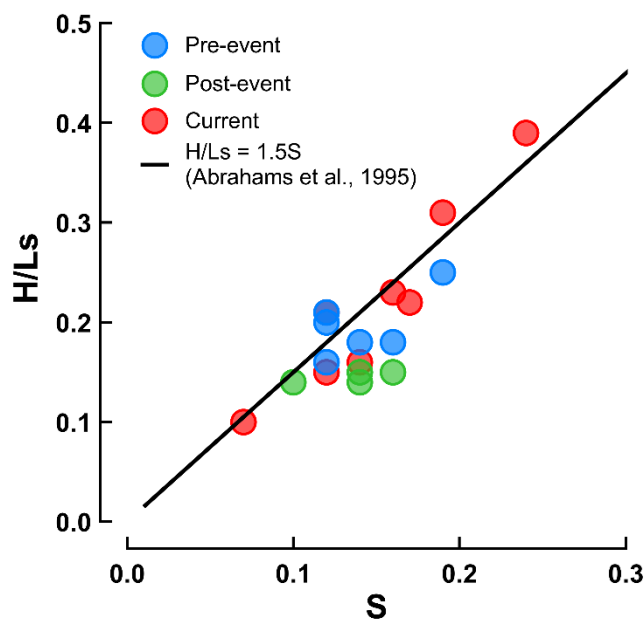


Figure 3.7. Relationship between S and mean steepness (H/Ls) for each step-pool sequence observed pre-event, post-event and in the current conditions. Black line is the function $H/Ls = 1.5S$ found by (Abrahams et al., 1995), describing the maximized flow resistance.

Variation in grain size distributions

Post-event, the grain size distribution of the Rio Cordon surficial material resulted overall finer than in the pre-event (Fig. 3.8). Particularly, the 16th (D_{16}), 50th (D_{50}) and 84th (D_{84}) percentiles were 29, 114 and 358 mm in the pre-event, decreasing to 26, 78 and 302 mm in the post-event. The GSD measured in the current conditions was comparable to that found post-event (Fig. 3.8). However, D_{16} , D_{50} and D_{84} equal 24, 76 and 423 mm suggesting a certain coarsening of the larger grain size fraction. Such tendency is explicated by the 84th percentile which increased by 40.1%.

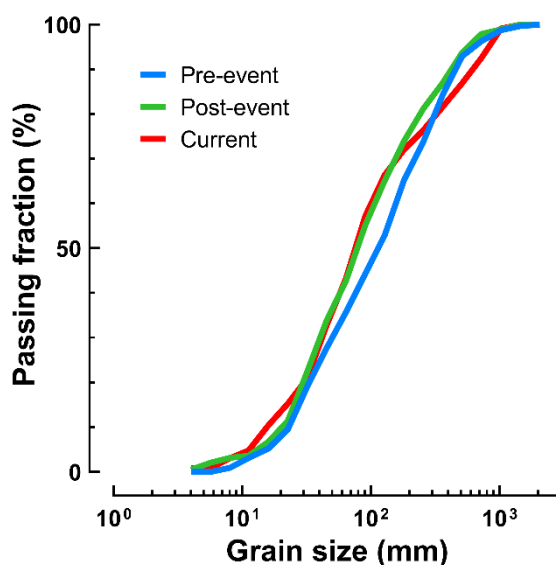


Figure 3.8. Grain size distributions of Rio Cordon surficial material measured pre-event, post-event and in the current conditions.

DISCUSSION

The pre-Vaia storm conditions, outlined by both the analysis on the pre-event planimetric pattern and GSD are to be considered the results of a long and stable phase of the Rio Cordon distinguished by persistent ordinary hydraulic forcing conditions (Rainato et al., 2020). In fact, prior to the Vaia storm, the only flood able to significantly modify the Rio Cordon morphology was registered in September 1994. However, this latter event, which registered a $Q_p = 10.40 \text{ m}^3 \text{ s}^{-1}$, affected more the hillslope rather than the main channel, creating numerous new sediment source areas (Pagano et al., 2019). Particularly, since the bedload transport of 1994 flood was around 7 times lower than the Vaia flood (Rainato et al., 2021), the stream changed substantially in terms of bedforms configuration but slightly in terms of planimetric pattern. Large planimetric changes, instead, were registered during Vaia, which created an 82.3 m channel avulsion close to the outlet of the basin (Fig. 3.9). In mountain fluvial systems, avulsion channel can be the result of the combination of different factors such as large flooding events and its consequent aggradation effect (Ashworth et al., 2004) that triggers the creation of a new and steeper channel (Brizga and Finlayson, 1994; Leenman and Eaton, 2021; Nanson and Knighton, 1996) able to provide new downstream pulses of sediment transport and yield (Sims and Rutherford, 2017). In the Rio Cordon, such changes go together with the increase of around 80% of the mean channel width and 68% of the channel area. Notwithstanding, the talweg length increased of only 0.48% featuring a relatively similar planimetric path. The talweg length increase documented in the Rio Cordon resulted lower than what experienced by the Erlenbach consequently to the 50-year flood of June 2007. In fact, such event induced an augment of 3.82% in the Erlenbach talweg length (Molnar et al., 2010). Interestingly, the increase of mean channel width detected in the Rio Cordon between pre- and post-event was in line with the range + 40% – 105% observed in the mountain Biała River consequently to an 80-year flood (Hajdukiewicz et al., 2016). However, it is worth comparing the widening observed in the Rio Cordon with that documented in the Grimmbach and Orlacher Bach after the May 2016 flash flood (Lucía et al., 2018). In fact, the larger (30 km²) and flatter (1.5%) Grimmbach mountain basin experienced a mean channel width increase (+ 590%) clearly higher than the Rio Cordon. Instead, the Orlacher Bach, which features basin area (5 km²) and stream slope (5.5 %) closer to the Rio Cordon, exhibited an increase of mean channel width equal to + 210 %. In this sense, it is worth noting that the widening in the Rio Cordon was induced by a unit peak discharge equal to $3.3 \text{ m}^3 \text{ s}^{-1} \text{ km}^{-2}$, notably lower than the $20.9 \text{ m}^3 \text{ s}^{-1} \text{ km}^{-2}$ expressed in the Erlenbach by the June 2007 flood and the $20.0 \text{ m}^3 \text{ s}^{-1} \text{ km}^{-2}$ experienced by the Orlacher Bach during the May 2016 flash flood, stressing the high geomorphic effectiveness of the Vaia storm in the alteration of main channel. Such hypothesis is supported also by the large variation experienced by the Rio Cordon in terms of active channel area (+ 68%).



Figure 3.9 Examples of planimetric changes experienced by the Rio Cordon in the (A) middle and (B) upstream part of the lower Cordon.

The planimetric changes observed between post-event and current periods resulted one order of magnitude lower than those registered between the pre and post-event. This result is mainly related to the persistent ordinary flow conditions occurred during the last years ($Q_p = 1.7 \text{ m}^3 \text{ s}^{-1}$). However, the capacity of these conditions to further augment the active channel area by 10.5% and the mean channel width by 7.5% seems to suggest that the geomorphic status of the Rio Cordon is still unstable after two years from the Vaia storm. Moreover, the current talweg reduced its length by around 1.6% implying a certain simplification in the channel path, especially in the downstream part of the study reach (Fig. 3.4C). Interestingly, this result is consistent to what observed in the Erlenbach after 3 years from the large June 2007 flood. During these 3 years (2007-2010), the Erlenbach experienced only ordinary floods, reducing the talweg length by 4.74% and restoring similar values to those of the pre-2007 period (Molnar et al., 2010). In the Rio Cordon, worth mentioning is the degree of uncertainty given by the two different technique of remote sensing data acquisition, precisely between the LiDAR and SfM from UAV technology. Although both provide high-resolution products, SfM DEMs and aerial photos offer lower cell dimension, reducing considerably the possible errors made by the operators in measuring the planimetric features of the channel. On the contrary, LiDAR technology offers more reliability when filtering the water and vegetation cover (Smith et al., 2016). In the end, despite the analysis was carried out by the same operator, the two different data sources might have affected the results of the present work.

The changes in the planimetric pattern of the Rio Cordon led to the alteration of the step-pool configuration. In this sense, the step-pool investigation realized between the pre-event and the current condition can be compared with the analysis made by Lenzi (2001) during the period 1993-1998, offering the rare opportunity to understand how the step-pool configuration can respond to different large floods. Interestingly, the increase observed in L_s (+ 53.9%), L_p (+ 53.3%) and H (+ 30.4%) after the Vaia storm resulted higher than the + 22.7 %, + 36.7 % and + 2.1% documented by Lenzi

(2001) as consequence of September 1994 event. This different response can be ascribed to the different magnitude of the two flood events, in particular in terms of flood duration (Rainato et al., 2021). However both cases, fall within those exceptional floods that (Turowski et al., 2009) highlighted to be able to generate total step-pool alteration. The same authors, in fact, demonstrated that 40- and 50-year floods in the Erlenbach were capable of disrupting the step-pool morphology, while a 27-year event produced only a partial alteration of this bedform configuration. This also matched with Beylich and Sandberg (2005), who proved that an extreme rainfall event caused the step-pool system failure in the Latnjavagge basin. Particularly, in the Rio Cordon, the removal of the step-pool units by the Vaia storm seems to be attributable to the outstanding hydraulic forcing conditions that produced also boulder mobility (Rainato et al., 2021). Such conditions suggest that the direct entrainment of the keystone and the impact of these by large particles could have been the main processes by which the steps were removed. Such hypothesis would support what documented in the Erlenbach by Turowski et al. (2009) as well as the flume experiments made by Zhang et al. (2018), in which the motion of keystone accounted for 90% of the total step-pool failure events.

The Ls (- 40.2%), Lp (- 36.7%) and H (- 22.6%) variations detected after 2 years from the Vaia storm (current conditions) were in line to those revealed 4 years since the September 1994 event. In fact, in 1998-1999, Lenzi (2001) found - 36.4% in Ls, - 36.7% in Lp and - 19.1% in H. Therefore, these results seem to suggest that after October 2018 flood, the Rio Cordon is recovering the step-pool configuration faster than after September 1994 event, likely due to the post-event hydraulic forcing. In fact, the period between the post-event and the current situation was characterized by persistent under-bankfull flows ($Q_p = 1.7 \text{ m}^3 \text{ s}^{-1}$). Differently, the post-large flood period (1994-1999) analyzed by Lenzi (2001) featured an over-bankfull flood ($Q_p = 4.7 \text{ m}^3 \text{ s}^{-1}$) that can have further disturbed the re-establishment of step-pool configuration. In 2020, the decrease in Ls, Lp, H and Z may also be caused by the large widening experienced by the Rio Cordon, which, combined with the persistent ordinary flow conditions, can have promoted flow velocity reduction over the step-pool units and, then, prevalence of deposition over erosion (Liro et al., 2020). This dynamic may have further supported by the large sediment availability characterizing the post-event period. Interestingly, the step-pool responses observed in the Rio Cordon differed from what document in the Erlenbach after the large June 2007 event (Molnar et al., 2010). In fact, this latter event has not substantially changed the mean step height and the mean step spacing, but strongly increased their variability. Also, in 2010, after 3 years of ordinary flow conditions, the Erlenbach step-pool configuration showed an increase of 4.41% and 8.86% in the mean step height and the mean step spacing, respectively. Therefore, the Erlenbach exhibited a different response in terms of step-pool evolution, in particular, in the variations induced by the ordinary flow conditions. This stresses how

the step-pool configurations can respond in a complex way to the different hydraulic forcings, especially, if they were previously altered by large flood events. However, the step-pool recovery currently observed in the Rio Cordon is consistent to what found in the Lainbach by Gintz' et al. (1996), who noticed the re-established of this bedform configuration two years after an exceptional flood event. In addition, the trend exhibited by the steepness and by the non-dimensional steepness (c) seems to confirm it. Particularly, the decrease of c from 1.41 (pre-event) to 1.11 (post-event) stressed, further, how Vaia flood has destabilized the step-pool morphology, which after that event has shown a more disorganized pattern. However, c equal to 1.44 (current conditions) pointed to a return to a more stable bedform configuration, with a c very close to 1.5, i.e., a condition of maximized flow resistance and well developed armour layer (Lenzi, 2001; Comiti et al., 2009; Turowski et al., 2009). As for the analysis on the planimetric patterns, the results obtained for the step-pool evolution include some uncertainty related to the methodological technique applied. For instance, the post-event longitudinal profile was built on fewer points per meter because it was surveyed in the weeks immediately after the Vaia flood, i.e., in highly unstable streambed conditions and with the presence of over 130 trees uprooted and laying perpendicularly to the main channel that made field activities particularly difficult and dangerous (Picco et al., 2020). However, we assume that the survey was good enough to provide information related to the step-pool configurations.

In light of the results achieved, it is evident how Vaia caused an evident expansion of the active channel (mean channel width and mean active channel area), to which the step-pool configuration responded by increasing its spacing (L_s , L_p) and height differences (H , Z). Moreover, the flood event triggered a general fining of surficial material of Rio Cordon (Fig. 3.8). Differently, the persistent under-bankfull flow conditions occurred after Vaia flood induced no significant variations in the GSD apart from an increase in the coarse fraction of the distribution ($> D_{70}$). As above-mentioned, even the planimetric pattern responded modestly to 2 years of ordinary flow conditions, which, instead, induced a significant change in the step-pool units and sequences that returned to a configuration very similar to the pre-event. This result seems to suggest that, in the Rio Cordon, the outstanding hydraulic forcing expressed by Vaia were capable to totally altering the fluvial system, while the under-bankfull flow conditions occurred after such event acted on the step-pool configuration but not significantly on the streambed grain size and on the planimetric pattern. Such conclusion is in line with Rainato et al. (2020), who stressed that even low hydraulic forcing conditions can influence the fluvial system, acting in particular on the setting of streambed material. To conclude, in a future scenario, with more frequent extreme events, understanding the primary response of mountain step-pool streams to diverse flood magnitudes will be a major topic in terms of both management strategies and ecological purposes. In this sense, this work offers the rare chance

to investigate the morphological response of a mountain step-pool stream to a large and infrequent flood as well as its evolution two years after that event. Furthermore, thanks to a long-term monitoring programme it was possible to compare the results to a previous exceptional flood in the same catchment.

CONCLUSIONS

This study presents the response of a step-pool mountain stream to an exceptional flood and its evolution during two years of ordinary flow conditions. The results provide evidence of step-pool destruction and recovery. Specifically, the analysis on the planimetric patterns suggested clear changes in both the width and the talweg path of the Rio Cordon. Such consequence led to an in-channel morphological alteration. In fact, significant changes have emerged between the analysis on the pre-event, post-event and current step-pool configuration. A distinct increase on the value of the step-pool descriptive parameters, as well as a decrease in the number of sequences immediately after the Vaia storm was highlighted. Furthermore, an ongoing process of morphological stabilization after two years from the large disturbance was identified. The data registered concerning L_s , L_p , Z and H , in fact, are heading back to the pre-event values. Therefore, our results underline that the step pool morphology can be destroyed only by large exceptional events and can recover even during a 2 years period of ordinary flow conditions.

However, the comparison of the results with worldwide studies concerning step-pool alteration and recovery from large infrequent disturbances, highlighted evidence of complex and non-univocal responses. Therefore, further verification of such dynamics are required. We suggest to apply future flume and field experiments to both compare and validate such impacts and the cascading processes occurring in a mountain step-pool stream after an exceptional flood event.

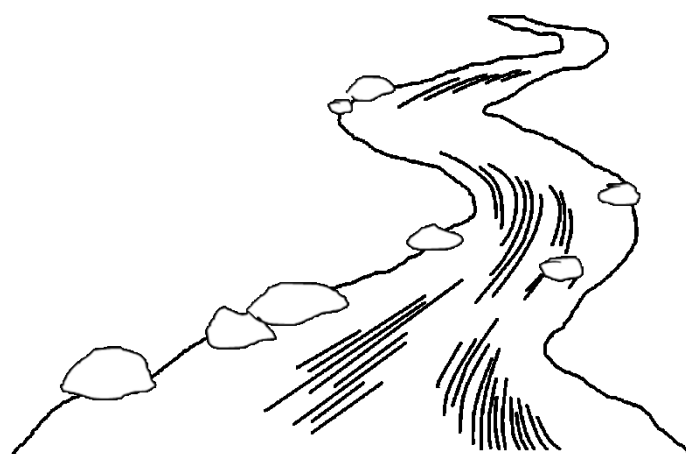
Chapter 4.

Surprising suspended sediment dynamics of an alpine basin affected by a large infrequent disturbance

Giacomo Pellegrini, Luca Mao, Riccardo Rainato, Lorenzo Picco

This chapter was published as Giacomo Pellegrini, Luca Mao, Riccardo Rainato, Lorenzo Picco (2023). Surprising suspended sediment dynamics of an alpine basin affected by a large infrequent disturbance. *Journal of Hydrology*, 617, 128933.

doi: 10.1016/j.jhydrol.2022.128933



ABSTRACT

In many environments, climate change causes an increase in the frequency and magnitude of Large Infrequent Disturbances (LIDs). LIDs make fragile areas, as mountain basins, even more vulnerable, along with local communities that could be severely affected by extreme events. Among all LIDs, windthrows are one of the most relevant and yet rather unpredictable disturbances affecting the Alpine region. Windthrows can affect the forest cover and morphological settings at the basin scale, changing the supply of sediments to river networks and affecting the sediment cascading processes. This work aims at (i) identifying the contribution of Suspended Sediment Load (SSL) from a windthrow-managed-affected area induced in an Alpine basin by a recent LID (Vaia rainstorm, 2018), (ii) assessing the annual, seasonal and monthly variation in the SSL, and (iii) analysing the changes in SSL fluxes and dynamics in the 2nd and 3rd year after the LID in comparison to those detected after a similar high magnitude event occurred in 1994. To do so, two multiparameter sondes measuring the water level and the turbidity were installed upstream and downstream the windthrow-affected area. Discharge measurements and water samples were collected to obtain the rating curves and calibrate the turbidity meters in order to derive suspended sediment loads (SSL). The results show that the windthrow-affected area was significantly contributing suspended sediment during events occurring two years after Vaia (2020) but less intensively in those occurred three years after the event itself (2021). Both the events average intensity rainfalls and the total precipitation appear to be the best predictors of both the peak of suspended sediment concentration (SSC_p), the total suspended sediment (SSL) and the suspended sediment percentage variation among the two cross-sections. The seasonal and monthly analysis revealed to be in line with those detected prior the disturbance. The analyzed LID affected the transport efficiency for near-bankfull events but not the annual sediment yield as it was found after the previous high magnitude flood event recorded in 1994. Unexpectedly, the mean rate of SSL ($42 \text{ t km}^{-2} \text{ yr}^{-1}$) is indeed comparable with what monitored during the decade before Vaia (2004-2014) ($40 \text{ t km}^{-2} \text{ yr}^{-1}$). Such surprising results may be explained by the fact that the Rio Cordon basin have had an alluvial response rather than colluvial during the Vaia rainstorm event and that the basin's resilience may be in a different stage as compared to the one of 1994, when the catchment featured different cascading processes that completely overturn the suspended sediment dynamics and fluxes for about a decade.

Keywords: Vaia rainstorm; Suspended sediment; Cascading processes; Mountain basin resilience

INTRODUCTION

The ongoing climate changes bring with them an increase in the frequency and magnitude of Large Infrequent Disturbances (LIDs, Foster et al., 1998). LIDs make fragile areas more vulnerable, especially mountain environments that are indicators of the planet Earth's responses to climatic changes (Pepin and Lundquist, 2008) and, particularly, when analysing the instability processes due to hydro-climatic hazards (Diodato et al., 2018). Most mountain basins drain into steep channels that are thus affected by changes in processes and dynamics especially related to runoff generation (e.g., rainfall, snow and glacier melting) and sediment production and delivery (Rainato et al., 2017), influencing the quantity, timing and size of material transported downstream (Yager et al., 2012). The occurrence of large disturbances, as high magnitude floods, determines, in a short time, large transport of coarse sediments but also cohesive soil and vegetation. This overturns the entire equilibrium of a basin system, renewing the availability of sediment and adjusting the pre-existing trend of transport processes and dynamics (Nanson and Huang, 2018).

Sediment transport is commonly classified into bedload and suspended load (Einstein et al., 1940; Turowski et al., 2010). Suspended sediment transport refers to sediments displaced for long distances within the water column, and not interacting with the channel bed (Einstein et al., 1940; Misset et al., 2021), although the fine fraction may also originate directly from the riverbed resuspension (Park and Hunt, 2017). The suspended sediment is the result of the interplay between different factors such as the impacts of natural and anthropogenic disturbances, thus climatic conditions, rainfall intensities, catchment topography (i.e., size and slope), geology and streambed stability (Soler et al., 2008; Mills and Bathurst, 2015; Picco et al., 2016; Mao and Carrillo, 2017; Pagano et al., 2019). The interactions among these factors change according to different spatial and temporal scales. However, the current changes in climate are expected to affect the suspended sediment contribution along worldwide mountain catchments, entailing alteration in the river system functioning. In fact, the increase in frequency of large disturbances, as well as the decrease in ordinary events (i.e., snowmelt and rainfall events) (Bakker et al., 2018; Comiti et al., 2019) is expected to completely rearrange the dynamic equilibrium of the mountain systems (Misset et al., 2021). Therefore, it is becoming even more important to study the suspended sediment dynamics, to understand soil degradation processes (Nadal-Romero et al., 2013) and to analyse and predict the future ecological status of the riverine environment (Albers and Petticrew, 2013). Recent literature shows that in Alpine streams the suspended sediment is typically transported during flood events (Pagano et al., 2019). However, the relationship between the suspended sediment concentration (SSC) and water discharge (Q) is dependent on many factors such as particle size, basin topography, erosional activity, bed morphology and hydraulic processes (Mouri et al., 2014; Sun et al., 2016; Mao

and Carrillo, 2017). Alpine catchments behave differently in different seasons due to limited sediment availability in winter (i.e., inactive hillslope processes; Bača, 2008; Recking, 2012; Rainato et al., 2017) and diverse sediment contributions among the spring and summer-autumn seasons (i.e., snowmelt vs. rainfall events; Rainato et al., 2017; Pagano et al., 2019). Nonetheless, the SSC-Q relationship differs also between and within single events (Williams, 1989; Mao, 2004; Seeger et al., 2004) showing a hysteretic pattern (García-Rama et al., 2016). Hysteresis can be clockwise or counterclockwise (e.g., Williams, 1989; Lenzi and Marchi, 2000; Gao and Josefson, 2012; Yeshaneh et al., 2014). In the former case, the SSC peak (hereinafter SSC_p) occurs before the Q peak (hereinafter Q_p), whereas in the latter, the SSC_p occurs after the Q_p (Mao and Carillo, 2017). At the scale of a single flood event, several studies associated clockwise hysteresis to nearby sediment sources, exhausted sediment sources and resuspended channel bed sediment (e.g., Asselman, 1999; Rovira and Batalla, 2006; Gao and Pasternack, 2007). Counterclockwise hysteresis is, instead, associated to suspended sediment coming from sediment sources far away from the monitoring site (Klein, 1984), bank failures (Rinaldi et al., 2004; Mao and Carillo, 2017) and condition of sediment exhaustion in the entire riverine system. Aich et al. (2014) developed a quantitative metric to quantify the degree of hysteretic loops, providing an index based on the size and direction of the loop itself. The idea of using normalized values of SSC and Q, improved the possibility of comparing events of different areas (Mao and Carillo, 2017). In this sense, suspended sediment contribution from anthropogenic practices (i.e., mining, land use, forest operation etc.) seems to cause considerable disturbance to the channel fluxes (Gomi et al., 2005; Glendell and Brazier, 2014) although, the major portion of suspended sediment fluxes in mountain streams is commonly provided by large rainfall events (Coynel et al., 2004; Moatar et al., 2006; Duvert et al., 2011). Therefore, in the context of climate change, where large disturbances are becoming more frequent and challenging to predict (Yildiz et al., 2022), a better understanding of sediment fluxes during and after extreme events is needed in order to improve land management and adaptation practices. This work aims at fulfilling this gap, analysing an Alpine basin throughout the first 2-3 years following the catastrophic Vaia rainstorm event (Rainato et al., 2021; Pellegrini et al., 2021a). More specifically, it focuses on (i) identifying the contribution of SSL from a windthrow-managed-affected area caused by the Vaia event in an alpine basin, (ii) quantifying the annual, seasonal and monthly variation of SSL, and (iii) analysing the changes in suspended sediment fluxes and dynamics in the 2nd and 3rd year after Vaia and in comparison to those detected after a similar high magnitude event occurred in 1994.

MATERIAL AND METHODS

Study area

The Rio Cordon basin is an alpine catchment located in the Northeast of Italy (Dolomites) (Fig. 4.1A). It has an extension of 5 km² with an altitude ranging between 1763 m a.s.l. and 2763 m a.s.l. and a mean slope of 27°. On the one hand, dolomite, and volcanic rocks (Wengen formation) compose the geology of the upper part of the basin, on the other hand, sandstones and calcareous-marly rocks (Buchenstein formation) feature the lower part. Alpine pastures cover most part of the basin area (61%), followed by shrubs (18%), bare lands (14%) and Norway spruce forests (*Picea abies*) (7%) (Oss Cazzador et al., 2020). Overall, the basin can be divided into three different physiographic and altimetric areas: the upper part constituted by exposed dolomites rocks, the middle flat one confined by a waterfall and belonging to the Wengen formation group and the lower part that is, from a sedimentological point of view, completely disconnected from the mid one and that is characterized by Buchenstein formation and quaternary deposits. In this area, the active channel featured cascade step-pool and riffle-pool morphologies.

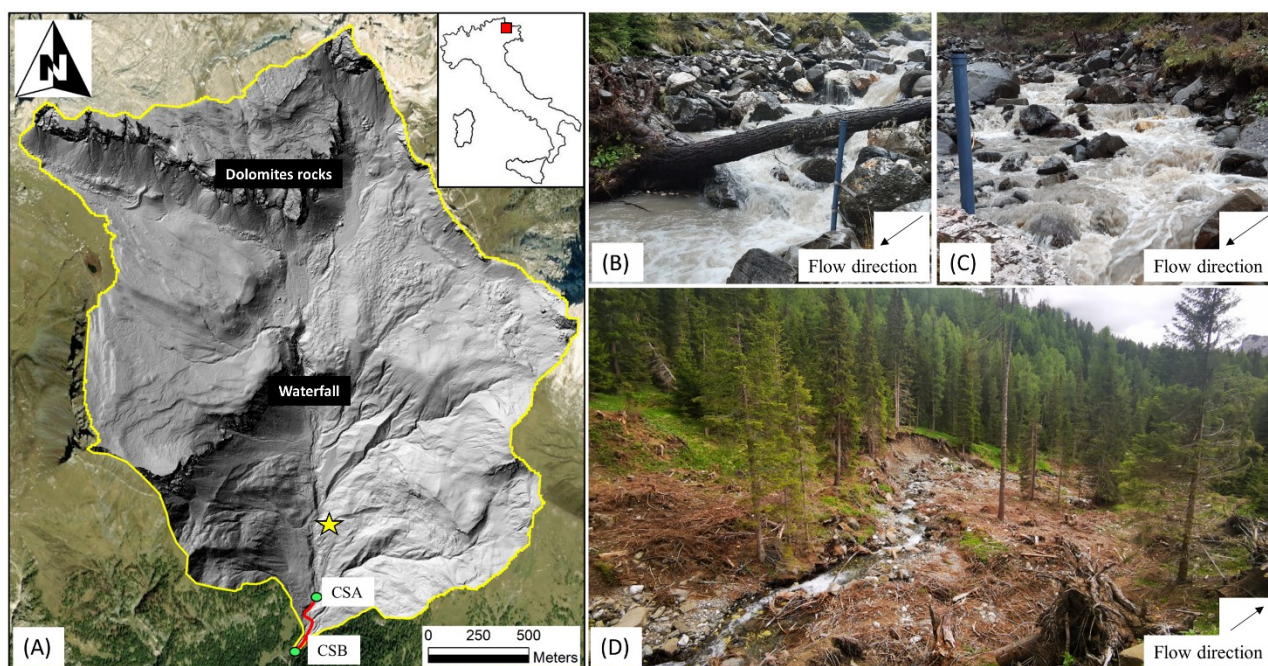


Figure 4.1. (A) Rio Cordon basin is located in the northeast of Italy. The presence of dolomites rocks and of a waterfall divides the basin into 3 physiographic zones: exposed dolomites rocks area (upstream), middle flat area (between dolomites and the waterfall) and lower area (downstream the waterfall). The yellow star indicates the location of the S-RGD-M002 Davis Rain Gauge Smart Sensor while the green dots indicate the two cross sections monitoring sites (CSA and CSB), captured in (B) CSA and (C) CSB which is located 10 m upstream the permanent monitoring station. The red stripe indicates the channel reach affected by windthrows and pictured, almost entirely, in (D).

The bankfull width and discharge are 5.3 m and 2.3 m³ s⁻¹ (Lenzi et al., 2006; Rainato et al., 2020), respectively. Between 1986 and 2018, the mean annual precipitation was around 1180 mm (Pellegrini et al., 2021b) while the mean temperature (2010 – 2021) was 3.9 °C. The Rio Cordon

basin features a nivo-pluvial regime, favouring snowfalls either during the early autumn, winter season and early spring or short and intense rainfall events during the rest of the year. A permanent station for a long-term monitoring program was installed in 1985 and allowed to characterize the climatic, hydrological, and sedimentological dynamics acting in this alpine basin (Fattorelli et al., 1988). Before the occurrence of Vaia rainstorm, the largest flood ever recorded at the experimental station occurred on 14th September 1994. It was a flash flood of an estimated return interval of 60 years, triggered by an average event rainfall intensity of 16 mm h⁻¹, which produced a peak water discharge of 10.4 m³ s⁻¹ (Lenzi et al., 2003). These conditions caused the transport of over 900 m³ of bedload (Picco et al. 2012) and 2432.9 t of suspended sediment load. However, the long-term monitoring program was interrupted in the Rio Cordon in October 2018 due to the occurrence of another large disturbance (i.e., the Vaia rainstorm).

Vaia rainstorm description

Between 27th and 30th October 2018, the Rio Cordon was highly affected by the Vaia rainstorm event (Chirici et al., 2019; Pellegrini et al., 2021b; Rainato et al., 2021). Along the entire Northeast of Italy such event caused over 41,000 ha of forest loss, and activated landslides, debris flows, floods and damages to villages, hydraulic structures and infrastructures. Indeed, wind gusts exceeding 200 km h⁻¹ (afternoon and evening of 29th October 2018) and cumulative precipitation over 500 mm were registered (Davolio et al., 2020; Giovannini et al., 2021). For the Rio Cordon, the analyses of Rainato et al. (2021) reported that the Vaia-induced precipitation was equal to 352 mm and lasted 80 h. The maximum intensity between the 6h and 72h characterized the event with a recurrence interval (RI) of > 50 years. During the event, however, a hiatus of around 9 h was detected. Such interruption permitted to split the event into two distinct phases. The first lasted 36.8 h and summed around 200 mm of rain, while the second lasted 34.2 h and counted over 150 mm. Although the lower amount of precipitation, the second phase registered the highest value of peak discharge, 16.4 m³s⁻¹, exceeding 100 years of RI (Rainato et al., 2021). These conditions caused a bedload volume of about 6800 m³. Overall, the event created and reactivated over 25 new sediment sources among landslides, debris flows channels and bank erosions (Martini et al., 2022). However, only 7 (5 landslides and 2 debris flows) sediment sources resulted as functionally connected to the channel network and, therefore, able to actively contribute in terms of sediment (Martini et al., 2022). Such analyses highlighted the fact that the Rio Cordon has had a predominant alluvial response, especially in the lower part where the morphology of the channel was completely naturally restructured (Rainato et al., 2021). In addition, 139 trees of *Picea abies* were blown down and uprooted (Picco et al., 2020), producing large and intense bank failures. In summer 2019, forest operations were made to remove the entire material

leaving the slopes completely bare (Fig. 4.1D) and with huge amounts of loose fine material (Pellegrini et al., 2021b).

Discharge and sediment monitoring

The discharge and sediments monitoring were conducted in two different cross sections (Fig. 4.1), one upstream (hereafter CSA) and one downstream (hereafter CSB) the windthrow-affected area. CSA and CSB are spaced 300 m and are located in a reach of the Rio Cordon characterized by the absence of tributaries. Since the end of August 2020, two multiparameter water quality sonde (OTT Hydrolab MS5 and Hydrolab HL4) were installed in order to monitor turbidity within a range between 0 and 3000 NTU ($\pm 1\%$ up to 100 NTU; $\pm 3\%$ from 100 to 400 NTU; $\pm 5\%$ from 400 to 3000 NTU) (Mao and Carrillo, 2017). Similarly, two pressure transducer sensors were mounted to monitor the water level (m) across two cross-sections rather stable due to the presence of large boulders. Additionally, rainfall information was obtained through a S-RGD-M002 Davis Rain Gauge Smart Sensor ($\pm 4.0\%$ accuracy). Rainfall, water levels and turbidity data were acquired with a 15 min resolution. To establish the two rating curves among the water level and the discharge, 30 and 28 discharge salt dilution measurements were realized in CSA and CSB, respectively. To this end, a variable quantity of 0.25 and 0.50 kg of NaCl mixed to stream water was used as tracer (Comiti et al., 2007), while a portable conductivity meters (WTW Cond340i) was used to record the electrical conductivity variations. Then, the discharge was computed according to Moore (2005), obtaining a range of 0.07-1.54 m³ s⁻¹ and 0.07-1.61 m³ s⁻¹ in CSA and CSB, respectively. The obtained water level-discharge rating curves exhibited a coefficient of determination (R²) of 0.89 in CSA and 0.85 in CSB (Fig. 4.2). Moreover, 24 water samples were collected in order to derive an empirical relationship between NTU and suspended sediment concentration (SSC g l⁻¹) applicable to both CSA and CSB. The samples were collected randomly during the rainfall events of the monitoring period and covered a range of NTU between 1 and 2109 (Fig. 4.2C). The collected samples were filtered through a fiberglass filter, dried at 105 °C and quantified as concentration of suspended sediment in g l⁻¹. The power-law empirical regression fitted with a coefficient of determination (R²) equal to 0.92. The monitoring activities ended in November 2021, defining a monitoring period of 16 months (August 2020 – November 2021).

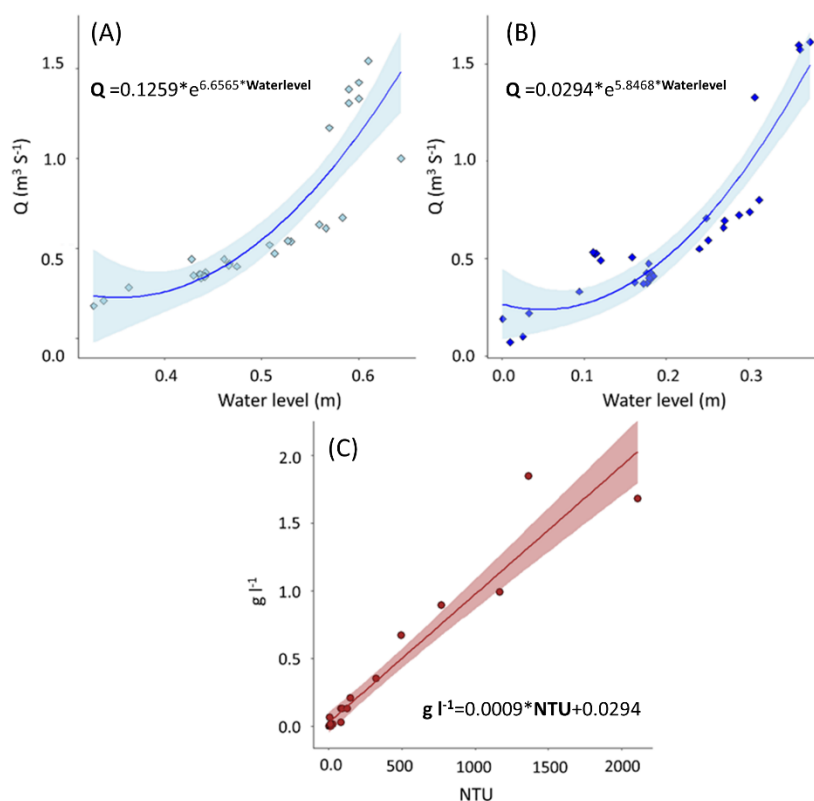


Figure 4.2. Discharge rating curves of the (A) CSA and (B) CSB cross sections. (C) represents the empirical relation $\text{NTU}-g \text{ l}^{-1}$ for both sites derived through field and laboratory analysis. On the one hand the range of Q in CSA is $0.07-1.54 \text{ m}^3 \text{ s}^{-1}$, while the water level covers a range between 0.33 m and 0.64 m . On the other hand, the range of Q in CSB is $0.07-1.61 \text{ m}^3 \text{ s}^{-1}$, while the water level is between 0.01 and 0.38 m .

Dataset preparation and analysis

To investigate the suspended sediment dynamics acting in the two monitored cross-sections, the analysis was divided into four different timescales: event, month, season and annual. Regarding the flood event, the starting and ending point of the flood were defined when the following dynamics were verified: (i) a significant and fast increase in the water discharge and (ii) a water discharge call-back to the initial flow (Fig. 4.3). In this sense, the analyses focused on 8 isolated flood events (hereafter FE1 to FE8) and considered precipitation, discharge and suspended sediment transport (see in Table 4.1). Because one of the aims was to detect changes among the area upstream (CSA) and downstream (CSB) the windthrow-affected area, the variables presented two sets of data, one for CSA and one for CSB (Fig. 4.1), respectively.

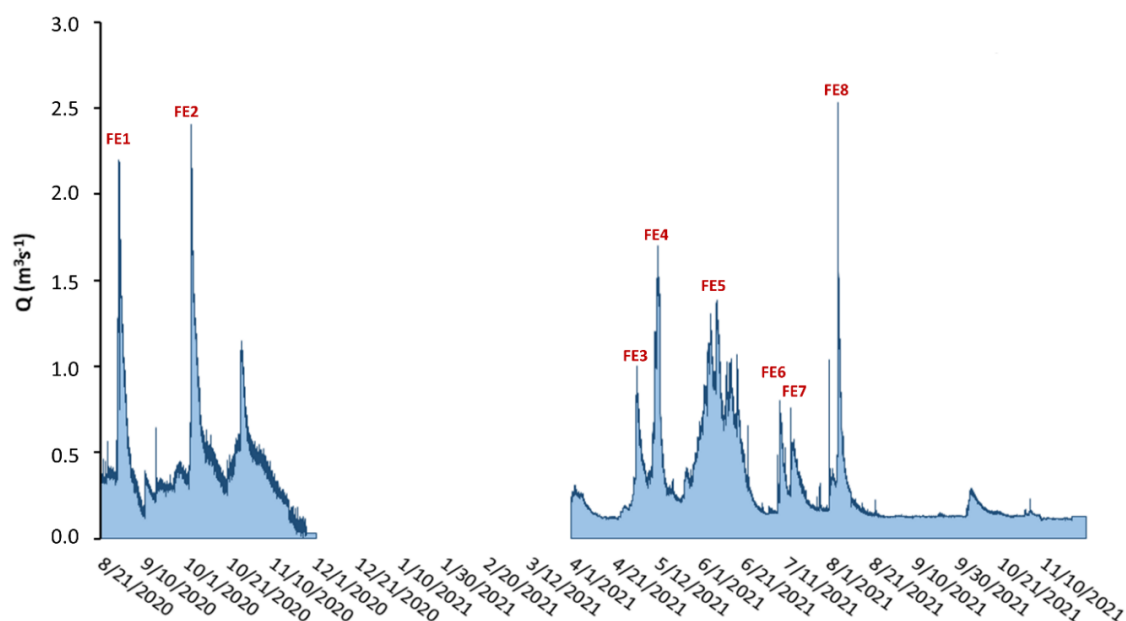


Figure 4.3. Water discharge experienced by the Rio Cordon in CSB during the monitoring period (August 2020 - November 2021). The discharge was determined using the procedure explained in section 2.3. FE1 – FE8 identify the 8 flood events analysed. The gap in the time series refers to the winter season 2020-2021, period in which the instrumentation were removed due to icing conditions.

For each cross section and event, descriptive statistical analysis and their correlation matrices were produced. To this end, the Pearson correlation test (hereinafter *cor.test*) with a level of significance equal to 95% was used using R Studio 2022.02.0. Moreover, the hysteresis relationship between Q and SSC was described. Both the shape (circular or eight-shaped) and the loop (clockwise or counterclockwise) of the hysteretic cycles were used to classify the events. Additionally, to quantitatively assess the degree of hysteresis, the index proposed by Aich et al. (2014) was used. The normalized values of Q and SSC were computed as to define a line starting from the value of Q_p and ending at the last value of the temporal series. Thus, the final value of the index (H) is computed summing the distances from the farthest SSC value in the rising and falling limb of the loop (Mao and Carrillo, 2017). The positive or negative values of the index (H) define whether the loop is clockwise or counterclockwise, respectively. Moreover, the data were used to provide information concerning the variations of SSL between the two cross sections. The results were then used to verify whether or not a regression among the percentages variation of SSL and hydrological data could be determined.

Furthermore, the analysis conducted at a month and seasonal scale took into consideration each month (16 months, from August 2020 to November 2021) of the monitoring period and the three main seasons: snowmelt (1st April- 15th June), summer (15th June-31st August) and autumn (1st September – 30th November). The dates of starting and ending periods of the seasons were retrieved by Rainato et al. 2017. To this end, only the data provided by the downstream section (CSB) were

used in order to provide possible comparisons with the historic suspended sediment budget measured at the measuring station.

Table 4.1. Variables investigated in the flood events

Flow event parameters	
Q_p ($m^3 s^{-1}$)	Peak discharge
Q_m ($m^3 s^{-1}$)	Mean water discharge
R_u ($10^3 m^3$)	Total runoff
SSC_p ($g l^{-1}$)	Suspended Sediment Concentration at peak
SSC_m ($g l^{-1}$)	Mean Suspended Sediment Concentration
SSL (t)	Total suspended sediment load (as $SSC \cdot Q \cdot \text{time interval}$)
P_{tot} (mm)	Total precipitation
I_{max} ($mm h^{-1}$)	Maximum hourly precipitation intensity
I_{av} ($mm h^{-1}$)	Mean hourly precipitation intensity
Δt (BSSC-BQ) (h)	Time lag between SSC_p and Q_p

RESULTS

Upstream (CSA) and downstream (CSB): comparing correlation matrices and changes in the sediment contribution at event-scale

During the eight events registered, CSA featured different variables as descriptors of the suspended sediment transport (Fig. 4.4A, Table 4.2). Taking the SSC_m into consideration, significant correlations (cor.test, p-value <0.05) were found with the precipitation i.e., with P_{tot} , I_{max} and I_{av} . However, the P_{tot} and the I_{av} were found significant (cor.test p-value<0.05) when taken into account also the SSC_p . The latter was also highly correlated (cor.test p-value<0.05) with SSC_m variable. When concentrating on the hydrological variables instead, the descriptors for the Q_p were the P_{tot} and the I_{av} , respectively. P_{tot} and I_{av} were mutually correlated.

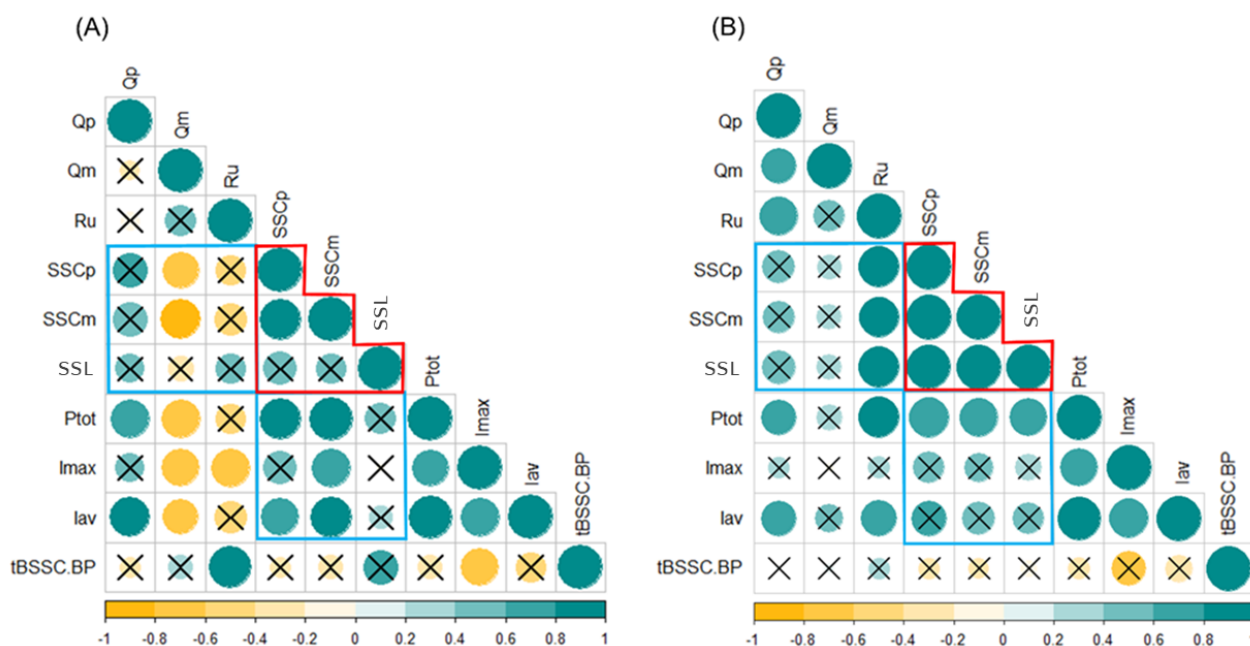


Figure 4.4. Correlation matrices obtained in CSA (A) and CSB (B). The matrices considered the parameters described in Table 4.1. The black cross indicates non-significant correlations according to a p -value > 0.05 . The red highlighted part gathers the correlation matrices concerning sedimentological parameters while the blue highlighted part gathers the parameters belonging to the hydrological conditions. The yellow and blue parts of the correlation matrix indicate negative and positive correlation, respectively.

Focusing on CSB (Fig. 4.4B), the suspended sediment descriptors seemed similar but not identical to those of CSA. As far as the SSC_m is concerned, along with the P_{tot} (cor.test, p -value < 0.05), the Ru and the SSL also resulted significantly correlated. A significant correlation was registered for the same descriptors when the SSC_p is considered. Unlike CSA, the SSL was also found positively and significantly correlated to the P_{tot} and the Ru , respectively. Regarding the hydrological variables, instead, the results of the correlation matrix were equal to those of CSA. Therefore, the Q_p was positively correlated to P_{tot} and I_{av} . P_{tot} and I_{av} that were again correlated to each other and to I_{max} .

Table 4.2. Summary of the parameters analysed for each flood event (FE) recorded during the study period in the cross sections CSA and CSB. The date format is mm/dd/yy.

Event	Date	P _{tot} (mm)	I _{av} (mm h ⁻¹)	I _{max} (mm h ⁻¹)	Ru (10 ³ m ³)	Q _p (m ³ s ⁻¹)	Q _m (m ³ s ⁻¹)	SSL (t)	SSC _p (g l ⁻¹)	SSC _m (g l ⁻¹)	Δt (h)
CSA-FE1			0.95	17.2	116402.1	2.20	0.21	10.32	0.95	0.07	-75
CSB-FE1	08/29-9/05/20	158.6	0.95	17.2	552308.5	2.20	0.98	46.33	0.88	0.07	-120
CSA-FE2			0.6	12.8	146074.8	1.82	0.18	13.86	1.71	0.06	195
CSB-FE2	10/02- 10/10/20	129.6	0.6	12.8	686674.7	2.40	0.88	160.0 2	2.19	0.15	105
CSA-FE3			0.22	4.6	203420.3	0.69	0.47	7.86	0.06	0.04	255
CSB-FE3	05/01- 05/06/21	26.8	0.22	4.6	241396.2	1.00	0.56	8.76	0.08	0.04	285
CSA-FE4			0.21	2.2	371849.7	1.12	0.63	14.61	0.06	0.04	1140
CSB-FE4	05/08- 05/15/21	34.6	0.21	2.2	472572.7	1.70	0.81	17.06	0.07	0.04	5010
CSA-FE5			0.27	6.4	161807.8	1.29	0.88	5.51	0.05	0.03	105
CSB-FE5	05/23- 06/16/21	13.8	0.27	6.4	211310.6	1.39	1.14	8.36	0.06	0.04	30
CSA-FE6			0.31	15.2	148087.9	0.62	0.36	7.82	0.20	0.05	60
CSB-FE6	07/08- 07/13/21	36.2	0.31	15.2	174450.1	0.80	0.42	6.99	0.25	0.04	150
CSA-FE7			0.30	9.4	175192.8	0.63	0.36	6.44	0.06	0.04	150
CSB-FE7	07/13- 07/19/21	41.0	0.30	9.4	207892.7	0.76	0.43	7.95	0.10	0.04	150
CSA-FE8			0.44	9.6	239148.0	1.81	0.59	8.78	0.08	0.04	45
CSB-FE8	08/04- 08/09/21	49.4	0.44	9.6	306266.5	2.54	0.75	11.62	0.10	0.03	15

Additionally, the percentage variation between the two monitoring sites was computed (Table 4.2). The flood event FE1 produced a huge variation in terms of SSL, i.e., +77.7% between CSB and CSA. Similarly, FE2 featured a percentage variation in SSL of over +90%. As far as FE3 and FE4 are concerned, both events featured similar variations of SSL, i.e., +10.3% the former and +14.3% the latter. FE5, which was registered halfway between the snowmelt and spring season, was the longest event ever monitored in this study and it led to a SSL variation of +34.1 %. During spring and summer 2021, instead, three overall events were monitored. FE6 featured a negative variation of -1.9%, while FE7 and FE8 registered a SSL percentage variation of +18.9 % and +24.4%, respectively.

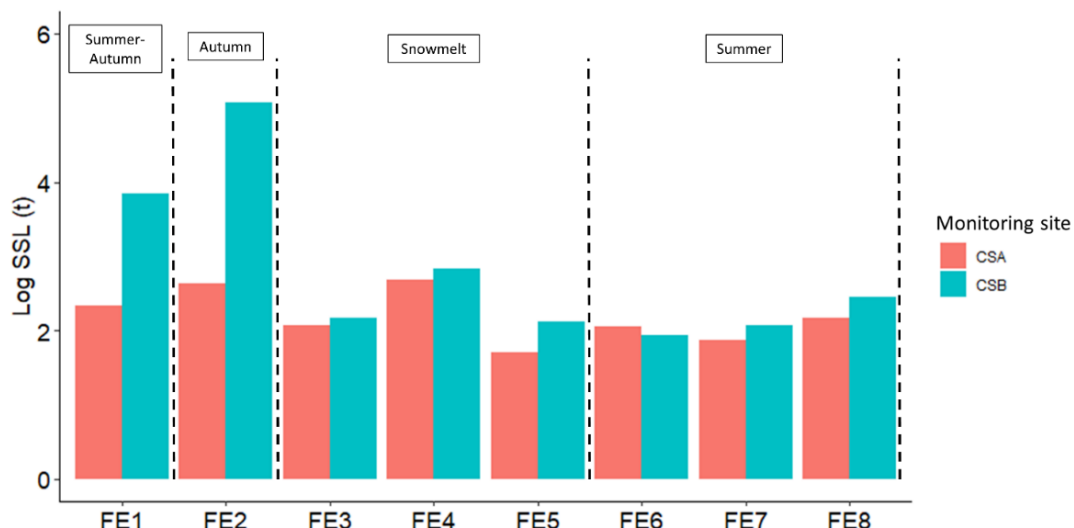


Figure 4.5. The logarithmic value of suspended sediment load registered at the upstream (CSA) and downstream (CSB) sites for each of the eight events recorded during the monitoring period. The FE1 occurred between the 29th August and 9th September 2020, the FE2 between 2nd and 10th October 2020, the FE3 between the 1st and 6th May 2021, the FE4 between 8th and 15th May 2021, the FE5 between 23rd of May and 16th June 2021, the FE6 between 8th and 13th July 2021, the FE7 between the 13th and 19th July 2021 while the FE8 between the 4th and 9th August 2021.

Upstream (CSA) and downstream (CSB) cross-sections: precipitation influence on SSL variations

A further analysis considering the correlation among the variation in SSL (%) and the three different precipitation variables (I_{\max} , P_{tot} and I_{av}) was carried out. Although showing a slight positive correlation with the suspended sediment percentage variation, I_{\max} did not provide any revealing trend (Fig. 4.6A; $R^2 = 0.17$). I_{av} of each event (Fig. 4.6B), instead, showed a positive correlation ($R^2 = 0.63$) with the variation in suspended sediment (%). Lastly, the P_{tot} was registered as the most correlated variable ($R^2 = 0.74$; Fig. 4.6C).

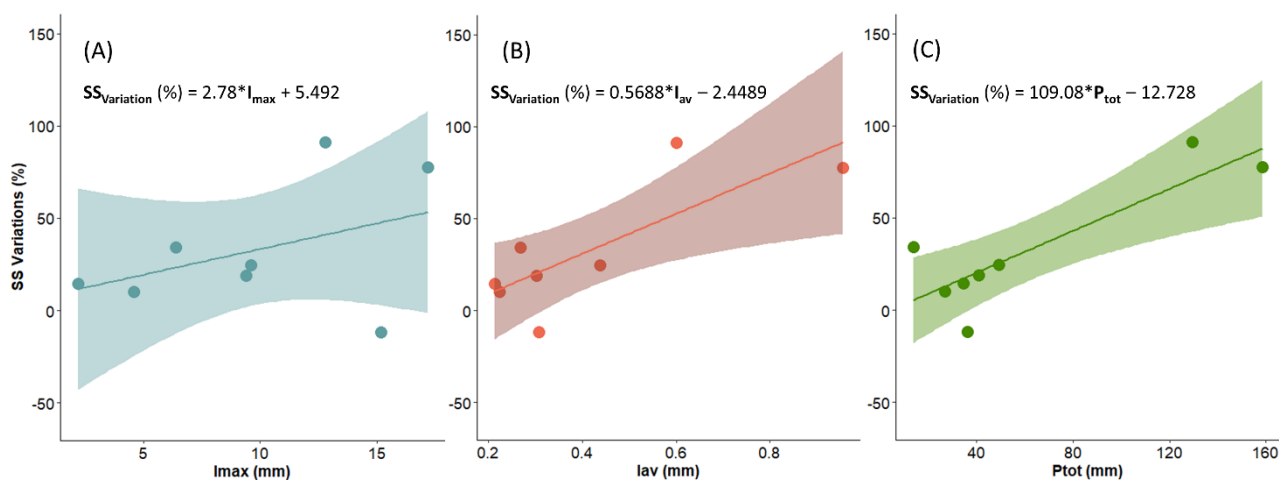


Figure 4.6. Linear correlation among the percentages of variation between the upstream and downstream sites and three different parameters of precipitation, (A) I_{\max} , (B) P_{tot} and (C) I_{av} respectively. The coloured bands represent the 95% confidence interval bands.

Upstream (CSA) and downstream (CSB) cross-sections: Hysteresis patterns analysis

In order to characterize the SSC-Q relationship for each event, the data collected on both cross-sections were analysed and quantified using the H index (Aich et al., 2014; Table 4.3). Six out of eight events, registered in both CSA and CSB, featured a rather circular clockwise (C) hysteresis loop (Fig. 4.7A). In fact, the index of the C loops was always between 0.01 and 0.17.

Table 4.3. Summary of the hysteresis loops analysed for each event at the CSA and CSB (CC: counterclockwise; C: clockwise). H is the hysteresis index proposed by Aich et al. (2014).

Event	Season	CSA				CSB			
		Q _p	Shape	Direction	H	Q _p	Shape	Direction	H
FE1	Summer-Autumn	2.20	Eight-shape	CC	-0.08	2.20	Eight-shape	CC	-0.73
FE2	Autumn	1.82	Eight-shape	CC	-0.99	2.40	Circular	CC	-1.05
FE3	Snowmelt	0.69	Circular	C	0.03	1.00	Circular	C	0.05
FE4	Snowmelt	1.12	Circular	C	0.10	1.70	Circular	C	0.01
FE5	Snowmelt	1.29	Circular	C	0.01	1.39	Circular	C	0.02
FE6	Summer	0.62	Circular	C	0.17	0.80	Circular	C	0.13
FE7	Summer	0.63	Circular	C	0.02	0.76	Eight-shape	C	0.06
FE8	Summer	1.81	Circular	C	0.04	2.54	Circular	C	0.06

The two remaining events that were all monitored during the summer and autumn seasons 2020 registered, for CSB and CSA, eight-shaped and circular counterclockwise loops (Fig. 4.7B). Conversely, the H index was found to be covering a higher range of negative values, from -0.08 to -1.05 respectively. The weakest value of -0.08 was represented by the FE1 in CSA while the strongest (0.99 and 1.05) by the FE2 for both CSA and CSB (Fig. 4.8A). Overall, the relations between the H index and Q_p showed a slight negative linear regression for both CSA and CSB (Fig. 4.8B).

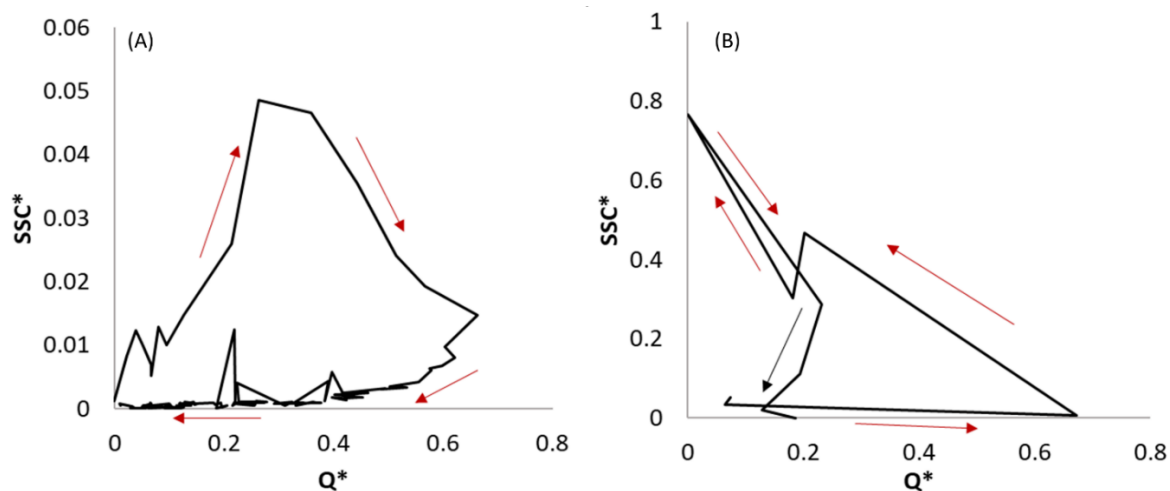


Figure 4.7. Example of hysteresis loop registered in the eight events monitored. (A) Represents a clockwise circular loop (FE3, downstream) while (B) an eight shaped counterclockwise and clockwise loop (FE1, downstream). The asterisk refers to the normalized Q and SSC (the data were subtracted by the minimum value of both Q and SSC).

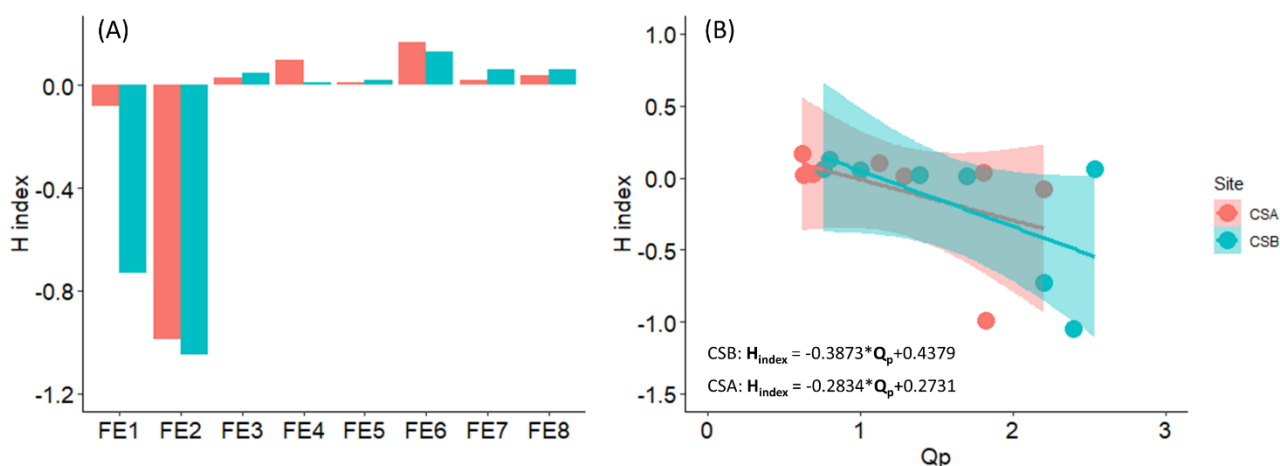


Figure 4.8. (A) Bar plot of the H index distribution for each event and monitoring sites. (B) Regression between the H index and the Q_p of both monitoring sites, CSA (orange, $R^2=0.22$) and CSB (sea-green, $R^2=0.39$) respectively.

Annual, monthly and seasonal averages variations

Herein the annual, monthly and seasonal values of precipitation, water discharge, and suspended sediment load are analysed along the monitoring period (August 2020-November 2021). The overall precipitation registered 1574.4 mm of which 523 mm attributable to the last portion of 2020 and the residual 1051.4 mm to the entire year 2021. The Q_m registered $0.34 \text{ m}^3 \text{ s}^{-1}$ while the total SSL measured 452.9 t (250.3 t produced in Autumn 2020 while the remaining 202.6 t during the entire 2020). This information provided an overall suspended sediment yield of $42 \text{ t km}^{-2} \text{ yr}^{-1}$ for the period August 2020-November 2021.

As far as the monthly precipitation is concerned, the highest value was registered in October 2020, featuring over 279 mm of cumulative precipitation and 9 mm daily average, while the lowest value of cumulative rainfall was detected in November 2020 (13.6 mm). The highest monthly Q_m was

measured in June 2021 and was about $0.66 \text{ m}^3 \text{ s}^{-1}$. This value represents a response to the snowmelt and rain-on-snow recorded in this month, especially over the first 15 days. The lowest value of discharge, instead, was measured in November 2021 ($0.12 \text{ m}^3 \text{ s}^{-1}$) even if the precipitation featured a value of over 160 mm. As for the precipitation, the month with the highest total SSL was October 2020 with 194.3 t and was clearly related to the number of rainy days detected during the month. Conversely, the month exhibiting the lowest SSL was, again, November 2021 with 10.8 t (Fig. 4.9). The most rainfall-contributing season was summer 2021 with over 435 mm of cumulative rain. The lowest was recorded during the snowmelt 2021, where the cumulative precipitation was 253 mm. During the monitoring period, the season with the highest value of Q_m was the snowmelt 2021 with a value of $0.50 \text{ m}^3 \text{ s}^{-1}$. The lowest was instead autumn 2021, with $0.13 \text{ m}^3 \text{ s}^{-1}$. Unlike Q_m and the precipitation, the highest SSL was registered in autumn 2020. In this case, the SSL reached a value of over 250 t. As for the minimum Q_m , the lowest value of SSL was found in autumn 2021 with less than 40 t.

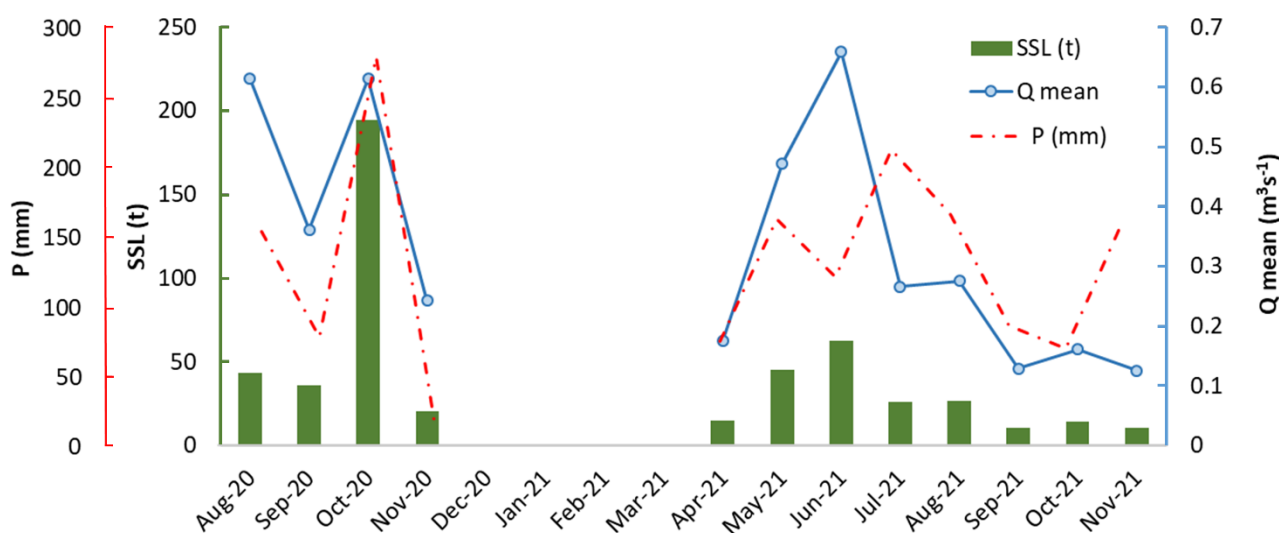


Figure 4.9. Monthly precipitation (P), monthly-suspended sediment load (SSL) and monthly discharge (Q) of the monitoring period. The green bars represent the load of SS, the solid line indicates the Q averages and the red dotted line indicates the P.

DISCUSSIONS

Sixteen months of monitoring: controlling factors and differences between upstream and downstream windthrow-affected area

In the Rio Cordon, eight events were registered during the monitoring period (August 2020 - November 2021). The factors controlling the suspended sediment load were identified among the extracted variables (Table 4.1) and the total precipitation (P_{tot}) was found to be the most correlated to SSC_m and SSC_p measured at both the monitoring sites (CSA and CSB). As pointed out by Penna et al. (2011), the limited area of the Rio Cordon basin (around 5 km^2) can induce a rapid response to

rainfall, generating fast floods and powerful erosion processes which could explain the detected dynamics. Nonetheless, the additional analysis showed a clear correlation between the percentage variation of SSL and both the I_{av} and the P_{tot} (Fig. 4.6). This seems to suggest that the contribution of SSL from the windthrow-affected area was controlled by the flood cumulative precipitation and average intensity (1h) rather than by the maximum intensity, indicating that the duration of the events rather than the peak is more important in determining the amount of suspended sediments recruited from the bank and low-lying berms. Overall, unlike the observations of Duvert et al. (2012) who analysed over eight catchments between Mexico, French Alps and Spanish Pyrenees, and those of Pagano et al. (2019) in the Rio Cordon pre-Vaia, the event peak discharge was not the best predictor of suspended sediment transport, both in terms of SSL and SSC_p . Being this a novel result for the Rio Cordon, further analysis should be needed. However, this result could be partially explained by the fast recovery of the Rio Cordon step-pool configuration which occurred after barely two years from the Vaia event (Pellegrini et al., 2021b). Indeed, in 2020, the step-pool non-dimensional steepness factor was 1.44, which is very close to 1.5, the value for which it's suggested that (i) flow resistance of the step-pool morphology is maximized and for which (ii) the armoured layer is well-developed (Abrahams and Atkinson, 1995). These conditions lead to a highly stable streambed and to a significant energy dissipation (Comiti et al., 2019) which could clarify the observed complex relations between flow conditions and sediment fluxes. Also, the structural and functional disconnectivity of the upper part of the basin (Martini et al., 2022) limits the downstream sediment supply.

When the hysteresis patterns are taken into account, it is worth noticing the different response of the catchment during the two years of monitoring (summer-autumn 2020 and 2021). In 2020, the Rio Cordon featured only counterclockwise loops in both CSA and CSB (Table 4.3), revealing the faster arrival of Q_p than SSC_p . This suggests that two years after the Vaia event, the sediment availability may have been still abundant. Given the fact that Vaia did not activate many new functionally connected sediment sources at the scale of basin (Martini et al., 2022), the high sediment availability is likely to be due to in-channel processes such as bank erosions and the progressive cleaning of finer sediments from the river network, which is also confirmed by the increase of armouring and the reestablishment of a marked step-pool morphology by means of pool scouring in the Rio Cordon (Pellegrini et al., 2021b). However, the differences of SSL among hysteresis measured at CSA and CSB monitoring sites suggest that the windthrow-affected area was active and functionally connected to the active channel during the first two events (FE1 and FE2). Interestingly, such dynamic did not change the hysteresis loop of the events (from counterclockwise to clockwise) meaning that the sediment contribution from the upstream basin prevailed over the sediment originated from the windthrow-affected area. Differently, during 2021, the basin featured a faster

response in terms of sediment transport rather than of water discharge, showing a prevalence of clockwise hysteresis loops. Such results are consistent with what presented by Seeger et al. (2004) in the Arnás catchment (Pyrenees) and by Bezak et al. (2016) in small Slovenian catchments, which showed that ordinary events along channel networks with close and ready-available sediment sources generate clockwise loops. However, as demonstrated by the computed index of hysteresis proposed by Aich et al. (2014), the loop appeared to be weak due to, probably, the ready-available sediment located in the active channel and very close to the two monitoring sites as was found by Mao and Carrillo (2017) in the Estero Morales Chilean basin. However, the results showed that the contribution sourced from the close in-channel available material rather than from the windthrow-affected area that did not provide any evidence of suspended sediment contribution during the 2021 events (Fig. 4.5). Once again, this result can be explained by the exhaustion of the upstream sediment availability and by the presence of the hanging valley lying in the centre of the basin that represents a major topographical feature that highly influence the sediment dynamics. Thus, the only sources able to contribute suspended sediment to the outlet are those located in the downstream connected half of the basin (Rainato et al., 2018; Lenzi and Marchi 2000; Martini et al., 2022). These changes in the hysteresis loops and indexes suggest that after the Vaia rainstorm, the ready-available is depleting progressively from upstream to downstream, likely adjusting the sediment storage along the active channel until the outlet of the basin. Nonetheless, it is possible that the ready-available sediment could have been originated, at least partially, during the last event of October 2020.

Comparison with historical data

By comparing the flood events occurred before and after the two large disturbances (i.e. September 1994 and October 2018), Fig. 4.10 shows that at discharges $\leq 3 \text{ m}^3 \text{ s}^{-1}$ the after LIDs events exhibited higher suspended sediment transport efficiency while, at higher discharges ($> 3 \text{ m}^3 \text{ s}^{-1}$), the suspended sediment transport is rather comparable with the events monitored after the LIDs. In this sense, as way of example, the before LID event of 3rd May 2003 exhibited a Q_p of $1.02 \text{ m}^3 \text{ s}^{-1}$ and a SSL equal to 0.2 t which is around one fortieth of the SSL (8.76 t) registered in the FE3 ($Q_p = 1.00 \text{ m}^3 \text{ s}^{-1}$) that fall within the after LIDs group. Also, the before LID event of the 5th October 1992 that featured a Q_p of $2.91 \text{ m}^3 \text{ s}^{-1}$ and a SSL of 4.8 t, diverged considerably from the after LID event of 16th October 1996 which exhibited a SSL of 294.4 t with a Q_p of $2.96 \text{ m}^3 \text{ s}^{-1}$. On the contrary, the largest before LID event of 3rd July 1989 ($Q_p = 4.39$) featured a value of SSL (223.9 t) in the same order of magnitude as compare to the after LID event of 7th October 1998 ($Q_p = 4.73 \text{ m}^3 \text{ s}^{-1}$) which transported around 294.4 t.

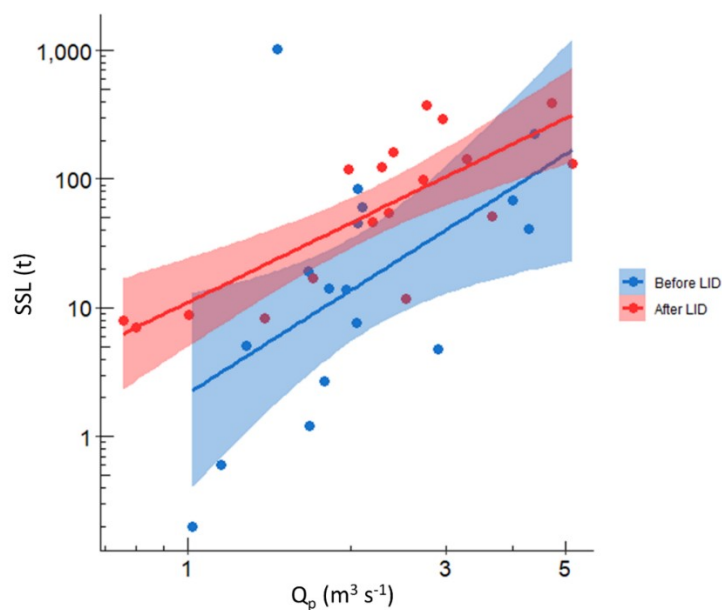


Figure 4.10. Scatter plot and regressions of the SSL and the Q_p of the event monitored before (blue; 1986-1994, 2002-2014) and after (red; 1994-2002, 2020-2021) the two LIDs (Large Infrequent Disturbances) recorded by the Rio Cordon monitoring program, i.e., 1994 flood and the Vaia rainstorm. The data between 1986 and 2014 were retrieved from Rainato et al. (2017).

In terms of sediment yield, the $42 \text{ t km}^{-2} \text{ yr}^{-1}$ of suspended sediment featured in the period August 2020 - November 2021 was comparable to the $40 \text{ t km}^{-2} \text{ yr}^{-1}$ measured in the stable and armoured period 2003 – 2014 (Rainato et al., 2017; Lenzi, 2001).

If on the one hand this value falls within the range of mean sediment delivery ($50\text{-}5000 \text{ t km}^{-2} \text{ yr}^{-1}$) noticed in over 200 alpine basins by Hinderer et al. (2013), on the other hand this result suggested that Vaia did not induce a subsequent increase in the sediment fluxes as, instead, observed in the Rio Cordon basin after the September 1994 flood event (sediment yield 1994-2002 = $149.4 \text{ t km}^{-2} \text{ yr}^{-1}$) (Rainato et al., 2017). Despite the fact that the suspended sediment amounts mobilized two years after Vaia were comparable to those monitored before it, the results have stressed a higher transport efficiency for lower- and near-bankfull events ($Q_p \leq 2.54 \text{ m}^3 \text{ s}^{-1}$). The limited influence of Vaia on the suspended sediment amounts could be explained by the fact that the Rio Cordon exhibited an alluvial rather than a colluvial response during the event (Rainato et al., 2021). In fact, most sediments transported during the event were likely provided by the channel and banks, and the number of sediment sources connected to the channel network remained rather constant (Martini et al., 2022). The limited contribution of sediment sources at the basin scale was also somehow confirmed by the comparison of the two monitored cross-sections, which demonstrated the exhaustion of sediment supply by the windthrow-affected area already after two years. Also, Pellegrini et al. (2021b) demonstrated that after barely two years of ordinary conditions, in the Rio Cordon, the step-pool configuration was re-established. Such process, as already demonstrate by Lenzi (2001),

reinforces the observation that a substantial change in the suspended sediment delivery and availability was not evident. However, although this work took into account eight events over 16 months, further analyses are required in the near future in order to implement the data with longer time monitoring to catch a larger magnitude range of floods and to see whether a formative flood allow the basin to jump to another resilience state. Additionally, due (i) to health and safety issues imposed by the logging interventions in 2019 and (ii) to Covid restrictions between March-June 2020, the post-event monitoring had to start in August 2020 which, limited the chances of including in the analysis the effects of the event occurred between November 2018 and August 2020. However, further fingerprinting investigations to understand which are the contributing sediment sources and how their functional connectivity changes during different seasons and/or floods event would be highly recommended. Nonetheless, as it seemed that the ready-available sediment is quickly moving from upstream to downstream, it would also be interesting to quantify the sediment storage along the active channel and, therefore, to understand how it moves.

CONCLUSIONS

The severe Vaia event produced different impacts on the alpine Rio Cordon basin, producing exceptional responses from hydrological to sedimentological and geomorphic points of view. As far as concerns the after-event processes, instead, no clues but only open questions were given. This work can be summarized taking inspiration by the two questions raised by Rainato et al. (2021): (i) What can be expected for the future? (ii) Has the October 2018 event represented the new ground zero for the Rio Cordon basin? The answer to the first question, although retrieved by sixteen months of suspended sediment monitoring, is that the Vaia LID seems not to have triggered the expected cascading processes as it occurred for the 1994 flood. Both the analysis at event and seasonal scale, in fact, show that the suspended sediment fluxes were pretty much in line with what registered during the pre-event condition (2003-2014) demonstrating that the equilibrium of the basin seems not to have been overturned. Indeed, not even the windthrow-affected area seemed to have contribute sediment to the active channel sediment transport. Benefiting from a long-term monitoring program that accounted two large and infrequent floods, it was possible to investigate the alteration induced by them on the suspended sediment dynamics. Interestingly, evidence of higher transport efficiency for the after LID events was mainly found for discharges lower than $3 \text{ m}^3 \text{ s}^{-1}$ (Fig. 4.10). In that case, apparently, the post LID condition seems to be more efficient in terms of suspended sediment contribution. However, as the monitoring of the events after Vaia covered only the suspended sediment analysis for lower than bankfull and near bankfull events, further monitoring to register higher magnitude floods and bedload dynamics is surely needed. The answer to the second question,

instead, seems clearer and, again, far from the expected results. Apparently, the ground zero was not achieved as, instead, seems to have happened after 1994 flood. Resilience seems to be the keyword that may explain the different dynamics that occurred after large disturbances. If we consider the resilience as a ladder, the different rungs can represent the stages of the Rio Cordon basin (lower rungs mean low resilience and vice-versa). Therefore, if we consider the two large disturbances affecting the Rio Cordon in the last 35 years, 1994 flood and the Vaia rainstorm, they can be placed at two different heights, lower and higher as far as concerns the former and the latter, respectively. However, to answer more precisely to these questions, further investigation is needed in order to cover up either or both ordinary and high magnitude events and considering a whole analysis of sediment transport, which takes into account suspended and bedload sediment.

Discussions and Conclusions

Understanding the state of dynamic *equilibrium* to which a hydro-system naturally tends is a key challenge to predict the behaviour of fluvial systems and its sensitivity and/or resilience to future disturbances (Phillips, 2009; Fryirs, 2017; Piégay et al., 2020).

Therefore, the main aim of my PhD thesis was to study the primary impacts and the ongoing cascading morphological and sedimentological processes of mountain basins following a specific large infrequent disturbance: the Vaia storm event. Specifically, I focused on the impacts and subsequent evolution at catchment- and reach -scale using either or both remote sensing, and field data. In the first two chapters, I reported findings from small and medium-large catchment-scales studies that focused on the hillslopes' and channel network's morphological and sedimentological responses. In the last two chapters, instead, I presented results from reach-scale studies aimed at exploring both the medium-term evolution of a mountain stream's morphology and the changes of suspended sediment fluxes following a large disturbance.

In the catchment-scale studies, I documented the effects of high magnitude/low frequency disturbances of mountain basins. To do so, I encompassed the hydrological, geomorphic and sedimentological responses. I outlined the importance of (i) combining different indirect methods to estimate and quantify the hydraulic forcings and of (ii) exploiting high-resolution remote sensing data (i.e. aerial images and LiDAR) to identify and characterized the geomorphic and sedimentological impacts of large disturbances on medium-large mountain basins. Specifically, in chapter one I demonstrated how the application and integration of such data on different softwares permitted an integrated vision of the sediment dynamics. On the one hand, the static and structural function of the sediment was described by the Index of Connectivity (IC) while, on the other hand, the factual dynamics were outlined by the Dem of Difference (DoD) analysis. Overall, in both chapters I clearly stressed the outstanding hydraulic forcing occurred during the flood. I showed how the two basins have had different predominant responses: mostly colluvial and alluvial for the on the one hand and alluvial on the other. In the former I found both the hillslope's sediment sources (landslides; debris flows) and the entire channel network (hyperconcentrated flows; debris flood) as the main sediment suppliers while, in the latter, I identified streambed remobilization, boulder mobility, incision and lateral erosion as the main sediment-contributing processes.

In the reach-scale studies, I explored the effects of a large disturbance on mountain streams' morphology and on the suspended sediment dynamics. In particular, I investigated the sensitivity of the Rio Cordon stream to the Vaia storm and its current state of dynamic *equilibrium*. In chapter 3, I

found evidence of morphological stabilization as the step-pool morphology, after being completely disrupted due to armouring removal and boulder mobility is heading back to the pre-Vaia conditions. This recovering of the step-pool configuration was much faster than what detected after the September 1994 large disturbance (Lenzi, 2001), likely due to the different resilience stage of the basin. In chapter 4, I investigated the hydrological and sedimentological conditions featuring the Rio Cordon two and three years after the disturbance. In this study, I had the chance to understand the ongoing hydro-sedimentological forcings and to compare the suspended sediment data at event-, monthly- and seasonal- scale with the Rio Cordon's old dataset (1986-2014). If on the one hand I underlined how the transport efficiency of the stream has increased during the first years following large disturbances and for lower than bankfull events, on the other I surprisingly demonstrated that, the annual sediment yield, as well as the monthly and seasonal loads of suspended sediments are in line with those detected before the Vaia storm. To this end, I hypothesized that the Rio Cordon may be in a different rung of the resilience ladder as compared to the one of 1994, when the catchment featured different cascading processes that completely overturn the suspended sediment dynamics and fluxes for about a decade.

Altogether, findings of my PhD thesis pointed out a main message on mountain basins' responses to LIDs. Large Infrequent Disturbances overturn the dynamic *equilibrium* of mountain fluvial systems leading to undefined secondary processes as demonstrated by the different secondary responses of the Rio Cordon basin to diverse large disturbances. The current condition suggests that the Rio Cordon is now heading back to the original state but with a new dynamic *equilibrium* since (i) the morphology of the system changed during the Vaia event and (ii) the sediment fluxes and stability of the step-pool configuration resulted in line with the prior event condition (Fig. 1B1).

Within these four studies, I found answers to few questions, but, more importantly, I identified knowledge gaps and formulated new hypotheses. Answers to these questions await further research to provide insight into the prediction of future fluvial systems' behaviours to Large "Infrequent" Disturbances.

Future challenges and perspectives

In this brief paragraph, I want to underline the limitations of my thesis and my view on future challenges of mountain river science in a context of climate change.

Climate change in mountain environments is causing variations to the entire fluvial systems, above all by altering the water cycle, worldwide. The increase of heavy rainfalls and the changes in the seasonal precipitation and temperature are driving mountain basins to rain dominant regimes (snowpack declining and heavy rainfall events increasing). Rain dominant regimes are effectively changing both the ecological and geo-hydro-morphological status of mountain environments. Thus, the perception and definition of mountain safety and hydrological risks are changing accordingly.

If, on the one hand, my thesis has tried to fulfill some of the gaps of knowledge concerning mountain basins' primary and secondary responses to large disturbances in a climate change context, using both field and remote sensing data, on the other hand, my research still lacked in delineating risk mitigation measures due to several limitations. Two of these limitations are the limited spatial and temporal scale of the analyses.

Therefore, in my opinion, the challenge of today's mountain river science is to do research based on combined field and remote data in an extended period of time and space. Thus, experimental designs should consider three main steps: (i) improving the monitoring activities and enlarging the (ii) spatial and (iii) temporal scales of analyses.

Improving the monitoring activities means having a well-rounded view of the mountain basins' responses to ordinary and extraordinary meteorological events. For example, the application of an experimental design that considers both colluvial and alluvial processes could provide fundamental knowledge on where, when, and how much to intervene in a mountain environment. Notwithstanding, the answers to these questions could also define practical guidelines or "on-air" warning systems to protect villages and structures/infrastructures from geo-hydrological hazards and to improve safety of mountain areas. This approach was partially applied in Chapter 1 and 2 where I tried to characterize and identify the holistic responses of two mountain basins during the Vaia storm event.

Increasing the temporal scale means collecting as much information as possible on mountain basins' responses to both ordinary and extraordinary events over a long period of time (>30 years). In my opinion, the need to constantly monitor mountain basins over a long period arises from the fact that the climatic conditions are changing along with the representativeness of the old datasets. Therefore, the opportunity of enlarging the timescale of analysis could provide information concerning the geomorphological-sedimentological responses of mountain basins to (i) a huge range

of future hydrological events (lower than bankfull, bankfull or over than bankfull) and, in the meantime, (ii) to similar events but during different stages of mountain basins' dynamic *equilibrium*. The availability of such information will permit the definition of mitigation measures according not only to the magnitude or recurrence interval of an event, but also depending on the evolutionary state of mountain basins that could be retrieved from several information, as for example the distance from the last extraordinary events, the activity of sediment sources or the morphological status of mountain stream. This approach has started to be applied only in Chapter 4 where I highlighted the different responses of the Rio Cordon catchment during ordinary flood events and before/after large disturbances over a 35-year period of monitoring.

Enlarging the spatial scale, instead, means establishing common responses of a large area to predict future developments/dynamics of a mountain system. The availability of a large dataset of various basins with similar or different topographic (slope, exposure, drainage area etc.) and geomorphological (sediment sources areas, grain sizes, channel width etc.) features, could be extremely important to predict common or uncommon trends of mountain areas in a changing scenario such as climate change. Obviously, this goal can be achieved if the responses of mountain basins are analysed as a whole, thus paying attention to both the colluvial and alluvial processes that are often activated by different triggering factors. Therefore, I believe that this approach is the most challenging and needs huge cooperation from multidisciplinary scientists (i.e., fluvial and hillslope geomorphologists). I think that my thesis can be an important piece in the puzzle of a future study on mountain basins and climate change.

Obviously, the power of this hypothetical design reaches its maximum when these three strategies are combined. Therefore, to succeed in research I believe that is crucial to work in multidisciplinary teams to share different expertise but common results.

Appendix

Appendix A (Chapter 1.)

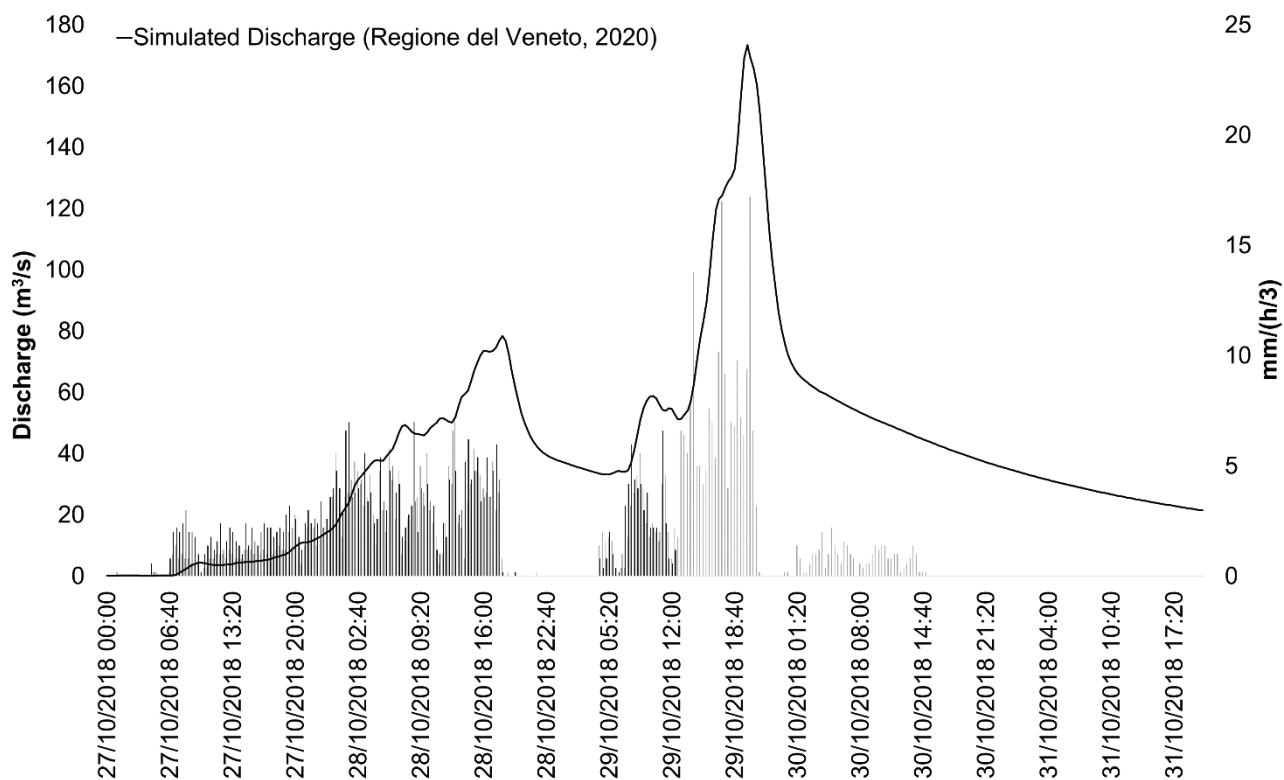


Figure A S1. Graphical representation of the Simulated Discharge of the Vaia storm with the factual precipitation registered by the ARPA Veneto agency in Biois di Cencenighe (grey) and Col di Prà (black) gauging stations, respectively.

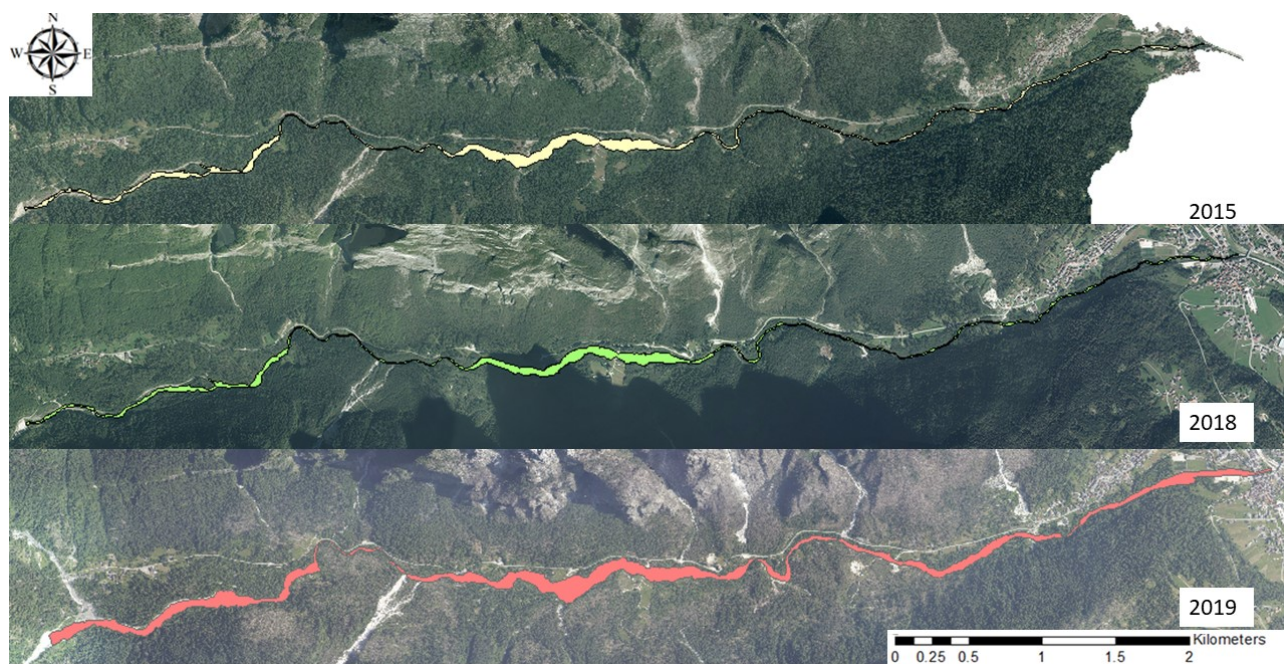


Figure A S2. Changes in the TTB active channels from 2015 to 2019.

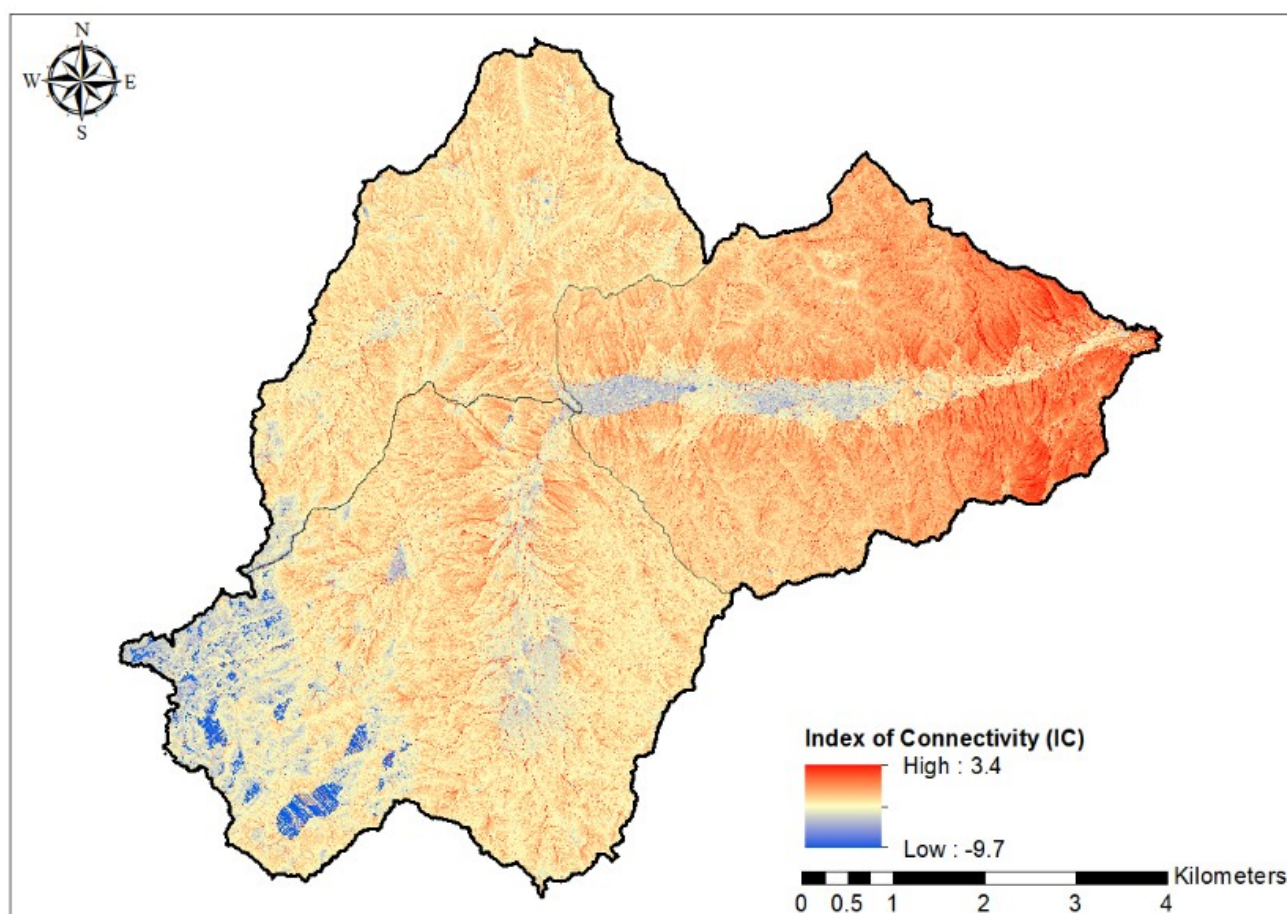


Figure A S3. Catchment-scale Index of Connectivity (IC); the target is the outlet of the TTB.

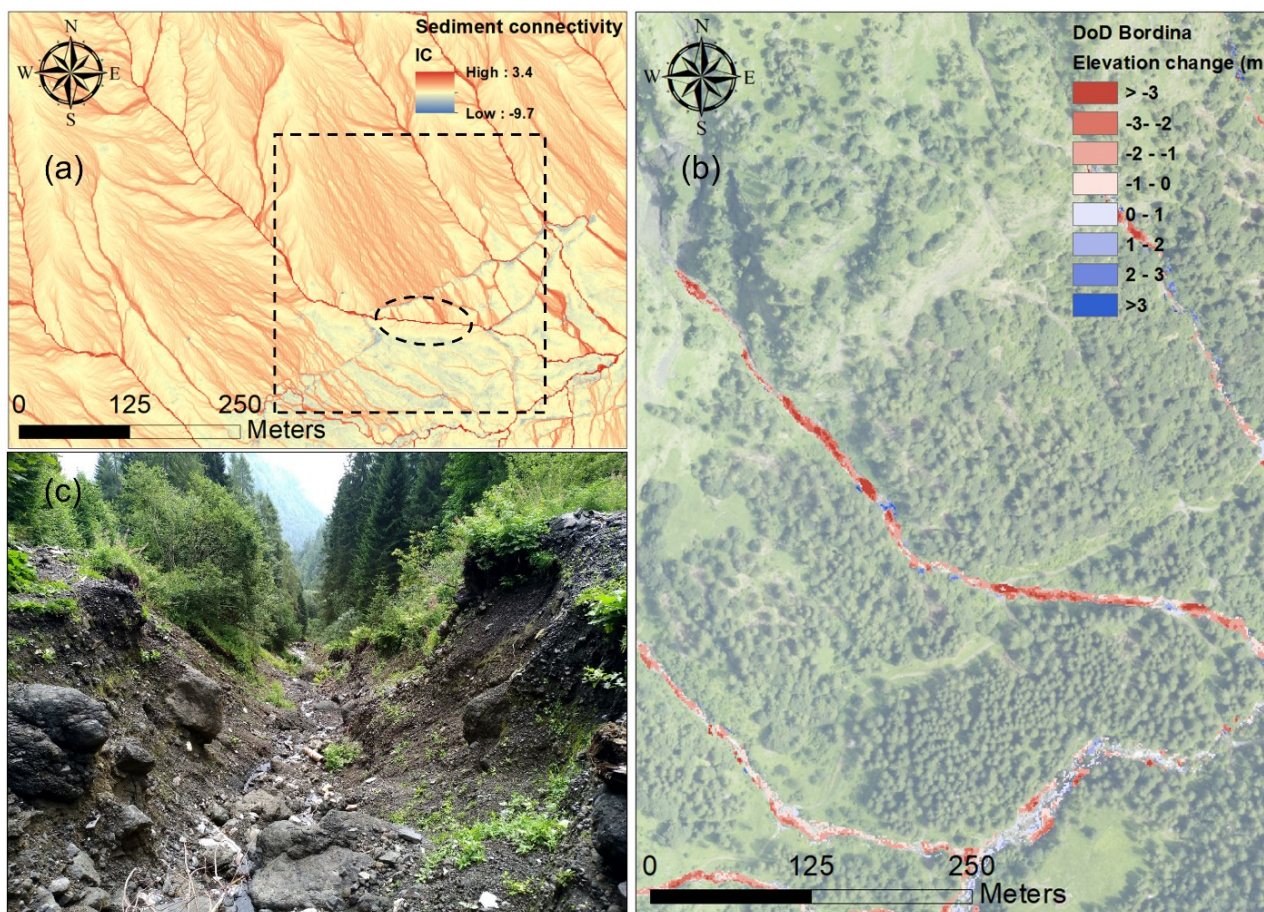


Figure A S4. (a) IC map, (b) DoD and (c) field evidence regarding the channel of the Bordina Sub-basin; (a) the dotted ellipse shows the position from where the picture was taken, (a) the dotted rectangle, instead, represent the zoom of the channel where the DoD analysis was made.

Appendix B (Chapter 2.)

Table B S1: Main features of the flood events recorded by the Rio Cordon monitoring station between September 1986 and September 2018: Q_P is the water discharge peak (in $\text{m}^3 \text{s}^{-1}$), RI the recurrence interval estimated (in years), BL the amount of coarse material transported at the monitoring station (both in m^3 and tons), SSL the suspended sediment load measured (in tons), ER is the effective runoff volume (in 10^3 m^3), BLr the bedload transport rate (in $\text{m}^3 \text{ h}^{-1}$), while D_{16} , D_{50} , D_{84} and D_{90} are, respectively, the 16th, 50th, 84th and 90th percentiles of the bedload grain size distribution.

	Q_P ($\text{m}^3 \text{ s}^{-1}$)	RI years	BL (m^3)	BL (t)	SSL (t)	ER (10^3 m^3)	BLr ($\text{m}^3 \text{ h}^{-1}$)	D_{16} (mm)	D_{50} (mm)	D_{84} (mm)	D_{90} (mm)
11 October 1987	5.15	11.5	54.8	85.6	131.7	79.9	6.9	-	-	-	-
15 July 1988	2.43	2.0	1.0	1.7	-	-	-	-	-	-	-
3 July 1989	4.39	7.1	85.0	145.6	223.9	103.4	3.1	54	103	207	242
22 May 1990	0.85	1.0	1.0	1.7	-	-	-	-	-	-	-
17 June 1991	4.00	5.5	39.0	67.2	68.1	57.9	2.0	30	51	100	135
5 October 1992	2.91	2.7	9.3	15.5	4.8	21.5	0.9	22	43	111	162
2 October 1993	4.28	6.6	13.7	17.2	41.1	30.7	2.3	29	61	135	186
18 May 1994	1.79	1.4	1.0	1.7	2.7	5.4	0.1	21	33	52	62
14 September 1994	10.42	> 100	900.0	1541.7	2435.1	26.6	323.6	65	116	226	281
13 August 1995	2.72	2.4	6.2	10.3	98.3	1.8	6.2	-	-	-	-
16 October 1996	2.96	2.8	57.0	94.7	294.4	22.0	3.8	40	79	143	163
27 June 1997	1.46	1.2	1.0	1.7	-	-	-	-	-	-	-
7 October 1998	4.73	8.8	300.0	516.8	393.5	91.8	17.6	40	78	157	188
20 September 1999	3.65	4.4	19.2	32.7	50.9	10.4	3.0	32	54	98	117
13 October 2000	3.28	3.5	55.6	92.2	142.0	110.6	1.6	39	61	111	123
11 May 2001	1.46	1.2	80.0	137.8	1017.6	8.5	6.2	33	48	69	77
20 July 2001	1.98	1.6	20.9	36.0	119.8	15.0	4.4	-	-	-	-
04 May 2002	2.29	1.8	27.4	47.2	123.0	29.4	1.4	39	59	99	119
16 November 2002	2.35	2.0	10.0	17.2	54.3	18.9	0.7	-	-	-	-
27 November 2002	2.77	2.5	69.1	119.0	373.7	70.3	2.3	26	44	78	89
03 May 2003	1.02	1.1	1.0	1.7	0.2	1.0	0.3	-	-	-	-
01 November 2004	2.05	1.6	4.6	7.9	7.6	-	-	25	38	62	77
6 October 2005	1.68	1.4	0.9	1.6	1.2	3.3	0.1	18	30	55	71
19 May 2006	1.28	1.1	0.7	1.2	5.1	1.0	0.1	-	-	-	-
24 May 2009	1.67	1.3	1.8	3.1	19.3	5.2	0.1	-	-	-	-
5 May 2010	1.82	1.5	0.8	1.4	14.2	3.7	0.1	-	-	-	-
8 June 2011	1.15	1.1	0.5	0.9	0.6	0.8	0.2	-	-	-	-
11 November 2012	2.10	1.7	14.2	24.4	60.8	4.6	2.3	23	38	70	79
17 May 2013	1.96	1.5	2.2	3.8	13.7	10.2	0.1	33	44	90	110
9 June 2014	2.06	1.7	65.6	113.0	76.8	16.6	4.7	24	41	64	113
5 November 2014	2.06	1.7	2.7	4.6	84.3	33.3	0.1	25	38	62	73
27 May 2016	1.09	1.0	0.5	0.9	-	1.0	-	25	35	51	60
24 May 2018	1.68	1.3	3.6	6.2	-	8.0	0.1	24	36	59	68

Acknowledgments

As a final step, I want to, firstly, express my gratitude to different people who helped me and believed in my research and me. Among all, (i) my Supervisor Prof. Lorenzo Picco, who has been able to convey to me the enthusiasm and passion for research and geomorphology,(ii) the whole team of Mountain Fluvial Morphology Research Group, especially Prof. Mario Aristide Lenzi, Dr. Lorenzo Martini and Dr. Riccardo Rainato with whom I shared most time of my experience, (iii) Dr. Marco Cavalli whose feedbacks were fundamental to publish my first scientific work, and (iv) Prof. Luca Mao, whose brilliant scientific vision helped (and is still helping) me in producing some innovative scientific works.

Secondly, I would like to thank (i) my family, especially Mom and Dad who have always invested in my education and have always believed in me and in my choices, (ii) my friends, in particular my PhD colleagues that contributed with happiness and light-heartedness this 3-year journey and (iii) my dear Costi, whose ambition, smartness and love have been essential to keep me on track and to keep me dreaming about my future and carrier.



References

- Abrahams, A.D., Li, G., Atkinson, J.F., 1995. Step-Pool Streams: Adjustment to Maximum Flow Resistance. *Water Resour Res* 31, 2593–2602. <https://doi.org/10.1029/95WR01957>
- Aich, V., Zimmermann, A., Elsenbeer, H., 2014. Quantification and interpretation of suspended-sediment discharge hysteresis patterns: how much data do we need? *Catena*, 122, 120–129. doi:10.1016/j.catena.2014.06.020.
- Albers, S.J., Petticrew, E.L., 2013. Biogeomorphic impacts of migration and disturbance: implications of salmon spawning and decay. *Geomorphology*, 202:43–50. doi:10.1016/j.geomorph.2013.02.002
- Amponsah, W.A., Ayrál, P.A., Boudevillain, B.B., Bouvier, C., Braud, I., Brunet, P., Delrieu, G., Didon-Lescot, J.F., Gaume, E., Lebouc, L., Marchi, L., Marra, F., Morin, E., Nord, G., Payrastre, O., Zoccatelli, D., Borga, M., 2018. Integrated high-resolution dataset of high-intensity European and Mediterranean flash floods. *Earth System Science Data* 10, 1783-1794.
- Ashworth, P.J., Best, J.L., Jones, M., 2004. Relationship between sediment supply and avulsion frequency in braided rivers. *Geology* 32, 21–24. <https://doi.org/10.1130/G19919.1>
- Asselman, N.E.M., 1999. Suspended sediment dynamics in a large drainage basin: the River Rhine. *Hydrological Processes*, 13, pp. 1437-1450. doi:10.1002/(SICI)1099-1085(199907)13:10<1437::AID-HYP821>3.0.CO;2-J.
- Bača, P., 2008. Hysteresis effects in suspended sediment concentration in the Rybáric basin, Slovakia. *Hydrological Sciences Journal*, 53 (1), 223–235. doi:10.1623/hysj.53.1.224.
- Baewert, H., Morche, D., 2014. Coarse sediment dynamics in a proglacial fluvial system (Fagge River, Tyrol). *Geomorphology* 218, 88-97.
- Baker, V.R., Costa, J.E., 1987. Flood power. In: Mayer, L., Nash, D. (Eds.), *Catastrophic Flooding*. Allen & Unwin, Boston, 1–20.
- Bakker, M., Costa, A., Silva, T. A., Stutenbecker, L., Girardclos, S., Loizeau, J. L., Molnar, P., Schlunegger, F., Lane, S. N., 2018. Combined flow abstraction and climate change impacts on an aggrading Alpine River. *Water Resources Research*, 54, 223– 242. doi:10.1002/2017WR021775.
- Ban, N., Rajczak, J., Schmidli, J., Schär, C., 2018. Analysis of Alpine precipitation extremes using generalized extreme value theory in convection-resolving climate simulations. *Climate Dynamics*, 55, 61–75. <https://doi.org/10.1007/s00382-018-4339-4>.

- Ban, N., Schmidli, J., Schär, C., 2015. Heavy precipitation in a changing climate: Does short-term summer precipitation increase faster? *Geophysical Research Letters*, 42, 1165–1172. <https://doi.org/10.1002/2014GL062588>.
- Bangen, S., Hensleigh, J., McHugh, P., Wheaton, J.M., 2016. Error modeling of DEMs from topographic surveys of rivers using fuzzy inference systems. *Water Resources Research*, 52, 1176–1193. doi:10.1002/2015WR018299.
- Batalla, R.J., De Jong, C., Ergenzinger, P., Sala, M., 1999. Field observations on hyperconcentrated flows in mountain torrents. *Earth Surface Processes and Landforms* 24, 247–253.
- Bauch, G.D., Hickin, E.J., 2011. Rate of floodplain reworking in response to increasing storm-induced floods, Squamish River, south-western British Columbia, Canada. *Earth Surface Processes and Landforms* 36(7), 872–884.
- Beechie, T., Liermann, M., Pollock, M., Baker, S., Davies, J., 2006. Channel pattern and river floodplain dynamics in forested mountain river systems. *Geomorphology*, 78 (1–2), 124–141. doi:10.1016/j.geomorph.2006.01.030.
- Benito, G., 2013. Hazardous processes: flooding. In: Shroder J (ed) *Treatise on geomorphology. Geomorphology of human disturbances, climate change, and natural hazards*, vol 13. Academic Press. San Diego, CA, pp 243–261. <https://doi.org/10.1016/B978-0-12-374739-6.00363-8>.
- Beylich, A.A., Sandberg, O., 2005. Geomorphic Effects of the Extreme Rainfall Event of 20-in the Latnjavagge, Source: *Geografiska Annaler. Series A, Physical Geography*.
- Bezak, N., Brilly, M., Šraj, M., 2016. Flood frequency analyses, statistical trends and seasonality analyses of discharge data: a case study of the Litija station on the Sava River. *J. Flood Risk Manag.*, 9, pp. 154–168. doi:10.1111/jfr3.12118.
- Biolchi, S., Denamiel, C., Devoto, S., Korbar, T., Macovaz, V., Scicchitano, G., Vilibić, I., Furlani, S., 2019. Impact of the October 2018 Storm Vaia on coastal boulders in the Northern Adriatic Sea. *Water* 11(11), 2229.
- Bohorquez, P., Darby, S.E., 2008. The use of one- and two-dimensional hydraulic modelling to reconstruct a glacial outburst flood in a steep Alpine valley. *Journal of Hydrology* 361 (3–4), 240–261.
- Bonat, M., Lucianetti, G., Mastrorillo, L., Viaroli, S., Mazza, R., 2019. The role of alpine valley fill deposits for groundwater storage (Dolomites, Italy). *Grundwasser - Zeitschrift der Fachsektion Hydrogeologie*, 25, 3–14. doi:10.1007/s00767-019-00438-7.
- Borga, M., Stoffel, M., Marchi, L., Marra, F., Matthias, J., 2014. Hydrogeomorphic response to extreme rainfall in headwater systems: flash floods and debris flows. *Journal of Hydrology* 518, 194–205.

- Borselli, L., Cassi, P., Torri, D., 2008. Prolegomena to sediment and flow connectivity in the landscape: a GIS and field numerical assessment. *Catena*, 75 (3), 268-277. doi:10.1016/j.catena.2008.07.006.
- Bracken, L.J., Turnbull, L., Wainwright, J., Bogaart, P., 2015. Sediment connectivity: a framework for understanding sediment transfer at multiple scales. *Earth Surface Processes and Landforms*, 40 (2), 177–188. doi:10.1002/esp.3635.
- Brasington, J., Rumsby, B.T., McVey, R.A., 2000. Monitoring and modelling morphological change in a braided gravel-bed river using high-resolution GPS-based survey. *Earth Surface Processes and Landforms* 25, 973–990.
- Brasington, J., Langham, J., Rumsby, B., 2003. Methodological sensitivity of morphometric estimates of coarse fluvial sediment transport. *Geomorphology* 53, 299–316.
- Bravard, J.P., Petit, F., 1997. *Les cours d'eau, Dynamique du système fluvial*. Armand Colin: Paris; 222 pp.
- Brenna, A., Surian, N., Ghinassi, M., Marchi, L., 2020. Sediment–water flows in mountain streams: Recognition and classification based on field evidence, *Geomorphology*, 371, 107413. doi:10.1016/j.geomorph.2020.107413.
- Brierley, G., Fryirs, K., Jain, V., 2006. Landscape connectivity: The geographic basis of geomorphic applications. *Area* 38(2), 165–174. <https://doi.org/10.1111/j.1475-4762.2006.00671.x>
- Brizga, S.O., Finlayson, B.L., 1994. Interactions between upland catchment and lowland rivers: an applied Australian case study. *Geomorphology* 9, 189–201. [https://doi.org/https://doi.org/10.1016/0169-555X\(94\)90062-0](https://doi.org/https://doi.org/10.1016/0169-555X(94)90062-0)
- Brogan, D.J., MacDonald, L.H., Nelson, P.A., Morgan, J.A., 2019. Geomorphic complexity and sensitivity in channels to fire and floods in mountain catchments. *Geomorphology* 337, 53–68.
- Bucała-Hrabia, A., Kijowska-Strugała, M., Bryndal, T., Cebulski, J., Kiszka, K., Krocak, R., 2020. An integrated approach for investigating geomorphic changes due to flash flooding in two small stream channels (Western Polish Carpathians). *Journal of Hydrology: Regional Studies* 31, 100731.
- Buffington, J. M., 2012. Changes in channel morphology over human time scales. In: Church, M.; Biron, P.M.; Roy, A.G. (Ed.). *Gravel-bed rivers: processes, tools, environments*. Chichester: Wiley, pp. 433-463. <http://dx.doi.org/10.1002/9781119952497.ch32>.
- Buffington, J.M., Montgomery, D.R., 2013. 9.36 geomorphic classification of rivers. In: Shroder, J.F. (Ed.), *Treatise on Geomorphology*. Academic Press, San Diego, pp. 730–767. <https://doi.org/10.1016/B978-0-12-374739-6.00263-3>.
- Burt, T.P., Allison, R.J., 2010. *Sediment Cascades: An Integrated Approach*. *Sediment Cascades: An Integrated Approach*. John Wiley & Sons, Ltd, Chichester, UK. <https://doi.org/10.1002/9780470682876>

- Calle, M., Calle, J., Alho, P., Benito, G., 2020. Inferring sediment transfers and functional connectivity of rivers from repeat topographic surveys. *Earth Surface Processes and Landforms*, 45, 681–693. doi:10.1002/esp.4765.
- Carrivick, J.L., Smith, M.W., Quincey, D. J., 2016. *Structure from Motion in the Geosciences*. John Wiley & Sons, Ltd, Chichester, UK.
- Cassandro, C., Loglisci, N., Gandini, D., Qian, M.W., Niu, G.Y., Ramieri, P., Pelosini, R., Longhetto, A., 2002. The flood of November 1994 in Piedmont, Italy: A quantitative analysis and simulation. *Hydrological Processes* 16, 1275–1299.
- Castiglioni, B., 1939. Il Gruppo delle Pale di S. Martino e le valli limitrofe (Alpi Dolomitiche). *Mem. Ist. Geol. R. Univ. Padova*, Sez. 13, 1–104.
- Cavaleri, L., Bajo, M., Barbariol, F., Bastianini, M., Benetazzo, A., Bertotti, L., Chiggiato, J., Davolio, S., Ferrarin, C., Magnusson, L., Papa, A., Pezzutto, P., Pomaro, A., Umgiesser, G., 2019. The October 29, 2018 storm in northern Italy – an exceptional event and its modeling. *Progress in Oceanography*, 178, 102178.
- Cavalli, M., Marchi, L., 2008. Characterisation of the surface morphology of an alpine alluvial fan using airborne LiDAR. *Natural Hazards and Earth System Science* 8, 323–333.
- Cavalli, M., Trevisani, S., Comiti, F., Marchi, L., 2013. Geomorphometric assessment of spatial sediment connectivity in small Alpine catchments. *Geomorphology*, 188, 31–41. doi:10.1016/j.geomorph.2012.05.007.
- Cavalli, M., Tarolli, P., Dalla Fontana, G., Marchi, L., 2016. Multi-temporal analysis of sediment source areas and sediment connectivity in the Rio Cordon catchment (Dolomites). *Rendiconti Online Società Geologica Italiana*, 39(April), 27–30. <https://doi.org/10.3301/ROL.2016.39>.
- Cavalli, M., Goldin, B., Comiti, F., Brardinoni, F., Marchi, L., 2017. Assessment of erosion and deposition in steep mountain basins by differencing sequential digital terrain models. *Geomorphology*, 291, 4–16. doi:10.1016/j.geomorph.2016.04.009.
- Cavalli, M., Vericat, D., Pereira, P., 2019. Mapping water and sediment connectivity. *Science of The Total Environment*, 673, 763–767. doi:10.1016/j.scitotenv.2019.04.071.
- Chalov, S.R., Tsyplenkov, A.S., Pietron, J., Chalova, A.S., Shkolnyi, D.I., Jarsjö, J., Maerker, M., 2017. Sediment transport in headwaters of a volcanic catchment—Kamchatka Peninsula case study. *Frontiers in Earth Science*, 11, 565–578. doi:10.1007/s11707-016-0632-x.
- Cheng, L., Chen, S., Liu, X., Xu, H., Wu, Y., Li, M., Chen, Y., 2018. Registration of laser scanning point clouds: A review. *Sensors*, 18, 1641. doi:10.3390/s18051641.

- Chin, A., 2003. The geomorphic significance of step-pools in mountain streams. *Geomorphology* 55, 125–137. [https://doi.org/10.1016/S0169-555X\(03\)00136-3](https://doi.org/10.1016/S0169-555X(03)00136-3)
- Chin, A., Solverson, A.P., O'Dowd, A.P., Florsheim, J.L., Kinoshita, A.M., Nourbakhshbeidokhti, S., Sellers, S.M., Tyner, L., Gidley, R., 2019. Interacting geomorphic and ecological response of step-pool streams after wildfire. *Bulletin of the Geological Society of America* 131, 1480–1500. <https://doi.org/10.1130/B35049.1>
- Chirici, G., Giannetti, F., Travaglini, D., Nocentini, S., Francini, S., D'Amico, G., Calvo, E., Fasolini, D., Broll, M., Maistrelli, F., Tonner, J., Pietrogiovanna, M., Oberlechner, K., Andriolo, A., Comino, R., Faidiga, A., Pasutto, I., Carraro, G., Zen S., Contarin, F., Alfonsi, L., Wolynski, A., Zanin, M., Gagliano, C., Tonolli, S., Zoanetti, R., Tonetti, R., Cavalli, R., Lingua, E., Pirotti, F., Grigolato, S., Bellingeri, D., Zini, E., Gianelle, D., Dalponte, M., Pompei, E., Stefani, A., Motta, R., Morresi, D., Garbarino, M., Alberti, G., Valdevit, F., Tomelleri, E., Torresani, M., Tonon, G., Marchi, M., Corona, P., Marchetti, M., 2019. Stima dei danni della tempesta “Vaia” alle foreste in Italia. *Forest@* 16: 3-9. doi:10.3832/efor3070-016.
- Church, M., Zimmermann, A., 2007. Form and stability of step-pool channels: Research progress. *Water Resour Res* 43, 1–21. <https://doi.org/10.1029/2006WR005037>
- Clubb, F.J., Mudd, S M., Attal, M., Milodowski, D.T., Grieve, S.W.D., 2016. The relationship between drainage density, erosion rate, and hilltop curvature: Implications for sediment transport processes, *Journal of Geophysical Research: Earth Surface*, 121, 1724–1745. doi:10.1002/2015JF003747.
- Coe, J. A., Bessette-Kirton, E. K., Geertsema, M., 2018. Increasing rock-avalanche size and mobility in Glacier Bay national park and preserve, Alaska detected from 1984 to 2016 landsat imagery. *Landslides*, 15(3), 393–407. <https://doi.org/10.1007/s10346-017-0879-7>.
- Comiti, F., Mao, L., Wilcox, A., Wohl, E. E., Lenzi, M. A., 2007. Field-derived relationships for flow velocity and resistance in high-gradient streams. *J Hydrol (Amst)* 340, 48–62. <https://doi.org/10.1016/j.jhydrol.2007.03.021>
- Comiti, F., Cadol, D., Wohl, E., 2009. Flow regimes, bed morphology, and flow resistance in self-formed step-pool channels. *Water Resour Res* 45. <https://doi.org/10.1029/2008WR007259>
- Comiti, F., Mao, L., Penna, D., Dell'Agnese, A., Engel, M., Rathburn, S., Cavalli, M., 2019. Glacier melt runoff controls bedload transport in Alpine catchments. *Earth and Planetary Science Letters*, 520, 77– 86. doi:10.1016/j.epsl.2019.05.031.
- Costa, J.E., O'Connor, J.E., 1995. Geomorphologically effective floods. In: Costa, J.E., Miller, A.J., Potter, K.P., Wilcock, P.R. (Eds.), *Natural and Anthropogenic Influences in Fluvial Geomorphology (The Wolman Volume)* AGU Geophysical Monograph 89. American Geophysical Union, Washington, D.C., 45–56.

- Coyne, A., Schafer, J., Hurtrez, J.E., Dumas, J., Etcheber, H., Blanc, G., 2004. Sampling frequency and accuracy of SPM flux estimates in two contrasted drainage basins. *Science of the Total Environment*, 330, 233–247. doi:10.1016/j.scitotenv.2004.04.003.
- Crema, S., Cavalli, M., 2018. SedInConnect: A stand-alone, free and open source tool for the assessment of sediment connectivity. *Computers and Geosciences*, 111, 39–45. doi:10.1016/j.cageo.2017.10.009.
- Croke, J., Todd, P., Thompson, C., Watson, F., Denham, R., Khanal, G., 2013. The use of multi temporal LiDAR to assess basin-scale erosion and deposition following the catastrophic January 2011 Lockyer flood, SE Queensland, Australia, *Geomorphology*, 184, 111–126. doi:10.1016/j.geomorph.2012.11.023.
- Crowe, J. C., Wilcock, P. R., 2002. An Experimental Study of the Step-Pool Bedform, in: AGU Fall Meeting Abstracts. pp. H21G-01.
- Cucchiaro, S., Cazorzi, F., Marchi, L., Crema, S., Beinat, A., Cavalli, M., 2019. Multi-temporal analysis of the role of check dams in a debris-flow channel: Linking structural and functional connectivity, *Geomorphology*, 345. doi:10.1016/j.geomorph.2019.106844.
- Cucchiaro, S., Maset, E., Cavalli, M., Crema, S., Marchi, L., Beinat, A., Cazorzi, F., 2020. How does co-registration affect geomorphic change estimates in multi-temporal surveys? *GIScience and Remote Sensing* 57(5), 611–632. <https://doi.org/10.1080/15481603.2020.1763048>.
- Cyr, A.J., Granger, D.E., 2008. Dynamic equilibrium among erosion, river incision, and coastal uplift in the northern and central Apennines, Italy. *Geology*, 36 (2), 103–106. doi:10.1130/G24003A.1
- D’Agostino, V., Lenzi, M.A., 1999. Bedload transport in the instrumented catchment of the Rio Cordon: Part II: Analysis of the bedload rate. *Catena* 36, 191–204.
- Dalla Fontana, G., Marchi, L., 1994. Sediment source areas in a small alpine basin. *International Symposium on Forest Hydrology*, Oct. 24–28, Tokyo, Japan, 455–462.
- Davies, T.R., Korup, O., 2010. Sediment cascades in active landscapes. In: Burt, T., Allison, R.J. (Eds.), *Sediment Cascades: An Integrated Approach*. John Wiley and Sons, Chichester, 89–115.
- Davies, T.R., Sutherland, A.J., 1980. Resistance to flow past deformable boundaries. *Earth Surface Processes* 5, 175–179. <https://doi.org/https://doi.org/10.1002/esp.3760050207>
- Davolio, S., Della Fera, S., Laviola, S., Miglietta, M.M., Levizzani, V., 2020. Heavy precipitation over Italy from the Mediterranean storm “Vaia” in October 2018: Assessing the role of an atmospheric river. *Monthly Weather Review* 148, 3571–3588.
- Dean, D., Schmidt, J., 2013. The geomorphic effectiveness of a large flood on the Rio Grande in the Big Bend region: Insights on geomorphic controls and post-flood geomorphic response. *Geomorphology*, 201, 183–198. doi:10.1016/j.geomorph.2013.06.020.

- DiBiase, R.A., Heimsath, A.M., Whipple, K.X., 2012. Hillslope response to tectonic forcing in threshold landscapes, *Earth Surface Processes and Landforms*, 37 (8), 855–865. doi:10.1002/esp.3205.
- Diodato, N., Mao, L., Borrelli, P., Panagos, P., Fiorillo, F., Bellocchi, G., 2018. Climate-scale modelling of suspended sediment load in an Alpine catchment debris flow (Rio Cordon-northeastern Italy). *Geomorphology*, 309, 20–28. doi:10.1016/j.geomorph.2018.02.026.
- Dong, X., Grimm, N.B., Ogle, K., Franklin, J., 2016. Temporal variability in hydrology modifies the influence of geomorphology on wetland distribution along a desert stream. *Journal of Ecology*, 104, 18–30. doi:10.1111/1365-2745.12450.
- Duvert, C., Gratiot, N., Némery, J., Burgos, A., Navratil, O., 2011. Sub-daily variability of suspended sediment fluxes in small mountainous catchments-implications for community-based river monitoring. *Hydrology and Earth System Sciences*, 15, 703–713. doi:10.5194/hess-15-703-2011.
- Duvert, C., Nord, G., Gratiot, N., Navratil, O., Nadal-Romero, E., Mathys, N., Némery, J., Regüés, D., García-Ruiz, J.M., Gallart, F., Esteves, M., 2012. Towards prediction of suspended sediment yield from peak discharge in small erodible mountainous catchments (0.45–22 km²) of France, Mexico and Spain. *Journal of Hydrology*, 454–455, 42–55. doi: 10.1016/j.jhydrol.2012.05.048.
- Eaton, B.C., Giles, T.R., 2009. Assessing the effect of vegetation-related bank strength on channel morphology and stability in gravel bed streams using numerical models. *Earth Surface Processes and Landforms*, 34 (5), 712–724. doi:10.1002/esp.1768.
- Einstein, H. A., Anderson, A. G., Johnson, J. W., 1940. A distinction between bed-load and suspended load in natural streams. *Transactions: American Geophysical Union*, 21(2), 628–633. doi:10.1029/TR021i002p00628.
- Eiriksdottir, E.S., Louvat, P., Gislason, S.R., Óskarsson, N., Hardardóttir, J., 2008. Temporal variation of chemical and mechanical weathering in NE Iceland: evaluation of a steady-state model of erosion. *Earth and Planetary Science Letters*, 272(1–2), 78–88. doi: 10.1016/j.epsl.2008.04.005.
- Eltner, A., Maas, H.G., Faust, D., 2018. Soil micro-topography change detection at hillslopes in fragile Mediterranean landscapes. *Geoderma*. 313, 217–232. doi: 10.1016/j.geoderma.2017.10.034.
- Fattorelli, S., Lenzi, M.A., Marchi, L., Keller, H.M., 1988. An experimental station for the automatic recording of water and sediment discharge in a small alpine watershed, *Hydrological Sciences Journal*, 33:6, 607–617. doi:10.1080/02626668809491293
- Fernández, C., Fernández-Alonso, J.M., Vega, J.A., 2020. Exploring the effect of hydrological connectivity and soil burn severity on sediment yield after wildfire and mulching. *Land Degrad. Dev.*, 31, pp. 1611–1621, doi: 10.1002/ldr.3539.

- Ferrato, C., De Marco, J., Tarolli, P., Cavalli, M., 2017. An updated source areas inventory in the Rio Cordon catchment (Dolomites). *Rendiconti Online Società Geologica Italiana* 42, 10-13.
- Fischer, L., Huggel, C., Kääb, A., Haeberli, W., 2013. Slope failures and erosion rates on a glacierized high-mountain face under climatic changes. *Earth Surface Processes and Landforms*, 38(8), 836–846. <https://doi.org/10.1002/esp.3355>
- Fischer, E.M., Knutti, R., 2015. Anthropogenic contribution to global occurrence of heavy-precipitation and high-temperature extremes. *Nature Climate Change* 5, 560–564.
- Foster, R., Knight, D., Dennis, F.J., 1998. Landscape Patterns and Legacies Resulting from Large, Infrequent Forest Disturbances. *Ecosystems*, 1, 497-510.
- Friele, P., Millard, T.H., Mitchell, A., Allstadt, K.E., Menounos, B., Geertsema, M., Clague, J.J., 2020. Observations on the May 2019 Joffre Peak landslides, British Columbia. *Landslides* 17 (4), 913–930.
- Fryirs, K.A., Brierley, G.J., Preston, N.J., Kasai, M., 2007. Buffers, barriers and blankets: The (dis)connectivity of catchment-scale sediment cascades. *Catena* 70(1), 49–67. <https://doi.org/10.1016/j.catena.2006.07.007>
- Fryirs, K., 2013. (Dis)Connectivity in catchment sediment cascades: A fresh look at the sediment delivery problem. *Earth Surface Processes and Landforms* 38(1), 30–46. <https://doi.org/10.1002/esp.3242>
- Fryirs, K., Brierley, G.J., 2013. *Geomorphic Analysis of River Systems: An Approach to Reading the Landscape*. Chichester: Wiley.
- Fryirs, K. A., 2017. River sensitivity: a lost foundation concept in fluvial geomorphology. *Earth Surf. Process. Landforms*, 42: 55– 70. doi: 10.1002/esp.3940.
- Gao, P., Pasternack, G., 2007. Dynamics of suspended sediment transport at field-scale drain channels of irrigation-dominated watersheds in the Sonoran Desert, south-eastern California. *Hydrological Processes*, 21, 2081-2092. doi:10.1002/hyp.6398.
- Gao, P., Josefson, M., 2012. Event-based suspended sediment dynamics in a central New York watershed. *Geomorphology: 139-140*: 425– 437. doi: 10.1016/j.geomorph.2011.11.007.
- García-Rama, A., Pagano, S.G., Gentile, F., Lenzi, M.A., 2016. Suspended sediment transport analysis in two Italian instrumented catchments. *Journal of Mountain Science*, 13, 957–970. doi:10.1007/s11629-016-3858-x.
- Gariano, S. L., Guzzetti, F., 2016. Landslides in a changing climate. *Earth-Science Reviews*, 162, 227–252. <https://doi.org/10.1016/j.earscirev.2016.08.011>.
- Gaume, E., Borga, M., 2008. Post-flood field investigations in upland catchments after major flash floods: proposal of a methodology and illustrations. *Journal of Flood Risk Management* 1, 175–189.

- Gianolla, P., 2008. Geology. In: Nomination of the Dolomites for inscription on the World Natural Heritage List UNESCO; Dolomiti, Belluno, 1, 363.
- Gintz', D., Hassan, M.A., Schmidt', K.-H., 1996. Frequency and magnitude of bedload in a mountain river. *Earth Surf Process Landf* 21, 433–445.
- Giordano, D., 2011. La Valle di San Lucano: il progetto Tegas: gli aspetti geomorfologici. In: Aldighieri B, Testa B (eds) *L'armonia fra uomo e natura nelle valli dolomitiche. Atti delle giornate di studio di Agordo, 12–13 novembre 2010*. Aracne, Roma, 49–82. doi:10.4399/9788854841714.
- Giorgi, F., Torma, C., Coppola, E., Ban, N., Schär, C., Somot, S., 2016. Enhanced summer convective rainfall at Alpine high elevations in response to climate warming. *Nature Geoscience*, 9(8), 584–589. <https://doi.org/10.1038/ngeo2761>.
- Giovannini, L. Davolio, S., Zaramella, M., Zardi, D., Borga, M., 2021. Multi-model convection-resolving simulations of the October 2018 Vaia storm over Northeastern Italy. *Atmospheric Research* 253, 105455.
- Glendell, M., Brazier, R.E., 2014. Accelerated export of sediment and carbon from a landscape under intensive agriculture. *Science of the Total Environment*, 476, 643–656. doi:10.1016/j.scitotenv.2014.01.057.
- Gob, F., Bravard, J.P., Petit, F., 2010. The influence of sediment size, relative grain size and channel slope on initiation of sediment motion in boulder bed rivers. A lichenometric study. *Earth Surface Processes and Landforms* 35, 1535–1547.
- Gomi, T., Sidle, R.C., Woodsmith, R.D., Bryant, M.D., 2003. Characteristics of channel steps and reach morphology in headwater streams, southeast Alaska. *Geomorphology* 51, 225–242. [https://doi.org/10.1016/S0169-555X\(02\)00338-0](https://doi.org/10.1016/S0169-555X(02)00338-0)
- Gomi, T., Dan Moore, R., Hassan, M.A., 2005. Suspended sediment dynamics in small forest streams of the Pacific Northwest. *Journal of the American Water Resources Association*, 41(4), 877–898. doi:10.1111/j.1752-1688.2005.tb03775.x.
- Gorczyca, E., Krzemień, K., Wrońska-Wałach, D., Sobucki, M., 2013. Channel changes due to extreme rainfalls in the Polish Carpathians. In: Loczy, D. (Ed.), *Geomorphological Impacts of Extreme Weather, Case Studies from Central and Eastern Europe*. Springer, Dordrecht, 23–35.
- Guzzetti F., Ardizzone F., Cardinali M., Rossi M., Valigi D., 2009. Landslide volumes and landslide mobilization rates in Umbria, central Italy, *Earth and Planetary Science Letters*, 279, 222–229. doi:10.1016/j.epsl.2009.01.005.
- Hajdukiewicz, H., Wyżga, B., Mikuś, P., Zawiejska, J., Radecki-Pawlik, A., 2016. Impact of a large flood on mountain river habitats, channel morphology, and valley infrastructure. *Geomorphology* 272, 55–67.

- Harris, C., Arenson, L. U., Christiansen, H. H., Etzelmüller, B., Frauenfelder, R., Gruber, S., et al., 2009. Permafrost and climate in Europe: Monitoring and modelling thermal, geomorphological and geotechnical responses. *Earth-Science Reviews*, 92(3–4), 117–171. <https://doi.org/10.1016/j.earscirev.2008.12.002>
- Heckmann, T., Schwanghart, W., 2013. Geomorphic coupling and sediment connectivity in an alpine catchment - Exploring sediment cascades using graph theory. *Geomorphology* 182, 89–103. <https://doi.org/10.1016/j.geomorph.2012.10.033>.
- Heckmann, T., Cavalli, M., Cerdan, O., Foerster, S., Javaux, M., Lode, E., Smetanová, A., Vericat, D., Brardinoni, F., 2018. Indices of sediment connectivity: opportunities, challenges and limitations. *Earth-Science Reviews*, 187, 77–108. doi:10.1016/j.earscirev.2018.08.004.
- Hirschberg, J., Fatichi, S., Bennett, G. L., McArdell, B. W., Peleg, N., Lane, S. N., et al., 2021. Climate change impacts on sediment yield and debris-flow activity in an Alpine catchment. *Journal of Geophysical Research: Earth Surface*, 126, e2020JF005739. <https://doi.org/10.1029/2020JF005739>.
- Hlásny, T., Kočický, D., Mareta, M., Sitková, Z., Barka, I., Konôpka, M., Hlavatá, H., 2015. Effect of deforestation on watershed water balance: hydrological modelling-based approach / Vplyv odlesnenia na vodnú bilanciu povodia: prístup na báze hydrologického modelovania, *Central European Forestry Journal*, 61(2), 89-100. doi:10.1515/forj-2015-0017.
- Hinderer, M., Kastowski, M., Kamelger, A., Bartolini, C., Schlunegger, C., 2013. River loads and modern denudation of the Alps — a review. *Earth-Science Reviews*, 118, 11-44. doi:10.1016/j.earscirev.2013.01.001.
- Hooke, J.M., 2016. Geomorphological impacts of an extreme flood in SE Spain. *Geomorphology*, 263, 19–38. <https://doi.org/10.1016/j.geomorph.2016.03.021>.
- Hurst, M.D., Mudd, S.M., Walcott, R., Attal, M., Yoo, K., 2012. Using hilltop curvature to derive the spatial distribution of erosion rates, *Journal of Geophysical Research*, 117, F02017. doi:10.1029/2011JF002057.
- Iheaturu, C.J., Ayodele, E.G., Okolie, C.J., 2020. An assessment of the accuracy of Structure-from-Motion (SfM) photogrammetry for 3D terrain mapping. *Geomatics, Landmanagement and Landscape* 2, 65–82. <https://doi.org/10.15576/GLL/2020.2.65>
- IPCC, 2012. Managing the risks of extreme events and disasters to advance climate change adaptation. A special report of working groups I and II of the intergovernmental panel on climate change. Cambridge, UK: Cambridge University Press. <https://doi.org/10.1596/978-0-8213-8845-7>
- Ivy-Ochs, S., Martin, S., Campedel, P., Hippe, K., Alfimov, V., Vockenhuber, C., Andreotti, E., Carugati, G., Pasqual, D., Rigo, M., Viganò, A., 2017. Geomorphology and age of the Marocche di Dro rock avalanches (Trentino, Italy). *Quaternary Science Reviews*, 169, 188–205. doi:10.1016/j.quascirev.2017.05.01.

- Jautzy, T., Maltais, M., Buffin-Bélanger, T., 2021. Interannual evolution of hydrosedimentary connectivity induced by forest cover change in a snow-dominated mountainous catchment. *Land Degrad. Dev.*, 32, pp. 2318-2335. doi:10.1002/ldr.3902.
- Joyce, H., Hardy, R., Warburton, J., Large, A., 2018. Sediment continuity through the upland sediment cascade: geomorphic response of an upland river to an extreme flood event. *Geomorphology*, 317, 45-61. doi:10.1016/j.geomorph.2018.05.002.
- Keiler, M., Knight, J., Harrison, S., 2010. Climate change and geomorphological hazards in the eastern European Alps. *Phil. Trans. R. Soc. A*. 3682461–2479. <http://doi.org/10.1098/rsta.2010.0047>.
- Keiser, A.D., Knoepp, J.D., Bradford, M.A., 2016. Disturbance Decouples Biogeochemical Cycles Across Forests of the Southeastern US. *Ecosystems*, 19, 50–61. doi:10.1007/s10021-015-9917-2.
- Klein, M., 1984. Anti clockwise hysteresis in suspended sediment concentration during individual storms: Holbeck Catchment; Yorkshire, England, *Catena*, 11, 251-257. doi:10.1016/0341-8162(84)90014-6.
- Knighton, D., 1998. *Fluvial Forms and Processes: A New Perspective* (2nd ed.). Routledge. <https://doi.org/10.4324/9780203784662>.
- Knox, J.C., 2006. Floodplain sedimentation in the Upper Mississippi Valley: Natural versus human accelerated. *Geomorphology*, 79, 286–310. doi:10.1016/j.geomorph.2006.06.031.
- Koci, J., Sidle, R.C., Jarihani, B., Cashman, M.J., 2020. Linking hydrological connectivity to gully erosion in the catchment of a savanna rangelands tributary which flows to the Great Barrier Reef using structure-from-motion photogrammetry. *Land Degradation and Development*, 31, 20– 36. doi:10.1002/ldr.3421.
- Krapesch, G., Hauer, C., Habersack, H., 2011. Scale orientated analysis of river width changes due to extreme flood hazards. *Natural Hazards and Earth System Sciences*, 11 (8), 2137–2147. doi:10.5194/nhess-11-2137-2011.
- Lane, E. W., Borland, W. M., 1951. Estimating bedload. *Trans. Am. Geophys. Union* 32(1), 121–123.
- Lane, S.N., Bakker, M., Costa, A., Girardclos, S., Loizeau, J-L., Molnar, P., Silva, T., Stutenbecker, L., Schlunegger, F., 2019. Making stratigraphy in the Anthropocene: Climate change impacts and economic conditions controlling the supply of sediment to Lake Geneva. *Scientific Reports* 9, 1–11. doi:10.1038/s41598-019-44914-9.
- Lane, S.N., Westaway, R. M., Hicks, D. M., 2003. Estimation of erosion and deposition volumes in a large, gravel-bed, braided river using synoptic remote sensing. *Earth Surface Processes and Landforms* 28(3), 249–271. <https://doi.org/10.1002/esp.483>

- Lange, O.L., Nobel, P.S., Osmond, C.B., Ziegler, H., 1981. *Physiological Plant Ecology I: Responses to the Physical Environment*. Springer-Verlag Berlin Heidelberg, 12 (A), XVI, 628. doi:10.1007/978-3-642-68090-8.
- Langhammer, J., Su Y., Bernsteinova, J., 2015. Runoff response to climate warming and forest disturbance in a mid-mountain basin. *Water*, 7(7), 3320–3342. doi:10.3390/w7073320.
- Lawlor, S., 2004. Determination of channel-morphology characteristics, bankfull discharge, and various design-peak discharges in western Montana. Scientific Investigations Report. doi:10.3133/sir20045263.
- Leenman, A., Eaton, B., 2021. Mechanisms for avulsion on alluvial fans: Insights from high-frequency topographic data. *Earth Surf Process Landf* 46, 1111–1127. <https://doi.org/10.1002/esp.5059>
- Lenzi, M.A., D'Agostino, V., Billi, P., 1999. Bedload transport in the instrumented catchment of the Rio Cordon: Part I: Analysis of bedload records, conditions and threshold of bedload entrainment. *Catena* 36 (3), 171-190.
- Lenzi, M.A., Marchi, L., 2000. Suspended sediment load during floods in a small stream of the Dolomites (northeastern Italy). *Catena* 39(4), 267–282. [https://doi.org/10.1016/S0341-8162\(00\)00079-5](https://doi.org/10.1016/S0341-8162(00)00079-5).
- Lenzi, M.A., 2001. Step-pool evolution in the Rio Cordon, Northeastern Italy. *Earth Surface Processes and Landforms* 26(9), 991–1008. <https://doi.org/10.1002/esp.239>.
- Lenzi, M.A., Mao, L., Comiti, L., 2003. Interannual variation of suspended sediment load and sediment yield in an alpine catchment, *Hydrological Sciences Journal*, 48(6), 899-915. doi: 10.1623/hysj.48.6.899.51425.
- Lenzi, M.A., Mao, L., Comiti, F., 2004. Magnitude-frequency analysis of bed load data in an Alpine boulder bed stream. *Water Resources Research* 40(7). <https://doi.org/10.1029/2003WR002961>.
- Lenzi, M.A., Mao, L., Comiti, F., 2006a. Effective discharge for sediment transport in a mountain river: computational approaches and geomorphic effectiveness. *Journal of Hydrology* 326 (1-4), 257-276.
- Lenzi, M.A., Mao, L., Comiti, F., 2006b. When does bedload transport begin in steep boulder-bed streams? *Hydrological Processes* 20, 3517-3533.
- Liébault, F., Piégay, H., 2002. Causes of the 20th century channel narrowing in mountain and piedmont rivers of southeastern France. *Earth Surface Processes and Landforms* 27, 425-444.
- Liébault, F., Bellot, H., Chapuis, M., Klotz, S., Deschâtres, M., 2012. Bedload tracing in a high-sediment-load mountain stream. *Earth Surface Processes and Landforms* 37, 385-399.
- Liébault, F., Laronne, J.B., Klotz, S., Bel, C., 2022. Seasonal bedload pulses in a small alpine catchment, *Geomorphology*, Volume 398, 108055. <https://doi.org/10.1016/j.geomorph.2021.108055>.

- Lin, W.T., Chou, W.C., Lin, C.Y., Huang, P.H., Tsai, J.S., 2006. Automated suitable drainage network extraction from digital elevation models in Taiwan's upstream watersheds. *Hydrological Processes*, 20: 289-306. doi:10.1002/hyp.5911.
- Liro, M., Ruiz-Villanueva, V., Mikuš, P., Wyżga, B., Bladé Castellet, E., 2020. Changes in the hydrodynamics of a mountain river induced by dam reservoir backwater. *Science of the Total Environment* 744. <https://doi.org/10.1016/j.scitotenv.2020.140555>
- Lizaga, I., Quijano, L. Palazón, L. Gaspar, L., Navas A., 2017. Enhancing connectivity index to assess the effects of land use changes in a Mediterranean catchment. *Land Degrad. Dev.*, 675 (2017), pp. 663-675, 10.1002/ldr.2676
- López-Vicente, M., Ben-Salem, N., 2019. Computing structural and functional flow and sediment connectivity with a new aggregated index: A case study in a large Mediterranean catchment, *Science of The Total Environment*, 651(1), 179-19. doi:10.1016/j.scitotenv.2018.09.170.
- López-Vicente, M., González-Romero, J., Lucas-Borja, M.E., 2020. Forest fire effects on sediment connectivity in headwater sub-catchments: Evaluation of indices performance. *Sci. Total Environ.*, 732, 139206. Doi: 10.1016/j.scitotenv.2020.139206.
- Lucía, A., Schwientek, M., Eberle, J., Zarfl, C., 2018. Planform changes and large wood dynamics in two torrents during a severe flash flood in Braunsbach, Germany 2016. *Science of the Total Environment* 640–641, 315–326.
- Lucianetti, G., Mastrorillo, L., Mazza, R., Partel, P., 2019. Groundwater response to precipitation extremes: the case of the “Vaia” storm (Eastern Italian Alps). *Acque Sotterranee - Italian Journal of Groundwater*, 8(4). doi:10.7343/as-2019-429.
- Macchi, G., Crema, S., Arzillero, L., Boretto, G., Fanti, B., Marchi, L., Monegato, G., Cavalli, M., 2022. Assessing debris-flow activity and geomorphic changes caused by an extreme rainstorm: the case study of the Liera catchment (Dolomites, northeastern Italy). *Rendiconti Online della Società Geologica Italiana*. 58. 1-7. 10.3301/ROL.2022.13.
- Mackin, J.H., 1948. Concept of the graded river. *Geological Society of America Bulletin* 59, 463-511.
- Magilligan, F.J., 1992. Thresholds and the spatial variability of flood power during extreme floods. *Geomorphology* 5, 373–390.
- Magilligan, F.J., Buraas, E.M., Renshaw, C.E., 2015. The efficacy of stream power and flow duration on geomorphic responses to catastrophic flooding. *Geomorphology* 228, 175–188.
- Mao, L., Lenzi, M.A., 2007. Sediment mobility and bedload transport conditions in an alpine stream. *Hydrological Processes* 21, 1882-1891.

- Mao, L., Uyttendaele, G.P., Iroumé, A., Lenzi, M.A., 2008. Field based analysis of sediment entrainment in two high gradient streams located in Alpine and Andine environments. *Geomorphology*, 93, pp. 368-383.
- Mao, L., Carrillo, R., 2017. Temporal dynamics of suspended sediment transport in a glacierized Andean basin. *Geomorphology*, 287, 116–125. doi: 10.1016/j.geomorph.2016.02.003.
- Mao, L., Toro, M., Carrillo, R., Brardinoni, F., Fraccarollo, L., 2020. Controls over particle motion and resting times of coarse bed load transport in a glacier-fed mountain stream. *J. Geophys. Res. Earth Surf.*, 125. doi: 10.1029/2019jf005253.
- Marchi, L., Cavalli, M., Sangati, M., Borga, M., 2009a. Hydrometeorological controls and erosive response of an extreme alpine debris flow. *Hydrological Processes* 23 (19), 2714–2727
- Marchi, L., Borga, M., Preciso, E., Sangati, M., Gaume, E., Bain, V., Delrieu, G., Bonnifait, L., Pogačnik, N., 2009b. Comprehensive post-event survey of a flash flood in Western Slovenia: observation strategy and lessons learned. *Hydrological Processes* 23, 3761–3770
- Marchi, L., Cavalli, M., Amponsah, W., Borga, M., Crema, S., 2016. Upper limits of flash flood stream power in Europe. *Geomorphology* 272 (1), 68–77.
- Marston, R.A., 1982. The Geomorphic Significance of Log Steps in Forest Streams1. *Annals of the Association of American Geographers* 72, 99–108. <https://doi.org/10.1111/j.1467-8306.1982.tb01386.x>
- Martini, L., Faes, L., Picco, L., Iroumé, A., Lingua, E., Garbarino, M., Cavalli, M., 2020. Assessing the effect of fire severity on sediment connectivity in central Chile, *Science of The Total Environment*, Volume 728, 139006. doi:10.1016/j.scitotenv.2020.139006.
- Martini, L., Cavalli, M., Picco, L., 2022. Predicting sediment connectivity in a mountain basin: A quantitative analysis of the index of connectivity. *Earth Surface Processes and Landforms*, 47 (6), 1500– 1513. doi:10.1002/esp.5331.
- Martinsen, O., 1994. Mass movements. In: Maltman, A. (eds) *The Geological Deformation of Sediments*. Springer, Dordrecht. https://doi.org/10.1007/978-94-011-0731-0_5
- Wohl E., 2000. *Mountain Rivers*. American Geophysical Union Press, Washington, DC.
- Mazzorana, B., Picco, L., Rainato, R., Iroumé, A., Ruiz-Villanueva, V., Rojas, C., Valdebenito, G., Iribarren-Anacona, P., Melnick, D., 2019. Cascading processes in a changing environment: Disturbances on fluvial ecosystems in Chile and implications for hazard and risk management. *Science of the Total Environment*, 655, 1089-1103. doi:10.1016/j.scitotenv.2018.11.217.
- Mazzuoli, M., Vittori, G., Blondeaux, P., 2022. The dynamics of sliding, rolling and saltating sediments in oscillatory flows, *European Journal of Mechanics - B/Fluids*, Volume 94, Pages 246-262, <https://doi.org/10.1016/j.euromechflu.2022.03.006>.

- McColl, S.T., 2015. Chapter 2- Landslide causes and triggers. In J. F. Shroder, T. Davies, 2015, *Landslide hazards, risks and disasters* (Chap. 2, pp. 17–42). Academic Press. doi:10.1016/B978-0-12-396452-6.00002-1.
- McEwen, L.J., Werritty, A., 1988. The hydrology and long-term geomorphic significance of a flash flood in the Cairngorm mountains, Scotland. *Catena* 15, 361–377.
- Megahan, W.F., King, J.G., 2004. Erosion, sedimentation, and cumulative effects in the northern Rocky Mountains. In: Ice GG, Stednick D (eds) *A century of forest and wildland watershed lessons*. The Society of American Foresters, Bethesda, 201–222.
- Messenzehl, K., Hoffmann, T., Dikau, R., 2014. Sediment connectivity in the high-alpine valley of Val Mütschans, Swiss National Park - linking geomorphic field mapping with geomorphometric modelling. *Geomorphology* 221, 215–229. <https://doi.org/10.1016/j.geomorph.2014.05.033>.
- Miller, A.J., 1990. Flood hydrology and geomorphic effectiveness in the central Appalachians. *Earth Surface Processes and Landforms* 15, 119–134.
- Mills, C.F., Bathurst, J.C., 2015. Spatial variability of suspended sediment yield in a gravel bed river across four orders of magnitude of catchment area. *Catena*, 133, 14–24. doi:10.1016/j.catena.2015.04.008.
- Misset, C., Recking, A., Legout, C., Bakker, M., Bodereau, N., Borgniet, L., Cassel, M., Geay, T., Gimbert, F., Navratil, O., Piegay, H., Valsangkar, N., Cazilhac, M., Poirel, A., Zanker, S., 2020. Combining multi-physical measurements to quantify bedload transport and morphodynamics interactions in an Alpine braiding river reach. *Geomorphology* 351. <https://doi.org/10.1016/j.geomorph.2019.106877>
- Misset, C., Recking, A., Legout, C., Bakker, M., Gimbert, F., Geay, T., Zanker, S., 2021. Using continuous turbidity and seismic measurements to unravel sediment provenance and interaction between suspended and bedload transport in an Alpine catchment. *Geophysical Research Letters*, 48, e2020GL090696. doi:10.1029/2020GL090696.
- Moatar, F., Person, G., Meybeck, M., Coynel, A., Etcheber, H., Crouzet, P., 2006. The influence of contrasting suspended particulate matter transport regimes on the bias and precision of flux estimates, *Science of the Total Environment*, 370, 515–531. doi:10.1016/j.scitotenv.2006.07.029.
- Molnar, P., Densmore, A.L., McArdeell, B.W., Turowski, J.M., Burlando, P., 2010. Analysis of changes in the step-pool morphology and channel profile of a steep mountain stream following a large flood. *Geomorphology* 124, 85–94. <https://doi.org/10.1016/j.geomorph.2010.08.014>
- Montgomery, D.R., Buffington, J.M., 1997. Channel-reach morphology in mountain drainage basins. *Geological Society of America Bulletin*, 109(5), 596–611.
- Moore, R.D., 2005. Slug injection using salt in solution. *Streamline, Watershed Manag. Bull.*, 8 , 1-6. doi:10.1592/phco.23.9.1S.32890.

- Motta, R., Ascoli, D., Corona, P., Marchetti, M., Vacchiano, G., 2018. Selvicoltura e schianti da vento. Il caso della “tempesta Vaia”. *Forest@* 15: 94-98. - doi: 10.3832/efor2990-015
- Mouri, G., Ros, F.C., Chalov, S., 2014. Characteristics of suspended sediment and river discharge during the beginning of snowmelt in volcanically active mountainous environments. *Geomorphology*, 213, 266–276. doi:10.1016/j.geomorph.2014.02.001.
- Muddle, D., Briggs, K.M., Dashwood, C., Dijkstra, T., 2015. The influence of slope geology on landslide occurrence during extreme rainfall. *Geotechnical Engineering for Infrastructure and Development*, 1813-1818. doi:10.1680/ecsmge.60678.vol4.271.
- Murphy, B. P., Czuba, J. A., Belmont, P., 2019. Post-wildfire sediment cascades: A modeling framework linking debris flow generation and network-scale sediment routing. *Earth Surf. Process. Landforms*, 44: 2126–2140. <https://doi.org/10.1002/esp.4635>.
- Nadal-Romero, E., Lasanta, T., García-Ruiz, J.M., 2013. Runoff and sediment yield from land under various uses in a Mediterranean mountain area: long-term results from an experimental station. *Earth Surface Processes and Landforms*, 38 (4), pp. 346-355. doi:10.1002/esp.3281.
- Najafi, S., Dragovich, D., Heckmann, T., Sadeghi S.H., 2021. Sediment connectivity concepts and approaches, *Catena*, 196, 104880. doi:10.1016/j.catena.2020.104880.
- Nannoni, A., Vigna, B., Fiorucci, A., Antonellini, M., De Waele, J., 2020. Effects of an extreme flood event on an alpine karst system. *Journal of Hydrology* 590, 125493.
- Nanson, G.C., Knighton, A.D., 1996. Anabranching rivers: their cause, character and classification. *Earth Surf Process Landf* 21, 217–239.
- Nanson, G.C., Huang, H.Q., 2018. A philosophy of rivers: equilibrium states, channel evolution, teleomatic change and least action principle. *Geomorphology*, 302, 3-19. doi:10.1016/j.geomorph.2016.07.024.
- Neverman, A.J., Fuller, I.C., Procter, J.N., 2016. Application of geomorphic change detection (GCD) to quantify morphological budgeting error in a New Zealand gravel bed river: A case study from the Makaroro River, Hawke’s Bay. *Journal of Hydrology (NZ)*, 55, 45–63.
- Orlandini, S., Lamberti, A., 2000. Effect of Wind on Precipitation Intercepted by Steep Mountain Slopes. *Journal of Hydrologic Engineering*, 5, 346-354. doi:10.1061/(ASCE)1084-0699(2000)5:4(346).
- Ortíz-Rodríguez, A. J., Borselli, L., Sarocchi, D., 2017. Flow connectivity in active volcanic areas: use of index of connectivity in the assessment of lateral flow contribution to main streams, *Catena*, 157, pp. 90-111. doi:10.1016/j.catena.2017.05.009.
- Oss Cazzador, D., Rainato, R., Cavalli, M., Lenzi, M.A., Picco L., 2020. Integrated analysis of sediment source areas in an Alpine basin, *Catena*, 188, 104416, ISSN 0341-8162. doi:10.1016/j.catena.2019.104416.

- Oss Cazzador, D., Rainato, R., Mao, L., Martini, L., Picco, L., 2021. Coarse sediment transfer and geomorphic changes in an alpine headwater stream. *Geomorphology* 376, 107569. <https://doi.org/10.1016/j.geomorph.2020.107569>.
- Parida, S., Singh, V., Tandon, S., 2019. Sediment connectivity and evolution of gravel size composition in Dehra Dun – an Intermontane Valley in the Frontal Zone of NW Himalaya. *Zeitschrift für Geomorphologie*, 2 (62), 83-105. doi:10.1127/zfg/2019/0568.
- Pagano, S.G., Rainato, R., Garcia-Rama, A., Gentile, F., Lenzi, M.A., 2019. Analysis of suspended sediment dynamics at event scale: comparison between a Mediterranean and an Alpine basin, *Hydrological Sciences Journal* 64(8), 948-961.
- Pampalone, V., Di Stefano, C., Nicosia, A., Palmeri, V., Ferro, V., 2021. Analysis of rill step–pool morphology and its comparison with stream case. *Earth Surf Process Landf* 46, 775–790. <https://doi.org/10.1002/esp.5063>
- Park, J., Hunt, J.R., 2017. Coupling fine particle and bedload transport in gravel-bedded streams. *Journal of Hydrology*, 552, 532–543. doi:10.1016/j.jhydrol.2017.07.023.
- Pastorello, R., D'Agostino, V., Hürlimann, M., 2020. Debris flow triggering characterization through a comparative analysis among different mountain catchments, *Catena*, 186, 104348. doi:10.1016/j.catena.2019.104348.
- Peleg, N., Skinner, C., Fatichi, S., Molnar, P., 2020. Temperature effects on the spatial structure of heavy rainfall modify catchment hydro-morphological response. *Earth Surface Dynamics* 8, 17–36.
- Pellegrini, G., Martini, L., Cavalli, M., Rainato, R., Cazorzi, A., Picco, L., 2021a. The morphological response of the Tegnas alpine catchment (Northeast Italy) to a Large Infrequent Disturbance. *Science of the Total Environment* 770, 145209. <https://doi.org/10.1016/j.scitotenv.2021.145209>
- Pellegrini, G., Rainato, R., Martini, L., Picco, L., 2021b. The Morphological Evolution of a Step–Pool Stream after an Exceptional Flood and Subsequent Ordinary Flow Conditions. *Water*, 13(24), 3630. doi:10.3390/w13243630.
- Penna, D., Tromp-van Meerveld, H. J., Gobbi, A., Borga, M., and Dalla Fontana, G., 2011. The influence of soil moisture on threshold runoff generation processes in an alpine headwater catchment. *Hydrology and Earth System Sciences*, 15, 689–702. doi:10.5194/hess-15-689-2011.
- Pepin, N.C., Lundquist, J.D., 2008. Temperature trends at high elevations: Patterns across the globe, *Geophysical Research Letters*, 35, L14701. doi:10.1029/2008GL034026.
- Perucca, E., Camporeale, C., Ridolfi, L., 2007. Significance of the riparian vegetation dynamics on meandering river morphodynamics, *Water Resources Research*, 43, W03430. doi:10.1029/2006WR005234.

- Phillips, J. D., 2009. Changes, perturbations, and responses in geomorphic systems. *Progress in Physical Geography: Earth and Environment*, 33(1), 17–30. <https://doi.org/10.1177/0309133309103889>.
- Picco, L., Mao, L., Rigon, E., Moretto, J., Ravazzolo, D., Delai, F., Lenzi, M.A., 2012. An update of the sediment fluxes investigation in the Rio cordon (Italy) after 25 years of monitoring. *Journal of agricultural Engineering*. doi:10.4081/jae.2012.e17.
- Picco, L., Ravazzolo, D., Rainato, R., Lenzi, M., 2014. Characteristics of fluvial islands along three gravel-bed rivers of north-eastern Italy. *54 CIG 40*, 53–66.
- Picco, L., Sitzia, T., Mao, L., Comiti, F., Lenzi, M.A., 2016a. Linking riparian woody communities and fluviomorphological characteristics in a regulated gravel-bed river (Piave River, Northern Italy). *Ecohydrology*, 9, 101–112. doi: 10.1002/eco.1616.
- Picco, L., Tonon, A., Rainato, R., Lenzi, M.A., 2016b. Bank erosion and large wood recruitment along a gravel bed river. *Journal of Agricultural Engineering*, 47(2), 72-81. doi:10.4081/jae.2016.488.
- Picco, L., Rainato, R., Pellegrini, G., Martini, L., Lenzi, M.A., Mao, L., 2020. An extraordinary event changed the (morphological) appearance of a famous Alpine stream. *Proceedings of the 10th Conference on Fluvial Hydraulics (Delft, Netherlands, 7-10 July 2020)*. Taylor and Francis, ISBN 0367627736, pp. 1653-1658. <https://doi.org/10.1201/b22619>.
- Piégay, H., Arnaud, F., Belletti, B., Bertrand, M., Bizzi, S., Carbonneau, P., Dufour, S., Liébault, F., Ruiz-Villanueva, V., and Slater, L., 2020. Remotely sensed rivers in the Anthropocene: state of the art and prospects. *Earth Surf. Process. Landforms*, 45: 157–188. <https://doi.org/10.1002/esp.4787>.
- Piton, G, Recking, A., 2017. The concept of travelling bedload and its consequences for bedload computation in mountain streams. *Earth Surface Processes and Landforms* 42, 1505-1519.
- Pomeroy, J.W., Xing, F., Marks, D., 2016. The Cold Rain-on-Snow Event of June 2013 in the Canadian Rockies - Characteristics and Diagnosis. *Hydrological Processes* 30(17), 2899–2914.
- Rainato, R., Mao, L., García-Rama, A., Picco, L., Cesca, M., Vianello, A., Preciso, E., Scussel, G.R., Lenzi, M.A., 2017. Three decades of monitoring in the Rio Cordon instrumented basin: Sediment budget and temporal trend of sediment yield. *Geomorphology* 291, 45-56.
- Rainato, R., Mao, L., Picco, L., 2018a. Near-bankfull floods in an Alpine stream: effects on the sediment mobility and bedload magnitude. *International Journal of Sediment Research* 33(1), 27-34.
- Rainato, R., Picco, L., Cavalli, M., Mao, L., Neverman, A.J., Tarolli, P., 2018b. Coupling climate conditions, sediment sources and sediment transport in an alpine basin. *Land Degradation and Development* 29(4), 1154-1166.

- Rainato, R., Mao, L., Picco, L., 2020. The effects of low-magnitude flow conditions on bedload mobility in a steep mountain stream. *Geomorphology* 367, 107345.
- Rainato, R., Martini, L., Pellegrini, G., Picco, L., 2021. Hydrological, geomorphic and sedimentological responses of an alpine basin to a severe weather event (Vaia storm). *Catena (Amst)* 207, 105600. <https://doi.org/10.1016/j.catena.2021.105600>
- Recking, A., 2012. Influence of sediment supply on mountain streams bedload transport. *Geomorphology* 175-176, 139-150.
- Reid, D.E., Hickin, E.J., 2008. Flow resistance in steep mountain streams. *Earth Surface Processes and Landforms* 33, 2211-2240.
- Regione del Veneto – Consulenza tecnico scientifica dell’Università di Padova, 2020. Modellazione ed analisi delle portate al picco nel bacino del Cordevole a Ponte Alto.
- Rich, R.L., Frelich, L.E., Reich, P.B., 2007. Wind-throw mortality in the southern boreal forest: effects of species, diameter and stand age. *Journal of Ecology*, 95, 1261–1273. doi:10.1111/j.1365-2745.2007.01301.x
- Rickenmann, D., D’Agostino, V., Dalla Fontana, G., Lenzi, M., Marchi, L., 1998. New results from sediment transport measurements in two Alpine torrents. *IAHS-AISH Publication* 248, 283–289.
- Rickenmann, D., 1997. Sediment transport in Swiss torrents. *Earth Surface Processes and Landforms* 22 (10), 937-951.
- Rickenmann, D., 2020. Effect of sediment supply on cyclic fluctuations of the disequilibrium ratio and threshold transport discharge, inferred from bedload transport measurements over 27 years at the Swiss Erlenbach stream. *Water Resources Research* 56 (11), e2020WR027741.
- Rico, M., Benito, G., Barnolas, A., 2001. Combined palaeoflood and rainfall–runoff assessment of mountain floods (Spanish Pyrenees). *Journal of Hydrology* 245, 59–72.
- Rinaldi, M., Surian, N., Comiti, F., Bussetini, M., 2013. A method for the assessment and analysis of the hydromorphological condition of Italian streams: the Morphological Quality Index (MQI). *Geomorphology* 180-181, 96–108.
- Robson, B.J., Chester, E.T., Mitchell, B.D., Matthews, T.G., 2013. Disturbance and the role of refuges in mediterranean climate streams. *Hydrobiologia* 719, 77–91. <https://doi.org/10.1007/s10750-012-1371-y>
- Rovira, A., Batalla, R.J., 2006. Temporal distribution of suspended sediment transport in a Mediterranean basin: the lower Tordera (NE SPAIN). *Geomorphology*, 79, 58–71. doi:10.1016/j.geomorph.2005.09.016.
- Ruiz-Villanueva, V., Badoux, A., Rickenmann, D., Böckli, M., Schläfli, S., Steeb, N., Stoffel, M., Rickli, C., 2018. Impacts of a large flood along a mountain river basin: the importance of channel widening and

- estimating the large wood budget in the upper Emme River (Switzerland). *Earth Surface Dynamics* 6, 1115–1137.
- Rusnák, M., Sládek, J., Pacina, J., Kidová, A., 2019. Monitoring of avulsion channel evolution and river morphology changes using UAV photogrammetry: Case study of the gravel bed Ondava River in Outer Western Carpathians. *Area* 51, 549–560. <https://doi.org/10.1111/area.12508>
- Schoklitsch, A., 1962. *Handbuch des Wasserbaues*, 3rd ed., Springer, Wien.
- Schuerch, P., Densmore, A.L., McArdeell, B.W., Molnar, P., 2006. The influence of landsliding on sediment supply and channel change in a steep mountain catchment. *Geomorphology* 78, 222–235. <https://doi.org/10.1016/j.geomorph.2006.01.025>
- Schulte, L.A., Mladenoff D.J., 2005. Severe wind and fire regimes in northern forests: historical variability at the regional scale. *Ecology*, 86, 431–445.
- Scorpio, V., Crema, S., Marra, F., Righini, M., Ciccacese, G., Borga, M., Cavalli, M., Corsini, A., Marchi, L., Surian, N., Comiti, F., 2018. Basin-scale analysis of the geomorphic effectiveness of flash floods: A study in the northern Apennines (Italy). *Science of the Total Environment* 640–641, 337–351. <https://doi.org/10.1016/j.scitotenv.2018.05.252>.
- Seeger, M., Errea, M.P., Beguería, S., Arnáez, J., Martí, C., García-Ruiz, J.M., 2004. Catchment soil moisture and rainfall characteristics as determinant factors for discharge/suspended sediment hysteretic loops in a small headwater catchment in the Spanish Pyrenees. *Journal of Hydrology*, 288, 299–311. doi:10.1016/j.jhydrol.2003.10.012
- Shakti, P.C., Nakatani, T., Misumi, R., 2017. Hydrological simulation of small river basins in northern Kyushu, Japan, during the extreme rainfall event of July 5–6. *Journal of Disaster Research* 13(2), 396–409.
- Sholtes, J.S., Yochum, S.E., Scott, J.A., Bledsoe, B.P., 2018. Longitudinal variability of geomorphic response to floods. *Earth Surface Processes and Landforms* 43, 3099–3113.
- Sims, A.J., Rutherford, I.D., 2017. Management responses to pulses of bedload sediment in rivers. *Geomorphology* 294, 70–86. <https://doi.org/10.1016/j.geomorph.2017.04.010>
- Soler, M., Latron, J., Gallart, F., 2008. Relationships between suspended sediment concentrations and discharge in two small research basins in a mountainous Mediterranean area (Vallcebre, Eastern Pyrenees). *Geomorphology*, 98, 143–152. doi:10.1016/j.geomorph.2007.02.032.
- Smith, M.W., Carrivick, J.L., Quincey, D.J., 2016. Structure from motion photogrammetry in physical geography. *Prog Phys Geogr* 40, 247–275. <https://doi.org/10.1177/0309133315615805>
- Stoffel, M., Bollschweiler, M., 2008. Tree-ring analysis in natural hazards research – an overview. *Natural Hazards and Earth System Science* 8, 187–202

- Stueve, K.M., Hobie Perry, C.H., Nelson, M.D., Healey, S.P., Hill, A.D., Moisen, G.G., Cohen, W.B., Gormanson, D.D., Huang, C., 2011. Ecological importance of intermediate windstorms rivals large, infrequent disturbances in the northern Great Lakes. *Ecosphere*, 2, 1–21. doi:10.1890/ES10-00062.1
- Sun, L., Yan, M., Cai, Q., Fang, H., 2016. Suspended sediment dynamics at different time scales in the Loushui River, south-central China. *Catena*, 136, 152–161. doi:10.1016/j.catena.2015.02.014.
- Taylor, J., 1997. *An Introduction to Error Analysis: the Study of Uncertainties in Physical Measurements*, 2nd edn. University Science Books: Sausalito, CA.
- Tasser, E., Mader, M., Tappeiner, U., 2003. Effects of land use in alpine grasslands on the probability of landslides. *Basic and Applied Ecology*, 4, 271–280. doi:10.1078/1439-1791-00153.
- Testa, B., Aldighieri, B., Bertini, A., Blendinger, W., Caielli, G., De Franco, R., Giordano, D., Kustatscher, E., 2013. Geomorphodiversity of the San Lucano Valley (Belluno Dolomites, Italy): A Well-Preserved Heritage. *Geoheritage*, 5, 151–172. doi:10.1007/s12371-013-0079-3.
- Thouret, J.C., Oehler, J.F., Gupta, A., Solikhin, A., Procter, J.N., 2014. Erosion and aggradation on persistently active volcanoes: A case study from Semeru Volcano, Indonesia. *Bull Volcanol*, 76(10), 857. doi:10.1007/s00445-014-0857-z.
- Tiranti, D., Deangeli, C., 2015. Modeling of debris flow depositional patterns according to the catchment and sediment source area characteristics, *Frontiers in Earth Science*, 3, art. no. 8. doi:10.3389/feart.2015.00008.
- Tiranti, D., Crema, S., Cavalli, M., Deangeli, C., 2018. An integrated study to evaluate debris flow hazard in alpine environment, *Frontiers in Earth Sciences*, 6, art. no. 60. doi:10.3389/feart.2018.00060.
- Tonon, A., Picco, L., Rainato, R., 2018. Test of methodology for developing a large wood budget: A 1-year example from a regulated gravel bed river following ordinary floods. *Catena (Amst)* 165, 115–124. <https://doi.org/10.1016/j.catena.2018.01.035>
- Tsvetanov, N., Dountchev, A., Panayotov, M., Zhelev, P., Bebi, P., Yurukov, S., 2018. Short- and long-term natural regeneration after windthrow disturbances in Norway spruce forests in Bulgaria. *iForest*, 11 (5), 675–684. doi:10.3832/ifor2754-011.
- Turkington, T., Rемаître, A., Ettema, J., Hussin, H., van Westen, C., 2016. Assessing debris flow activity in a changing climate. *Climatic Change*, 137(1–2), 293–305. <https://doi.org/10.1007/s10584-016-1657-6>
- Turner, M.G., Dale, V.H., 1998. Comparing large, infrequent disturbances: what have we learned? *Ecosystems* 1, 493–496. doi:10.1007/s100219900045.

- Turowski, J.M., Yager, E.M., Badoux, A., Rickenmann, D., Molnar, P., 2009. The impact of exceptional events on erosion, bedload transport and channel stability in a step pool channel. *Earth Surface Processes and Landforms* 34, 1661-1673.
- Turowski, J.M., Rickenmann, D., Dadson, S.J., 2010. The partitioning of the total sediment load of a river into suspended load and bedload: A review of empirical data. *Sedimentology* 57 (4), 1126–1146. <https://doi.org/10.1111/j.1365-3091.2009.01140.x>.
- Uchida, T., Sakurai, W., Iuchi, T., Izumiyama, H., Borgatti, L., Marcato, G., Pasuto, A., 2018. Effects of episodic sediment supply on bedload transport rate in mountain rivers. Detecting debris flow activity using continuous monitoring. *Geomorphology* 306, 198-209.
- Valenza, J.M., Edmonds, D.A., Hwang, T., Roy, S., 2020. Downstream changes in river avulsion style are related to channel morphology. *Nat Commun* 11. <https://doi.org/10.1038/s41467-020-15859-9>
- Vericat, D., Smith, M.W., Brasington, J., 2014. Patterns of topographic change in sub-humid badlands determined by high resolution multi-temporal topographic surveys. *Catena* 120, 164–176. <https://doi.org/10.1016/j.catena.2014.04.012>
- Vericat, D., Wheaton, J.M., Brasington, J., 2017. Revisiting the morphological approach: opportunities and challenges with repeat high-resolution topography. In: Tsutsumi, D., Laronne, J.B. (Eds.), *Gravel-bed Rivers: Processes and Disasters*, First edition. John Wiley & Sons Ltd, pp. 121–158.
- Victoriano, A., Díez-Herrero, A., Génova, M., Guinau, M., Furdada, G., Khazaradze, G., Calvet, J., 2018. Four-topic correlation between flood dendrogeomorphological evidence and hydraulic parameters (the Portainé stream, Iberian Peninsula). *Catena* 162, 216–229.
- Walling, D. E., Webb, B. W., 1987. Suspended load in gravel-bed rivers: UK experience. In: *Sediment Transport in Gravel-Bed Rivers* (ed. by C. R. Thorne, J. C. Bathurst & R. D. Hey), 545–579. John Wiley & Sons, Chichester, West Sussex, UK.
- Wheaton, J.M., Brasington, J., Darby, S.E., Sear, D.A., 2010. Accounting for uncertainty in DEMs from repeat topographic surveys: improved sediment budgets. *Earth Surface Processes and Landforms*, 35, 136–156. doi:10.1002/esp.1886.
- Wheaton, J., Brasington, J., Darby, S.E., Kasprak, A., Sear, D., Vericat, D., 2013. Morphodynamic signatures of braiding mechanisms as expressed through change in sediment storage in a gravel-bed river, *Journal of Geophysical Research: Earth Surface*, 118, 759–779. doi:10.1002/jgrf.20060.
- Whittaker, J.G., Jaeggi, M.N.R., 1982. Origin of step-pool systems in mountain streams. *Journal of Hydraulic Engineering* 108, 758–773.
- Wicherski, W., Dethier, D.P., Ouimet, W.B., 2017. Erosion and channel changes due to extreme flooding in the Fourmile Creek catchment, Colorado. *Geomorphology* 294, 87–98.

- Wilcox, A.C., Wohl, E.E., Comiti, F., Mao, L., 2011. Hydraulics, morphology, and energy dissipation in an alpine step-pool channel. *Water Resour Res* 47. <https://doi.org/10.1029/2010WR010192>
- Williams, G.P., 1989. Sediment concentration versus water discharge during single hydrological events in rivers. *Journal of Hydrology*, 111, 89–106. doi:10.1016/0022-1694(89)90254-0.
- Wohl, E., 2010. *Mountain Rivers Revisited*. Washington, DC: American Geophysical Union Press.
- Wyżga, B., Radecki-Pawlik, A., Galia, T., Plesiński, K., Škarpich, V., Dušek, R., 2020. Use of high-water marks and effective discharge calculation to optimize the height of bank revetments in an incised river channel. *Geomorphology* 356, 107098
- Wyżga, B., Liro, M., Mikuś, P., Radecki-Pawlik, A., Jeleński, J., Zawiejska, J., Plesiński, K., 2021. Changes of fluvial processes caused by the restoration of an incised mountain stream. *Ecol Eng* 168. <https://doi.org/10.1016/j.ecoleng.2021.106286>
- Yager, E.M., Turowski, J.M., Rickenmann, D., McArdell, B.W., 2012. Sediment supply, grain protrusion, and bedload transport in mountain streams, *Geophys. Res. Lett.*, 39, L10402. doi:10.1029/2012GL051654.
- Yeshaneh, E., Eder, A., Blöschl, G., 2014. Temporal variation of suspended sediment transport in the Koga catchment, North Western Ethiopia and environmental implications, *Hydrol. Process.*, 28, 5972– 5984. doi:10.1002/hyp.10090.
- Yildiz, V., Hatipoglu, M.A., Kumcu, S.Y., 2022. Climate Change Impacts on Water Resources. In: Bahadir, M., Haarstrick, A. (eds) *Water and Wastewater Management*. Water and Wastewater Management. Springer, Cham. doi:10.1007/978-3-030-95288-4_2.
- Yochum, S.E., Sholtes, J.S., Scott, J.A., Bledsoe, B.P., 2017. Stream power and geomorphic change during the 2013 Colorado front range flood. *Geomorphology* 292, 178–192.
- Yousefi, S., Mirzaee, S., Keesstra, S., Surian, N., Pourghasemi, H.R., Zakizadeh, H., Tabibian, S., 2017. Effects of an extreme flood on river morphology (case study: Karoon River, Iran). *Geomorphology*, 304. doi:10.1016/j.geomorph.2017.12.034.
- Zhang, C., Xu, M., Hassan, M.A., Chartrand, S.M., Wang, Z., 2018. Experimental study on the stability and failure of individual step-pool. *Geomorphology* 311, 51–62. <https://doi.org/10.1016/j.geomorph.2018.03.023>
- Zink, J.M., Jennings, G.D., 2014. Channel roughness in North Carolina Mountain Streams. *Journal of the American Water Resources Association (JAWRA)* 50(5), 1354-1358.

Sites

CloudCompare (version 2.7) [GPL software]. (2016). Retrieved from <http://www.cloudcompare.org>
<https://idt2.regione.veneto.it>